Ab Initio Study of the chemical reactivity of metal clusters and metal oxide clusters

D I S S E R T A T I O N

zur Erlangung des akademischen Grades
doctor rerum naturalium
(dr. rer. nat.)
im Fach Chemie

eingereicht an der
Mathematisch-Naturwissenschaftlichen Fakultät I
Humboldt-Universität zu Berlin

von
Dipl.-Chem. Massimiliano Bienati
geborem am 04.06.1970 in Premosello (Italien)

Präsident der Humboldt-Universität zu Berlin:
Prof. Dr. J. Mlynek
Dekan der Mathematisch-Naturwissenschaftlichen Fakultät I:
Prof. Dr. B. Ronacher

Gutachter:

1. Prof. Dr. Vlasta Bonačić-Koutecký
2. Prof. Piercarlo Fantucci

eingereicht am: 24. Januar 2001
Tag der mündlichen Prüfung: 02. März 2001

Abstract

In this work the transition metal and metal oxide clusters has been investigated with the aim of gaining a better insight into the mechanisms which govern their reactivity. The theoretical study of the structural and energetic properties of the clusters has been carried out within the framework of the density functional theory by means of a new family of gradient-corrected hybrid density functionals which has been coded for the first time into quantum chemistry packages. The theoretical findings stimulated the experimental investigation of the gas phase reactivity of these species which confirmed the correctness of the reaction mechanism models proposed (A. Fielicke, Doctoral Thesis, Humboldt-Universität zu Berlin, 2001).

Keywords:
density functional theory, transition metal clusters, metal oxide cluster, bismuth oxide

Zusammenfassung

Mit der vorliegenden Arbeit wurden neue Erkenntnisse bei der Aufklärung der Mechanismen, die für die Reaktivität von Übergangsmetall- und Metalloxid-Clustern verantwortlich sind, gewonnen. Dies ist aus zwei Gründen gelungen: Zum einen erlaubt die gradienten-korrigierte Dichtefunktional-Methode eine zuverlässige Beschreibung von strukturellen und energetischen Eigenschaften dieser Cluster, insbesondere durch die Entwicklung einer neuen Generation von Hybrid-Austausch- und Korrelations-Funktionalen im Rahmen der verallgemeinerten Gradienten-Näherung. Diese wurden erstmalig in entsprechenden quantenchemischen Programmen implementiert und getestet. Zum zweiten stellte die fruchtbare Zusammenarbeit mit den experimentellen Bereichen, eine Herausforderung für die Theorie dar, mittels der gewonnenen Erkenntnisse zur konzeptionellen Planung der Experimente beizutragen (A. Fielicke, Dissertation, Humboldt-Universität zu Berlin, 2001).

Schlagwörter:
Dichtefunktional-Methode, Übergangsmetall-Cluster, Metalloxid-Cluster, Bismutoxid

To F.

Contents

Chapter 1

Introduction

The knowledge of principles of chemistry and physics of clusters has progressively developed in the last 15 years, to such a level that the whole cluster science had to split into well characterized and separated special topics. From this extremely intense research activity a general view emerged concerning the basic rules upon which the electronic structure of clusters can be built and understood. As a consequence, reliable theoretical models have been developed for basic properties of clusters considered as isolated species (shape, stability and isomerisation profiles), or a chemically reactive objects. In addition, clusters have been studied also in connection with their interaction with electromagnetic fields (studies of optical spectra of clusters considered as single points on the Born-Oppenheimer surface or clusters characterized by thermally excited nuclear motion) [1] or magnetic and electric fields (studies of polarizabilities and susceptibilities) [2]. This general view concerning the basic electronic properties of clusters support also the evidence that the specific nature of clusters is intimately correlated with the specific nature of atom-atom bonds. The present study will focus on two very different classes of clusters, characterized by very different chemical bonds. From one side, homonuclear transition metal Ni_X species will be considered, and on the other side the compound clusters $Bi_XO_y^+$ will be studied as prototypes of possible oxidation catalysts with respect to unsaturated hydrocarbons.

In order to point out the basic ideas which have inspired the present investigation, a brief review of the main characteristics of clusters of different nature will be reported. This will contribute also to frame our study within the general perspectives of the nowadays research in cluster science. It should be emphasized that the main aim of the present study is to investigate the behavior of “reactive” clusters, possibly in the

context of catalytic processes. This will give also a special character to the following brief review of classes of clusters, since it will point out mainly the reasons of cluster reactivity or non-reactivity.

In general, the elemental clusters (no reference will be made to molecular and rare gas species, that is to clusters dominated only by Van der Waals forces) may be classified as follows: i) homonuclear and heteronuclear (or mixed) metal clusters, ii) homonuclear or heteronuclear clusters of covalent elements, iii) compound clusters A_XB_y, where usually A is a metal and B a non metal atoms. A_XB_y species can be further separated into different classes, e.g. namely the ones with ionic, metallic bonds (Na_XF_y) or clusters characterized by covalent, partly polarized bonds (Bi_XO_y).

1.1 The general properties of homonuclear and heteronuclear metallic clusters

These are the species experimentally known since long time, due to the possibility of a relatively easy production of intense cluster beams, which is obviously connected with the melting and boiling temperature of the metal [3]. This is the reason why most of the work has been originally done on alkali metal (group Ia) clusters, mainly Na_X species and, more recently, also on the Li_X ones. The metal-metal bond in alkali metal clusters has been always considered as relatively week bond, a fact which should produce easy isomeric transitions and possible cluster fragmentation (evaporation of monomers and dimers from a given cluster). Such assumptions, formulated before a well grounded theoretical analysis could have been performed, led to the description of the electronic structure of clusters based on the very approximate jellium model, which contributed to spread oversimplified views (if not errors) in the cluster science literature. A more rigorous examination of the electron distribution in alkali metal clusters has suggested that the metal-metal bond in small-medium size species still has fingerprints of the molecular character, even if the tendency of the valence electron delocalization appears, which is a characteristic of the corresponding bulk metals. Static and dynamic properties of these clusters have been extensively investigated at ab initio theoretical level (cf. [4] and references therein). Due to the fact that the temperature range in which important isomerization processes can occur is relatively narrow (0-500K) and due to the relatively small size of representative clusters, dynamic properties have been investigated also at relatively accurate level of theory. In addition, the

nature of the excited states of Li_X and Na_X clusters are now well understood, being so well documented by numerous theoretical investigations.

In addition to the group Ia elements, also homonuclear clusters of group Ib elements (especially Ag_X) has been experimentally and theoretically investigated. All the bonding features in alkali and coinage metal clusters are dominated by the interaction among valence s electrons, which is accompanied, however, by an important s-p hybridization which is responsible for the appearance of specific cluster shapes, not necessarily connected with the symmetry of most compact forms. The mixed forms A_XB_y , where both A and B belong to the same group (e.g. Li_XNa_y) seem to be characterized by properties similar to those of pure A_{X+y} or B_{X+y} species. Clearly, in the case of ionization potential (IP), or electron affinity (AE) the cluster properties reflect the trend of the corresponding atomic properties. Thus, in general if IP(B) < IP(A) one can expect that IP(A_XB_y) < IP(A_{X+y}) (and similarly for AE values if AE(B) < AE(A)). Analogously, if the first transition energies (Te) in atoms obey the relation Te (B)< Te (A), then one can expect a red shift of all the transition in A_XB_y with respect to A_{X+y}. The basic feature of the electron distribution does not seem to be particularly affected by the presence of heteroatoms B, with exception of a very small increase in polarization of the bond when the electronegativity of B is smaller than that of A. Finally, the A_XB_y species are expected to be characterized by a number of low lying isomers larger than that occurring for A_{X+y}, a feature which is common to all the compound clusters.

The field of homonuclear and heteronuclear transition metal TM clusters is much less investigated experimentally, probably because of the high melting temperatures of the bulk metals. On the other hand, also the theoretical characterization of this class of clusters has been less frequent in the past, because of the well known difficulties of Hartree-Fock (HF) and post-HF methods when dealing with transition metal atoms. The drawback of such methods is related with the presence of d electrons and with the consequent complicated interplay of the inner- and inter-shell electron correlation (near degeneracy effects) which in turn is markedly dependent also on the extent of the d-s-p hybridization (and change in hybridization) present in clusters. Only recently the situation has considerably improved due to the availability of fairly accurate exchange-correlation functionals within the Density Functional Theory (DFT).

1.2 The general properties of homonuclear and heteronuclear covalent clusters

Covalent clusters are characterized, in general, by a stability much higher than the group Ia or Ib elemental clusters. Correspondingly, also the possibility of isomerization at relatively low temperature is expected to be fairly low. For instance, the pronounced covalent bonds in C_X [5] clusters are strongly localized for small x, while in large clusters a super-delocalization can take place giving rise to a graphite-like systems or systems with compact structure like the fullerenes. As well known, the strong localization of the bound electrons, or the extra stability provided by extended aromatic delocalization makes these clusters poorly reactive systems. This can be easily explained by the fact that C atoms can follow different hybridization schemes (sp, sp^2 or sp^3) with the corresponding possibility of forming triple, double or single bonds. This means that C atoms have a very pronounced tendency of saturating their own valences with direct C-C bonds. This implies that carbon clusters exhibit a very small tendency to have "dangling" bonds (i.e. possible reactive sites) and, in this respect, behave very differently from metallic clusters .

1.3 The reactive clusters: transition metal atom clusters and metal oxide clusters.

As pointed out above, the clusters formed by transition metal atoms or by metal oxides are the most favored representatives of reactive clusters. The metal clusters of small-medium size are characterized by atoms with a co-ordination number smaller than that of the bulk metal. Therefore, some atoms in the cluster (and in particular those belonging to the surface) are characterized by unsaturated valences, and therefore ready to react.

In particular, the TM clusters are interesting examples because, not only present unsaturated sites of co-ordination but also the constituent atoms are very active with respect to ligands, which -according to the point of view of the co-ordination chemistry- can behave as electron withdrawing group. When this occurs, metal atoms in TM clusters can act as bases (electron donors) better than acids (electron acceptors) with respect to unsaturated ligands (e.g. CO). It is very easy to accept that a TM clusters can

react easily with ligands, in an attempt to saturate the atom valences. Such a reaction is the subject of the part of the present study carried out on the specific example of nickel tetramers. It is accompanied by a deep change of the nature of the metal-metal bond, which in turn can determine also a pronounced variation of the magnetic properties of the cluster. In particular, it will be shown that in the complete absence of CO ligands, the nickel tetramers tend to assume the highest spin multiplicity (S=4*1/2=2) and that the cluster paramagnetism is progressively quenched by the further addition of CO ligands. Therefore, the nickel tetramers are not only very reactive with respect to CO, but they also undergo a deep change in their electronic structure. Therefore, this is a case in which the reactivity with ligands is accompanied by a strong variation of the metal-metal bond, to such an extent that in fully carbonylated clusters the stability is not longer determined by direct metal-metal interaction but is mediated by metal-ligand-metal bridges.

The second class of reactive clusters considered in this study is the class of bismuth oxide clusters. Here the behavior is very different from the above TM cluster example: the metal oxide cluster appear to be reactive in the sense that it can promote one or more reactant oxygen atoms to an electronic state suitable for reacting with unsaturated hydrocarbons. It is important to note that the metal oxide cluster keeps its own internal structure (and charge distribution) almost unaffected and that its reactivity takes place just because of the possibility of substituting a single oxygen atom (terminal M=O bond) with a peroxo group (M-O-O-M). This is a very characteristic reaction which reminds on the analogous reaction occurring with oxides of the transition metal atoms such as Mo and W (cf. [6] and references therein). Indeed, a second part of this study will show how it is possible to design a catalytic cycle which involve $Bi_XO_y^+$ clusters and unsaturated hydrocarbon like ethene or propene, with many similarities with the catalytic cycle involving Mo or W catalysts.

The present study is organized as follows. The Section 2 is devoted to the analysis of some aspects of the methodologies and computational strategies used in the theoretical investigation of the two considered classes of clusters. Section 3 report the discussion of the electronic structure of the series of neutral, positively and negatively charged nickel tetramers and their derivatives with one or more CO groups. Section 4 presents the results of a detailed investigation of the clusters $Bi_XO_y^+$ (x=3,4, y=3-6) and their reaction with ethylene and propylene. Section 5 reports some general conclusions and future perspectives in the field of theoretical investigations of cluster reactivity.

Chapter 2

Methodological and computational aspects

2.1 The Schrödinger equation

The principles of Quantum Mechanics can be equivalently formulated by two different approaches namely the Matrix Mechanics and the Wave Mechanics. The former is due to the pioneering work of Heisenberg, Born and Jordan and is based on a critical approach to the Old Quantum Theory which concerned with a whole set of notation without any experimental foundation[1] [8]. Matrix mechanics deals only with physically observable quantities such as frequencies and intensities of radiation emitted or adsorbed by matter. Wave Mechanics starts from a completely different point of view by considering the hypothesis of L. de Broglie on the *wave-particle* property of matter and seeking to establish the law of propagation of the wave function in the context of the *correspondence principle*[2] [7]. The law is based on the postulate that the wave

[1] As an example of this concept let us recall the notion of electronic orbit in the hydrogen atom suggested by Born. In order to observe this motion we should perform successive measurement of the position of the electron around the nucleus with a precision of several order of magnitude lager than the mean radius a of the orbit. This is conceivable by using X-rays of sufficiently short wavelenght: $\lambda \ll a$. However, it is known that the impact of the electron with such radiation would be accompained by a momentum transfer of the order of $\hbar/\lambda \gg \hbar/a$, (the Compton effect [7]) a finite perturbation which will affect the measurement of the motion one whishes to observe. Furthermore, the extent of the perturbation is the more appreciable the smaller is the quantum number n associated to the orbital motion of the electron which limits the precision of the measurement and prevents a complete success of the experiment.

[2] The correspondence principle states that there exists a formal analogy between Quantum Theory and Classical Theory, ergo Quantum Theory must approach Classical Theory asymtotically in the limit of large quantum numbers.

function $\Psi(\mathbf{r},t)$ of a quantum system completely defines its dynamical state, i.e. the dynamical properties of the system at a given time t can be deduced from the knowledge of $\Psi(\mathbf{r},t)$ itself[3]. Hence the problem becomes the determination of wave function at a given initial time t_0. The choice of the propagation's law of Ψ should be postulated and its justification lies in the success of predicting experimental results. Nevertheless, in order to keep fixed the interpretation of Ψ as well as to observe the correspondence principle some *a priori* conditions[4] restrict the choice of the wave equation to a *linear and homogeneous first order differential equation with respect to time*

$$i\hbar\frac{\partial}{\partial t}\Psi(\mathbf{r},t)=\left(-\frac{\hbar^2}{2m}\nabla^2-\frac{e^2}{r}\right)\Psi(\mathbf{r},t) \tag{2.1}$$

or in a more general form

$$\hat{H}\Psi(\mathbf{r},t)=\hbar\frac{\partial}{\partial t}\Psi(\mathbf{r},t) \tag{2.2}$$

which is the known as the time dependent Schrödinger equation. It is actually the fourth postulate of Quantum Mechanics: "The wave function $\Psi(\mathbf{r},t)$ must satisfy the fundamental law of motion expressed by the Schrödinger equation where $\hat{H}$ is the operator corresponding to the classical *Hamiltonian function* for the particle".

Notice, that the equation (2.2) is not a wave equation since it does not contain any second derivative terms with respect to time. It is rather a kind of diffusion equation [9] which has only a first derivative dependence of time. Nevertheless, for conservative systems Hamiltonians do not explicitly depend on time and allow the separation of variables in the wave function giving rise to a *standing wave equation* whose solutions $\Psi(\mathbf{r})$ are simply modulated by a phase factor $\mathrm{e}^{-iEt/\hbar}$ [10]. Consider a single particle in a potential well $\hat{V}(\mathbf{r})$[5]. Thus, the time dependent Schrödinger equation results

$$i\hbar\frac{\partial\Psi(\mathbf{r},t)}{\partial t}=-\frac{\hbar}{2m}\nabla^2\Psi(\mathbf{r},t)+\hat{V}(\mathbf{r})\Psi(\mathbf{r},t). \tag{2.3}$$

[3]This is known as the First Postulate of Quantum Mechanics [9]

[4]These are the postulates of Quantum Mechanics. The first has been reported in the previous footnote. Postulate II: Observables are represented by operators chosen to satisfy the commutaion relation $\hat{x}\hat{p}-\hat{p}\hat{x}=i\hbar$. Postulate III: Every measurable quantity is represented by a linear Hermitian operator Ω acting on Ψ such that the average result of many measurements of this quantity in a state $\Psi(\mathrm{r},t)$ is given by the expectation value of the operator: $\langle\Omega\rangle=\int\Psi^*\Omega\Psi d\tau/\int\Psi^*\Psi d\tau$.

[5]$\hat{V}(\mathrm{r})$ is assumed to be a real well-behaved function and represent the potential energy of the system.

The wave function can be now expressed as a product of spatial and temporal terms $\Psi(\mathbf{r},t) = \psi(\mathbf{r})f(t)$ and the equation (2.3) becomes

$$\psi(\mathbf{r})i\hbar\frac{df(t)}{dt} = f(t)\left[-\frac{\hbar^2}{2m}\nabla^2 + \hat{V}(\mathbf{r})\right]\psi(\mathbf{r}) \tag{2.4}$$

which can be written in a more compact form as

$$\frac{i\hbar}{f(t)}\frac{df(t)}{dt} = \frac{1}{\psi(\mathbf{r})}\left[-\frac{\hbar^2}{2m}\nabla^2 + \hat{V}(\mathbf{r})\right]\psi(\mathbf{r}). \tag{2.5}$$

Since the left hand side of (2.5) is a function of t only and the right hand side is a function of $\mathbf{r}$ only, the two sides must equal a constant. For classical conservative systems the energy is a constant of the motion. Looking for a solution $\Psi(\mathbf{r},t)$ representing a dynamical state of well-defined energy E one can write

$$\frac{1}{f(t)}\frac{df(t)}{dt} = -\frac{iE}{\hbar} \tag{2.6}$$

and

$$-\frac{\hbar^2}{2m}\nabla^2\psi(\mathbf{r}) + V(\mathbf{r})\psi(\mathbf{r}) = E\psi(\mathbf{r}). \tag{2.7}$$

The solutions of the equation (2.6) are of the form

$$f(t) = e^{-iEt/\hbar} \tag{2.8}$$

which are purely oscillatory functions[6] and affect the form of the solution of the wave equation (2.4) by a phase factor of constant magnitude. The equation (2.7) is the *time independent* Schrödinger equation[7] whose solutions represent *stationary states* of a quantum particle[8].

[6] Recall Euler's formula $e^{\pm i\zeta} = cos\zeta \pm isin\zeta$.

[7] In the language of the theory of partial differential equations an equation of the type $\hat{H}\psi = E\psi$ is known as an eigenvalue equation whose solutions are eigenfunctions of the corresponding eigenvalues [9].

[8] States having wave functions for which $\psi^*\psi$ is independent of time are called stationary states.

2.2 The adiabatic and Born-Oppenheimer approximation

A molecule arises from binding of several atoms and its energy can be obtained by the solutions of the time-independent Schrödinger equation associated with the non-relativistic molecular Hamiltonian (in atomic units [11])

$$\hat{H} = -\frac{1}{2}\sum_{A}^{nucl.}\frac{1}{M_A}\nabla_A^2 + \sum_{A>B}^{nucl.}\frac{Z_A Z_B}{R_{AB}} - \frac{1}{2}\sum_{i}^{el.}\nabla_i^2 - \sum_{i}^{el.}\sum_{A}^{nucl.}\frac{Z_A}{r_{iA}} + \sum_{i>j}\frac{1}{r_{ij}} \qquad (2.9)$$

where capital letters indicate the nuclei and small letters the electrons. To find the eigenfunctions of such a complex operator is a very difficult task. However, the problem can be simplified by considering that the mass of the nuclei is several order of magnitude larger than that of the electrons[9] whereas both particles are subjected to forces of comparable magnitude. To a good approximation, the electrons feel the nuclei as force centers and their dynamical state adiabatically follows the evolution of the potential created by the slow motion of the nuclei. Therefore, the nuclei are essentially subjected to only the average potential created by the electron motion. This is the essence of the *adiabatic approximation* which allows the separation of nuclear and electron variables when solving the Schrödinger equation. The *Born-Oppenheimer* (BO) approximation may be considered as a special case of adiabatic approximation in which the electrons moves in the presence of fixed nuclei.

Let us outline the procedure of finding the stationary state of a molecular system described by the Hamiltonian (2.9) which in a more compact form become

$$\hat{H} = \hat{T}_N(\mathbf{R}) + \hat{T}_e(\mathbf{r}) + \hat{V}_{eN}(\mathbf{r},\mathbf{R}) + \hat{V}_{NN}(\mathbf{R}) + \hat{V}_{ee}(\mathbf{r}). \qquad (2.10)$$

Unfortunately, in the (2.10) the term $\hat{V}_{eN}(\mathbf{r},\mathbf{R})$ prevents us from separating $\hat{H}$ into nuclear and electronic parts. $\hat{V}_{eN}(\mathbf{r},\mathbf{R})$ is large and cannot be neglected. However, due to the disparity of the masses of the electrons and nuclei we can make its $\mathbf{R}$ dependence *parametric* so that the total wave function can be written as $\psi(\mathbf{r};\mathbf{R})\chi(\mathbf{R})$. For a fixed nuclear configuration $\mathbf{R} = \mathbf{R_a}$, the full molecular Hamiltonian (2.10) reduces to the *clamped nuclei* electronic Hamiltonian

[9] Recall that the mass of the electron is of the order of 10^{-31} Kg while the mass of the proton and the neutron (as well as that of the nuclide) is of the order of 10^{-27} Kg (see [10], [11]).

$$\hat{H}_e(\mathbf{R_a}) = \hat{T}_e(\mathbf{r}) + \hat{V}_{eN}(\mathbf{r};\mathbf{R_a}) + \hat{V}_{NN}(\mathbf{R_a}) + \hat{V}_{ee}(\mathbf{r}), \tag{2.11}$$

which has its complete set of eigenvalues and eigenfunctions of the corresponding clamped nuclei Schrödinger equation

$$\hat{H}_e\psi_k(\mathbf{r};\mathbf{R_a}) = E_k\psi_k(\mathbf{r};\mathbf{R_a}). \tag{2.12}$$

Furthermore, since $\mathbf{R_a}$ is now a parameter the $\hat{V}_{NN}(\mathbf{R_a})$ term is just a constant and the Hamiltonian of the equation (2.12) can be written in a more compact form as

$$\hat{H}_e = \hat{T}_e(\boldsymbol{r}) + V_{eN}(\boldsymbol{r};\boldsymbol{R}) + \hat{V}_{ee}(\boldsymbol{r}). \tag{2.13}$$

In order to find out the wave equation of the nuclear motion let us consider again the molecular Hamiltonian (2.9). Without introducing any approximation, the solution of the associated wave equation can be written as expansion of electronic wave functions with coefficients as functions of the nuclear coordinates

$$\Psi(\mathbf{r},\mathbf{R}) = \sum_{k}^{\infty} \psi_k(\mathbf{r};\mathbf{R})\chi_k(\mathbf{R}) \tag{2.14}$$

where the $\psi_k(\mathbf{r};\mathbf{R})$ are known from (2.12). By substituting (2.14) into the time independent Schrödinger equation expressed by the Hamiltonian (2.10), one obtains

$$\hat{H}\sum_{k=1}^{\infty} \psi_k(\mathbf{r};\mathbf{R})\chi_k(\mathbf{R}) = E_{Tot}\sum_{k=1}^{\infty} \psi_k(\mathbf{r};\mathbf{R})\chi_k(\mathbf{R}) \tag{2.15}$$

For brevity, let ∇^2 and ∇ the operators associated with derivatives with respect to the nuclear coordinates. After some algebra and omitting writing the variables eq. 2.15 becomes**:**

$$\sum_{k=1}^{\infty}\Big\{\psi_k(\nabla^2\chi_k) + 2\nabla_N\psi_k\nabla\chi_k + \chi_k\nabla^2\psi_k + \chi_k E_k\psi_k\Big\} = E_{Tot}\sum_{k=1}^{\infty}\psi_k\chi_k. \tag{2.16}$$

By virtue of the orthonormality of the solutions of the electronic problem (2.12),[10] multiplying the eq. (2.16) by ψ_l and integrating over the electron coordinates **r**, one

[10]Since the Hamilton operator (2.11) is hermitian, the solutions of the associated Schrödinger equation can be chosen to be orthogonal and normalized.

obtains

$$\begin{aligned} &\int d\mathbf{r}\psi_l^* \sum_{k=1}^{\infty} [\psi_k(\nabla^2\chi_k) + 2(\nabla\psi_k)(\nabla\chi_k) + \chi_k(\nabla^2\psi_k) + \chi_k E_k\psi_k] \\ &= E_{Tot} \int d\mathbf{r}\psi_l^* \sum_{k=1}^{\infty} \psi_k\chi_k \end{aligned} \tag{2.17}$$

or, after some manipulation[11],

$$\nabla_N^2\chi_k + E_k\chi_k + \sum_{k=1}^{\infty} \left[2\left\langle\psi_l\right| \nabla \left|\psi_k\right\rangle (\nabla\chi_k) + \left\langle\psi_l\right| \nabla^2 \left|\psi_k\right\rangle \chi_k\right] = E_{Tot}\chi_k \tag{2.18}$$

which is the eigenvalue equation for nuclear motion in which the operators in square brackets are the *first and second order non-adiabatic coupling elements*, respectively and take into account the coupling between the electronic and nuclear motion.

In the adiabatic approximation the form of the total wave function is restricted to the electronic surface in which all the off-diagonal coupling elements in the eq. (2.18) are neglected. In the Born-Oppenheimer approximation also these diagonal terms are neglected and the resulting nuclear equation of motion takes the usual form

$$(\hat{T}_N + V_l(\mathbf{R}))\chi_l(\mathbf{R}) = E_{Tot}\chi_l(\mathbf{R}) \tag{2.19}$$

where the electronic energy E_k plays the role of an average potential energy $V_l(\mathbf{R})$. Thus, in the BO approximation the nuclei move on a *potential energy surface* (PES) which is a solution of the electronic Schrödinger equation (2.19).

2.2.1 Potential energy surface, geometry optimization techniques and vibrational analysis

The potential energy surface

The BO approximation is of central importance in describing chemical phenomena. As we have seen, its assumption that the electronic motion is uncoupled from that of the nuclei, leads to the concept of potential energy surface [13, 14] i.e. to a function

[11]The *bra-ket* notation introduced by Dirac [12, 7] deals with the short-hand notaion $|n\rangle$ (bra) and $\langle m|$ (ket) for expressing a wave function for the state *n* and the complex conjugate of wave function for the state *m*, respectively. By means of this notation the integral form of the eigenvalues problem $\int \psi^*\hat{H}\psi d\tau = E$ is written as $\langle\psi|\,\hat{H}\,|\psi\rangle = E$ and, in the case the Hamiltonian operator is Hermitian, the orthornormality condition of the solutions is expressed as $\int \psi_k^*\psi_l d\tau = \langle\psi_k\,|\psi_l\rangle = \delta_{kl}$.

which describes the energy of a molecular system at fixed nuclear configurations. Stable chemical compounds correspond to minima on the PES with a structure in which bond lengths and bonds angles are well defined. Reactions can be visualized as the movement of the nuclei from the *valley* representing the reactants to the *valley* of the products whereas the reaction mechanism can be designed by considering the *path* connecting these two limit forms. The transition state is the highest points along the reaction path and governs the rate of the reactions (cf. Sect. 2.3). Thus, in order to describe the structural properties of molecules and their reactivity one should be able to locate minima, transition states and reaction paths on the PES.

The forces acting on the atoms of a molecule are the negative gradients of the PES. At critical (or stationary) points on the PES (usually associated to minimum or saddle points) the the forces vanish. However, using only information based on gradient of the energy, one cannot distinguish between minimum, maximum and transition state or higher order saddle points and therefore second derivatives are needed. The matrix of the second derivatives of the PES is called *Hessian matrix* or *force constant matrix*. From simple mathematical analysis concepts [15] the eigenvectors and eigenvalues resulting by diagonalizing the Hessian matrix give all the necessary information on the shape of the function for a given specific configuration. For a null-gradient point, a minimum has all positive eigenvalues of the Hessian matrix and a maximum negative eigenvalues. A transition state, defined as first order saddle point on the PES, is a maximum along one direction and a minimum along all other directions and therefore is characterized by only one negative eigenvalue. Reaction paths can be defined as the steepest descent path from a transition structure down to reactants and down to products.

Molecular geometry optimization

The molecular geometry optimization belongs to the more general field of the minimizing of a *N-dimensional* function (the PES) with respect to a set of the coordinates. Optimization methods can be divided essentially into three groups, corresponding to the computation *i)* of the function only; *ii)* the function and the gradient; and *iii)* the function, the gradients and the Hessian matrix. The first type of approaches are known in computational chemistry as *energy only* methods [16]: they are widely applicable but converge slowly, especially for high number of variables and are often coupled with numerically computed gradient methods. Among the gradient based procedures

particular efficiency has been achieved in the framework of analytical conjugate gradients methods known as Fletcher-Revees or Polak-Rieber methods [16] whereas the third class of approaches mostly deals with the Newton-Rapson method [16] and its modifications known as quasi-Newton-based methods [13] in which the Hessian is first estimated and subsequently numerically upgraded at each step of the optimization. All these methods are applicable to cartesian and internal coordinates as well[12]. Nevertheless, it has been found that the same algorithms implemented by using mass-weighted redundant internal coordinates improve the efficiency of the location of the critical points of the PES [17].

The search for a transition state structure is more difficult than the location of an equilibrium geometry. When studying chemical process, very often the structural topology of the reactants and the products can be obtained by empirical rules and this knowledge allows the choice of a reasonable starting geometry and Hessian in order to ensure rapid convergence by one of the methods mentioned above. Transition state structures are mostly unknown in a precise manner. Often only guessed structures can be defined based on chemical intuition. Clearly a more quantitative way of guessing the TS structures is needed. In this contest one of the most powerful method is based on the transformation of the problem in the minimizing of a good guess of the TS geometry with the quasi-Newton based method under the constraint that the Hessian must posses a negative eigenvalue corresponding to a dominant coordinate (cf. the reaction coordinate). This is the strategy followed by the linear and quadratic *Synchronous Transit-Guided Quasi Newton* (STQN) method developed by Schlegel and Peng [18], [13], in which the first guess of the TS structure is obtained by linear or quadratic interpolation between the reactants and the products structures [19].

Obviously, the accuracy of all the gradient and Hessian based optimization methods depend on the accuracy reached in solving the electronic problem within the BO approximation. For a given nuclear configuration the clamped nuclei Schrödinger equation (2.12) is solved, the corresponding (analytical) gradients are computed and the critical points on the PES are located. This procedure is valid in principle for all stationary points. However, particular care must be exercised especially when dealing with the transition state theory and the calculation of reaction rates using exponential laws (cf. Sect. 2.3).

[12] Internal coordinates are elements of the non-redundant set of $3N-6$ parameters (e.g bond distances, valence and dihedral angles) which univocally describe a molecular conformation.

Harmonic approximation and vibrational analysis

The aforementioned methods generally converge to a stationary point on the PES and they do not give further information whether the located molecular geometry is a local minima or a transition state. Thus, it can happen that in the attempt to optimize a particular transition state structure the method converges to a closely lying intermediate which is not a saddle point but a local minima. However, the nature of a stationary point is closely related to the solutions of the equation of motion of the nuclei (2.19) which can be easily obtained by means of the harmonic approximation of the point on the PES.

In the framework of the BO approximation the potential energy $V(\mathbf{R})$ of the eq. (2.19) in the vicinity of a reference geometry $\mathbf{R}_0$ can be expanded in a Taylor series as [20]

$$\begin{aligned} V(\mathbf{R}) &= \mathbf{V}^{(0)}(\mathbf{R}_0) + \textstyle\sum_i \mathbf{V}_i^{(1)}(\mathbf{R}_0)\Delta R_i + \frac{1}{2}\sum_{i,j} \mathbf{V}_{ij}^{(2)}(\mathbf{R}_0)\Delta R_i \Delta R_j \\ &\quad + \tfrac{1}{6}\textstyle\sum_{i,j,k} \mathbf{V}_{ijk}^{(3)}(\mathbf{R}_0)\Delta R_i \Delta R_j \Delta R_k + ... \end{aligned} \tag{2.20}$$

where $\mathbf{R}$ is the vector of the cartesian nuclear coordinates, ΔR_i is the displacement from the reference geometry of the *ith* coordinate and $\mathbf{V}^{(1)}(\mathbf{R}_0)$, $\mathbf{V}^{(2)}(\mathbf{R}_0)$, etc. are vector, matrix and hypermatrices collecting, respectively, the first, second and higher order derivatives of the molecular potential energy $V^{(0)}$ with respect to the reference geometry $\mathbf{R}_0$. In a stationary point the gradient of the energy is zero and the (2.20) becomes

$$V(\mathbf{R}) = V^{(0)}(\mathbf{R}_0) + \frac{1}{2}\sum_{i,j} V_{ij}^{(2)}(\mathbf{R}_0)\Delta R_i \Delta R_j + (higher\ terms). \tag{2.21}$$

To the second order, the potential energy function can be approximately described by a harmonic potential, using the force constant matrix elements

$$\mathbf{V}_{ij}^{(2)} = \frac{\partial^2 V(\mathbf{R}_0)}{\partial R_i \partial R_j} \tag{2.22}$$

in the following way:

$$\mathbf{V}(\mathbf{R}) = \mathbf{V}^{(0)}(\mathbf{R}_0) + \frac{1}{2}\sum_{i,j} \mathbf{V}_{ij}^{(2)}(\mathbf{R}_0)\Delta R_i \Delta R_j \tag{2.23}$$

where $\mathbf{V}^{(0)}(\mathbf{R}_0)$ is a constant defining the zero-energy point. Because of the nature of a stationary point is invariant with respect to any coordinate transformation, one can transform the force constant matrix to mass-weighted coordinates defined as

$$q_1 = \sqrt{m_1}\Delta X_1,\ q_2 = \sqrt{m_2}\Delta Y_2,\ q_3 = \sqrt{m_3}\Delta Z_3,\ \ldots q_N = \sqrt{m_N}\Delta Z_N\,. \tag{2.24}$$

Furthermore, since $V_{ij}^{(2)}$ is symmetric we can perform an orthogonal transformation of the mass weighted coordinates q_i to the normal coordinates [21]

$$Q_k = \sum_{i}^{3N} \zeta_{ik} q_i \tag{2.25}$$

which preserves the diagonal quadratic form of the nuclear kinetic energy and transforms the second order Taylor expansion (2.23) to the form

$$V(\mathbf{Q}) = \frac{1}{2}\sum_{k}^{3N} \lambda_k Q_k^2 \tag{2.26}$$

in which λ_k and ζ_{ik} are the eigenvalues and components of the eigenvectors of the force constant matrix, respectively. Of course, the diagonalizing of the Hessian matrix defined in terms of atomic cartesian coordinates leads to a set of 6 (or 5 for linear molecules) zero eigenvalues corresponding to the translational and rotational degree of freedom of the system. The other $3N-6$ λ_k eigenvalues are proportional to the square of the *harmonic vibrational frequencies* of the molecule[13] and are of central importance for defining the nature of the stationary point of the PES as well as for defining the thermodynamic properties of a molecule (cf. Sect. 2.3). If all the λ_k of (2.26) are positive, the point on the molecular PES is a local (or global) minima and has all real vibrational frequencies. If one or more of the eigenvalues are negative the molecular structure corresponds to a saddle point of first or higher order. For a first-order saddle point (transition state) the normal mode of vibration corresponding to the imaginary frequency points along the reaction path between the reactants and the products.

[13]This is due to the fact that within the BO approximation, the nuclear Schrödinger equation (2.19) decouples into a set of $3N-6$ (or $3N-5$) harmonic oscillators.

2.3 Theoretical approach to chemical reactivity

A better understanding of the reactivity of chemical compounds can be pursued by a detailed knowledge of the intrinsic properties of the stable and transient states reached during their interaction. Of course, a chemical reaction involves either charge or mass transfer and represents a dynamical process the detailed description of which would require the knowledge of the instantaneous changes of the species involved. However, it can be also considered as a process in which substances undergo changes under the influence of driving forces, which in turn can be obtained as energy variations. Therefore, the information necessary to define the thermochemistry of a reactive process refer to the quantum chemical properties of reactants, products and the transition states only. The application of the *statistical thermodynamics* through the use of the molecular partition function would provide the complete information. A further insight in the reactivity can be obtained by the *kinetic* analysis of a chemical process which provides useful information about the mechanism of the reaction. The *transition state theory* (TST) combines the thermodynamic and kinetic of a chemical reaction.

In this section the basic concepts of statistical thermodynamics will be presented as working tools useful to translate quantum mechanical information about a molecular system into macroscopic thermodynamic properties such as internal energy, entropy, enthalpy and free energy. Furthermore, it will be outlined how these findings may be used for defining chemical reaction rate constants by means of the transition state theory, which will be widely applied in studying the reactivity of the species investigated in this thesis.

2.3.1 Concepts of statistical thermodynamics; The partition function

In order to determine how the thermodynamic properties of a system composed by a large number of particles in thermal equilibrium with the surrounding depend on the properties of the individual microscopic components it is useful to introduce the concept of statistical distributions and to determine how particles distribute themselves among permitted energy levels [22].

In the classical approximation, the “state” or energetic configuration of an *ensemble* of N non-interacting particles can be expressed as the product of the states of the

individual constituent particles[14]

$$\Psi_{tot} = \Psi_a(1)\Psi_b(2)...\Psi_m(N) \tag{2.27}$$

where the numbers $1,\ 2,\ ...,N$ label the particles and the letters *a, b, ..., m,* label the single wave functions. Of course, this also means that the total energy of the system is the sum of the individual energies. Furthermore, by interchanging any two particles we obtain a new state (cf. footnote 14), namely

$$\Psi'_{tot} = \Psi_a(2)\Psi_b(1).....\Psi_m(N).$$

Any individual particle may exist in quantum states with energies ϵ_i, $i = 0, 1, 2, ...$, which are solutions of the corresponding Schrödinger equation. Thus, at a given time there will be n_0 molecules in the state with energy ϵ_0, n_1 with ϵ_1, etc. and the instantaneous configuration of the system can be pictured as $\{n_0, n_1, n_2, ...\}$. Therefore, the number of ways in which N particles can be distributed in a (fixed) number of energy levels is expressed by the *weight of the configuration*

$$W = \frac{N!}{n_0!n_1!n_2!...} \tag{2.28}$$

and the most probable configuration would be that for which W is a maximum in the contest of the postulate of *equal a priori probabilities*[15]. The procedure of finding a maximum for W under the constraints of constant total energy, leads to the *Boltzmann distribution la*w

$$p_i = \frac{n_i}{N} = \frac{e^{-\beta\epsilon_i}}{\sum_j e^{-\beta\epsilon_j}} \tag{2.29}$$

where $\beta = 1/k_BT$, T is the temperature and k_B is the Boltzmann constant ($1.38066\ 10^{-23}$ J K^{-1}). p_i expresses the probability that at a given time the fraction of molecules n_i occupies the state with energy ϵ_i. The quantity at the denominator of the eq. (2.29) is called *molecular partition function,* q, and plays a very important role in statistical thermodynamics. Physically, it provides the average number of the accessible states of a system at a given temperature [23]. In fact, since all energies are computed with re-

[14]This would not be the case of particles in the quantum mechanical world for which the wave function should be either symmetric (bosons) or antisymmetric (fermions). In fact, the square of the wave function is invariant under the exchange of two identical particles. The classical approximation neglects any symmetry requirement and allow particles to be distinguishable.

[15]This is equivalent to assume that the intrinsic probabilities of all states of the system are equal.

spect to the lowest level, $\epsilon_0 = 0$ and $\epsilon_0/k_BT = 0$. Thus, for $T \to 0$, $q \to 1$ the only accessible states would be those associated to lowest energy levels[16]. On the contrary, for $T \to \infty$, $q \to \infty$ all accessible states would be populated.

Since the total energy of the system is the sum of the energy levels $E = \sum_i n_i\epsilon_i$ and the most likely configuration dominates, it can be espressed in terms of the Boltzmann distribution (2.29) as

$$E = \frac{N}{q}\sum_i \epsilon_i e^{\beta\epsilon_i} \tag{2.30}$$

or in an equivalent form

$$E = -\frac{N}{q}\frac{d}{d\beta}\sum_i e^{-\beta\epsilon_i} = -\frac{N}{q}\frac{dq}{d\beta}. \tag{2.31}$$

Indeed, E is the value of the internal energy U relative to its value at $T = 0$, $U(0)$ and can be espressed as

$$E = U - U(0) = -\frac{N}{q}\left(\frac{\partial q}{\partial\beta}\right)_V \tag{2.32}$$

which shows that by the knowledge of the partition function, the evaluation of the state function U is straightforward. Furthermore, from the *fundamental* equation of the thermodynamics[17]

$$dU = TdS - PdV, \tag{2.33}$$

which under *reversibility* conditions (*P*, *V* constant) becomes

$$dU = TdS, \tag{2.34}$$

one can derive the statistical definition of the *entropy*

$$S = \frac{U - U(0)}{T} + Nk_B\, lnq. \tag{2.35}$$

[16]Sometime, the partition function is written in terms of the degeneracy g_j of the energy levels instead of the states

$$q = \sum_j^{states} g_j e^{-\beta\epsilon_j}$$

and at $T = 0$ its value would correspond to the degeneracy g_0 of the ground state.

[17]The fundamental equation arises by combining the First and Second principles of the thermodynamic [24].

Once the internal energy and the entropy of a system are known, all the other thermodynamic functions can be derived. Thus, one can for example define the Helmholtz free energy

$$A = U - TS = -Nk_BT\, lnQ \tag{2.36}$$

the enthalpy

$$H = U + PV = -\left(\frac{\partial lnQ}{\partial \beta}\right)_V + k_BTV\left(\frac{\partial lnQ}{\partial V}\right)_T \tag{2.37}$$

and the Gibbs free energy

$$G = H - TS = k_BTV\left(\frac{\partial lnQ}{\partial V}\right)_T - k_BT\, lnQ. \tag{2.38}$$

Notice, that all these quantities are related to the knowledge of the molecular partition function, the temperature of the ensemble and universal constants only.

In order to determine the partition function *q* (or *Q*) all the molecular quantum states are needed. However, it is usually assumed that the energy of a molecule can be approximated as a *sum* of terms involving only *translational*, *rotational*, *vibrational* and *electronic* states[18]. Therefore, the total partition function is a *product* of terms and because the thermodynamic functions (2.32) to (2.38) show logarithmic dependence on *q* this product transforms into sums of contributions. Thus, for a molecular system one can write

$$\begin{aligned} \epsilon_{tot} &= \epsilon_{trans} + \epsilon_{rot} + \epsilon_{vib} + \epsilon_{elec} \\ q_{tot} &= q_{trans}q_{rot}q_{vib}q_{elec} \\ H_{tot} &= H_{trans} + H_{rot} + H_{vib} + H_{elec} \\ S_{tot} &= S_{trans} + S_{rot} + S_{vib} + S_{elec}. \end{aligned} \tag{2.39}$$

In principle, for each of the partition functions the sum $\sum_j e^{-\beta\epsilon_j}$ over the allowed quantum states runs to infinity[19]. However, since the energies become larger and the weight of the individual states exponentially decrease, only a finite number of states can in practice contribute to q.

[18]This hold true if the coupling among these motions can be neglected, i.e. if the separation between the vibrational and electronic motions is valid (the Born-Oppenheimer approximation) and the Coriolis forces [10] arising from the coupling of vibrational and rotational modes are very small.

[19]There are infinite quantum levels associated to the solutions of the Schrödinger equation.

Various contributions to the partition function

The model for determining the energy levels associated to the translational motion of a molecule is the particle in a "box" characterized by zero potential inside (the non-interacting particle approximation) and infinite outside (isolated system). The solution of the Schrödinger equation of such a system are stationary waves with energy levels very close each other [10] and the summation in the partition function can be replaced by an integral which gives

$$q_{trans} = \left(\frac{2\pi M k_B T}{h^2}\right)^{3/2} V \tag{2.40}$$

in which the only molecular parameter is the total mass *M*.

In the rigid rotor approximation, the rotational energy levels of a diatomic molecule result to be equal to

$$\epsilon_{rot} = J(J+1)\frac{h^2}{8\pi I} \qquad (J = 0, 1, 2, ...) \tag{2.41}$$

where J is the integer rotational quantum number and I is the inertia moment of the molecule. For a polyatomic molecule, I is a tensor [25] and the rotational energy levels cannot be written in a simple form. Nevertheless, a good approximation of the rotational partition function takes the form

$$q_{rot} = \frac{\sqrt{\pi}}{\sigma}\left(\frac{8\pi^2 k_B T}{h^2}\right)^{3/2}\sqrt{I_1 I_2 I_3} \tag{2.42}$$

where I_1, I_2 and I_3 are the principal values of the inertia tensor of the molecule and σ is the order of the rotational subgroup in the molecular symmetry point group. Thus, determining the rotational partition function requires only information about the atomic masses and molecular geometry.

The solution of the Schrödinger equation for a one-dimensional harmonic oscillator, leads to the energy levels

$$\epsilon_{vib} = \left(n + \frac{1}{2}\right) h\nu \tag{2.43}$$

where n is the quantum number running from zero to infinity and ν is the vibrational

frequency given in terms of the force constant k and reduced mass μ (cf. Sect. 2.2.1)

$$\nu = \frac{1}{2\pi}\sqrt{\frac{k}{\mu}}. \tag{2.44}$$

The vibrational energy levels compare to the product $k_B T$ and the summation determining the corresponding vibrational partition function cannot be transformed into an integral. However, in the assumption that the energy levels are regularly spaced the infinite summation of q_{vib} for the single mode of frequency v can be written in the closed form

$$q_{vib}(v) = \frac{e^{-\frac{h\nu}{2k_B T}}}{1 - e^{-\frac{h\nu}{k_B T}}} \tag{2.45}$$

which shows that for a molecular system, only the vibrational frequencies are needed in order to calculate the vibrational partition function. In the case of a polyatomic system the $3N$-dimensional Schrödinger equation decouples into $3N$ one-dimensional (harmonic) oscillator equations where the force constant k is replaced by the $3N \times 3N$ force constant matrix (cf. Sect. 2.2.1) and the total vibrational partition function can be expressed as a product of partition functions[20] (2.45)

$$q_{vib} = \prod_{i=1}^{3N-6(5)} q_{vib}(v_i) = \prod_{i=1}^{3N-6(5)} \frac{e^{-\frac{h\nu_i}{2k_B T}}}{1 - e^{-\frac{h\nu_i}{k_B T}}}. \tag{2.46}$$

Notice, that in the case of transition states, the imaginary vibrational frequency[21] is omitted in the evaluation of q_{vib}.

The electronic partition function involves the sum over the electronic quantum states which are solutions of the Schrödinger equation. However, because the energy difference between ground and excited states are normally much larger than $k_B T$, only the first term in the summation of q_{elec} is considered. Furthermore, because the ground state energy is usually referred as the zero point energy of the system, the electronic partition function reduces to the degeneracy of the electronic energy levels.

The basic thermodynamic functions used in this work have been derived by applying the equations reported in Table 2.1 [24].

[20] Of course, the energy contributions due to the translational motion (three) and to the rotational motion (three or two for diatomic molecules) belonging to the solutions of the *3N* one-dimensional oscillator equations should be counted out.

[21] These corresponds to the frequency of the vibration along the eigenvector with negative force constant (cf. Sect. 2.2.1).

$$
\begin{array}{rcl}
H_{trans} & = & \frac{5}{2}RT \\
S_{trans} & = & \frac{5}{2}R + Rln\left(\frac{V}{N_A}\left(\frac{2\pi M k_B T}{h^2}\right)^{3/2}\right) \\
H_{rot} & = & \frac{3}{2}RT \\
S_{rot} & = & \frac{1}{2}R\left[3 + ln\left(\frac{\sqrt{\pi}}{\sigma}\left(\frac{8\pi^2 k_B T}{h^2}\right)^{3/2}\right)\sqrt{I_1 I_2 I_3}\right] \\
H_{vib} & = & R\sum_{i=1}^{3N-6(5)}\left(\frac{h\nu_i}{2k_B} + \frac{h\nu_i}{k_B}\frac{1}{e^{-\frac{h\nu_i}{k_B T}}-1}\right) \\
S_{vib} & = & R\sum_{i=1}^{3N-6(5)}\left(\frac{h\nu_i}{k_B}\frac{1}{e^{-\frac{h\nu_i}{k_B T}}-1} - ln\left(1 - e^{\frac{h\nu_i}{k_B T}}\right)\right) \\
H_{elec} & = & 0 \\
S_{elec} & = & Rln(g)
\end{array}
$$

Table 2.1: Some basic thermodynamic functions which can be derived by the knowledge of the molecular partition function. N_{Av} is the Avogadro constant (6.02214×10^{23} mol^{-1}); k_B is the Boltzmann constant (1.38066×10^{-23} J K^{-1} mol^{-1}); $R = N_{Av}k_B$ is the gas constant (8.31451 J K^{-1}mol^{-1}); h is the Plank constant (6.62608×10^{-34} J s); S_{elec} is evaluated in terms of the degeneracy of the found electronic state, g.

2.3.2 The transition state theory; Reaction rates for chemical reactions

Let us consider an assembly of N_A molecules in the state A and N_B molecules in the state B in dynamical equilibrium

$$A \rightleftharpoons B$$

From the meaning of the partition function the *equilibrium constant* between the two species can be expressed as the ratio between the number of molecules in each state, namely

$$\frac{N_B}{N_A} = \frac{q_B}{q_A}e^{-\frac{\Delta E}{k_B T}} \tag{2.47}$$

where $\Delta E = E_B - E_A$ is the energy difference between the two states[22]. This statement holds also for a more general type of equilibrium like

$$aA + bB \rightleftharpoons cC + dD$$

[22]Notice, that the energies of both states should be measured from the same level, say the lowest one.

for which the constant K_N can be written as

$$K_N = \frac{N_C^c \, N_D^d}{N_A^a \, N_B^B} = \frac{q_C^c \, q_D^d}{q_A^a \, q_B^b} e^{-\frac{\triangle E}{k_B T}} \tag{2.48}$$

which shows that another important quantity in evaluating the reactivity of chemical species can be derived from the knowledge of the partition function of the reactants and the products, namely the form of the potential energy surface in the corresponding regions (cf. Sect. 2.2.1). Furthermore, the Liouville theorem [22] states that a system with an equilibrium distribution in one part of the phase space evolves into a system with an equilibrium distribution in the other parts of the phase space and it can be expressed as

$$\frac{\partial \rho}{\partial q_i} = \frac{\partial \rho}{\partial E} \frac{\partial E}{\partial q_i} = 0 \tag{2.49}$$

$$\frac{\partial \rho}{\partial p_i} = \frac{\partial \rho}{\partial E} \frac{\partial E}{\partial p_i} = 0 \tag{2.50}$$

where ρ is the classical density of states in the phase space with generalized coordinates and momenta $\{q_1, q_2, ..., q_f, p_1, p_2, ...p_f\}$. Thus, for a chemical process, once one imposes the condition of equilibrium between reactants, the *transition-state equilibrium*

$$A + B \rightleftharpoons (AB)^{\ddagger}$$

is a classical consequence of the Liouville theorem and the general equation (2.48) can be used to determine the number of particles in the state $(AB)^{\ddagger}$ [26]. The *transition-state theory* (TST) is directed to the calculation of the *one-way rate constant* for chemical reactions at equilibrium and makes use of this last statement[23].

The basic equation of TST for calculating the rate constant for a general chemical equation of the form

$$aA + bB \rightleftharpoons (AB)^{\ddagger} \rightarrow Products$$

is the Eyring equation [27]

$$k_r = \frac{k_B T}{h} \frac{q^{\ddagger}}{q_A^a q_B^b} e^{-\frac{E^{\ddagger}}{RT}} \tag{2.51}$$

[23]Indeed, the TST makes a furthrer assumption, which states that reactive trajectories originated at reactants passing through the surface dividing reactants and products (i.e. the transition state) in the products direction do not recross the surface before being thermalized in a product state. This is often called *quasi-equilibrium* assumption or *dynamical bottleneck* assumption. Of course, TST breaks down whenever any recrossing occours.

where k_B and h are the usual Boltzmann and Plank constants, respectively and q_A, q_B and $q^\ddagger$ indicate the the partition functions of the reactants and the transition state. There are several ways to derive the eq. (2.51), in connection with the kinetic theory of gases or from purely thermodynamic arguments. In this section this second approach will be briefly outlined[24] [28].

For a bimolecular reaction

$$XY + Z \rightleftharpoons [X \cdots Y \cdots Z]^\ddagger \rightarrow X + YX \tag{2.52}$$

the overall rate at which the transition state decomposes to the products can be expressed as the product of its concentration $c^\ddagger$ and the frequency with which it decomposes $\nu^\ddagger$, namely

$$Rate = c^\ddagger \nu^\ddagger. \tag{2.53}$$

Furthermore, by the assumption that reactants and TS are in a pre-equilibrium we have

$$c^\ddagger = K^\ddagger_{eq} c_{XY} c_Z.$$

Thus, one needs to calculate $\nu^\ddagger$ in order to obtain the rate constant of the chemical reaction. Of course, $\nu^\ddagger$ depends of the nature of the TS which can be actually considered as a quantum chemical metastable state with intrinsic energy. However, the metastability of TS is associated with to its vibrational mode along the reaction coordinate and it can be assumed that its properties may be derived by a modified total partition function $q_\ddagger$ in which the motion along the reaction coordinate s is treated separately in q_s. Therefore, eq. (2.48) can be written as

$$K^\ddagger_{eq} = \frac{q_\ddagger q_s}{q_{XY} q_Z} e^{-\frac{E^\ddagger}{RT}} \tag{2.54}$$

where only $q_\ddagger$ and q_s need to be derived. For this purpose, let us consider the three diagrams of Fig. (2.1) for the hypothetical evolution of a stable intermediate to a transition state through the decreasing of its fundamental vibration along the reaction coordinate. Referring to Fig. 2.1 a), equation (2.54) can be written as

$$K_N = \frac{q'_i q_s}{q_{XY} q_Z} e^{-\frac{\Delta E}{RT}} \tag{2.55}$$

[24]It is worth to emphasize, that all ways to derive the Eyring equation are based on the same quasi-equilibrium assumption and are strickly related.

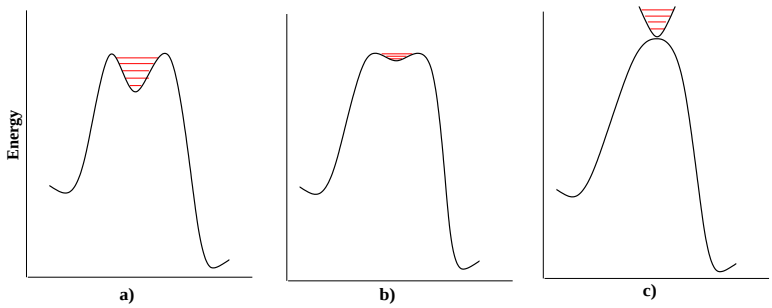

Figure 2.1: Modified PES diagrams for: a) stable intermediate; b)unstable intermediate; c) TS.

where q_i' is the partition function of the intermediate $[X \cdots Y \cdots Z]^{\ddagger}$ in which the contribution corresponding to its vibrational quantized motion along the reaction coordinate s has been separated in q_s expressed as

$$q_s = \frac{1}{1 - e^{-\frac{h\nu}{k_B T}}}. \tag{2.56}$$

Figure 2.1a) and 2.1b) are two examples of intermediate species characterized by smaller and smaller curvature. Correspondingly the two species have smaller force constant and more closely spaced vibrational levels. In the case of Fig. 2.1c) the system is not subjected to restoring force and leads to a complete reaction. Thus, it is now justified to assume that $h\nu \ll k_B T$ and the exponential expansion (2.56) becomes

$$q_s \cong \frac{1}{1 - \left(1 - \frac{h\nu^{\ddagger}}{k_B T} + ...\right)} = \frac{k_B T}{h\nu^{\ddagger}} \tag{2.57}$$

where $\nu^{\ddagger}$ corresponds to the vibration of the TS along the reaction coordinate. By substituting eq. (2.57) into (2.54) one obtains

$$K^{\ddagger} = \frac{q_{\ddagger}\left(\frac{k_B T}{h\nu^{\ddagger}}\right)}{q_{XY} q_Z} e^{-\frac{E^{\ddagger}}{RT}} \tag{2.58}$$

thus

$$\frac{c^{\ddagger}}{c_{XY} c_Z} = \frac{q_{\ddagger}\left(\frac{k_B T}{h\nu^{\ddagger}}\right)}{q_{XY} q_Z} e^{-\frac{E^{\ddagger}}{RT}} \tag{2.59}$$

and the rate constant of the reaction (2.53) results

$$Rate = k_r c_{XY} c_Z = \nu^{\ddagger} c^{\ddagger} = c_{XY} c_Z \frac{k_B T}{h} \frac{q_{\ddagger}}{q_{XY} q_Z} e^{-\frac{E^{\ddagger}}{RT}} \tag{2.60}$$

from which the equation (2.51) follows. Notice, that in this derivation of the Eyring equation all molecular motions but one are treated quantum mechanically.

The equilibrium constant (2.48) can be easily expressed in terms of partial pressure and can be further related to the classical thermodynamic Gibbs free energy function as

$$\Delta G^{\ddagger} = -RTlnK_P^{\ddagger} \tag{2.61}$$

from which the rate constant of the bimolecular reaction (2.52) can be written as

$$k_r = \frac{k_B T}{h} RT e^{-\frac{\Delta G^{\ddagger}}{RT}} \tag{2.62}$$

or, being $\Delta G^{\ddagger} = \Delta H^{\ddagger} - T\Delta S^{\ddagger}$

$$k_r = \frac{k_B T}{h} RT e^{\frac{\Delta S^{\ddagger}}{R}} e^{-\frac{\Delta H^{\ddagger}}{RT}} \tag{2.63}$$

which has an Arrehnius like form and become very helpful in connecting kinetics with thermodynamics for studying chemical reactions. In fact, in the approximation of an ideal gas, the activation energy [29] E_{act} for a bimolecular reaction can be expressed as

$$E_{act} = \Delta H^{\ddagger} + 2RT \tag{2.64}$$

and eq. (2.63) becomes

$$k_r = e^2 \frac{k_B T}{h} RT e^{\frac{\Delta S}{R}} e^{-\frac{E_{act}}{RT}} \tag{2.65}$$

which can be also written as

$$k_r = A e^{-\frac{E_{act}}{RT}} \tag{2.66}$$

where the pre-exponential factor A is a function of the entropy of the system only. The classical Arrehnius equation has exactly the form of (2.66) in which A is an empirical pre-exponential factor and is usually interpreted as a measure of the rate at which collisions between molecules occurs irrespective of their energy while the exponential gives the fraction of collisions with enough energy for the reaction to occur. In TST, A is defined by the entropy of the system thus, collisions between molecules can be

interpreted by entropy changes during the reaction.

2.4 Solving the Schrödinger equation

A quantum mechanical approach to chemical problems necessarily requires the solution of the Schrödinger equation. The ideal situation would be to obtain an a priori prediction of the structure, properties and reactivity of molecules formed by atoms of the whole periodic table and to derive an interpretation of the above mentioned results in terms of chemical concepts.

In the contest of wave function based methods, the impressive improvement of computer power in the last few years combined with the development of very efficient computational algorithms allow nowadays very sophisticate and accurate calculations of molecular properties by means of the post Hartree-Fock methods such as configuration interaction and coupled clusters methods. However, their scaling with the number of active electrons is very high and applications to many chemically interesting systems remain prohibitive. Less sophisticated conventional models such as the Hartree-Fock method or low-order many body perturbation technique like MP2 work very well for closed shell molecules formed by main group atoms. Nevertheless, they often provide a very poor description of open shell systems and chemical reaction energetics so that highly correlated methods are needed. In this respect, methods which have roots in the density functional (DF) theory are very promising since they are able to include large amount of correlation energy in a formalism which requires essentially similar resources as the HF method.

In this section a brief outline of the most used quantum chemical methods is presented. Starting from the Hartree-Fock model it will be examined the way how to improve the accuracy in describing molecular systems. Also, general considerations will be presented about the criteria adopted in the choice of the basis set. A general view of the theory of pseudopotentials will be presented since these methods have been largely used in the present study. The section will end with a presentation of the density functional theory (DFT) and its most recent developments. DFT is widely accepted as one of the most powerful and reliable method for treating chemical systems of relatively large size as those studied in this work.

2.4.1 The Hartree-Fock method

Within the Born-Oppenheimer approximation the Hartree-Fock method replaces the complicated many-electron problem defined by the Hamiltonian (2.11) by a set of one-electron non-linear problems in which the electron-electron repulsion is treated in an averaged way. The method deals with single Slater determinants wave functions $|\Psi_{HF}>$ constructed from molecular spin orbitals of the form

$$\chi_i(\mathbf{x}) = \psi(\mathbf{r})\eta(\omega) \tag{2.67}$$

and ensure that the best set of spin orbitals which variationally minimize the total energy

$$E_{HF} =< \Psi_{HF}|\hat{H}_e|\Psi_{HF} > \tag{2.68}$$

of the system are also eigenfunctions of the one-electron *HF integro-differential eigenvalue equations* [11, 30]

$$\hat{F}(1)\chi_j(1) = \epsilon_j\chi(1) \qquad j = 1, 2, ..., \infty. \tag{2.69}$$

The one-particle *Fock* operator $\hat{F}(1)$ is the sum of the *core-Hamiltonia*n operator

$$\hat{h}(1) = -\frac{1}{2}\nabla_i^2 - \sum_{A=1}^{nucl}\frac{Z_A}{r_{iA}} \tag{2.70}$$

and the *effective one-electron potential* operator (the Hartree-Fock potential)

$$\hat{v}(1)^{HF} = \hat{J}(1) - \hat{K}_j(1) \tag{2.71}$$

where $\hat{J}(1)$ and $\hat{K}(1)$ are the *Coulomb* and the *exchange* operators, respectively and represent the average electron-electron interaction. In details, $\hat{J}(1)$ replaces the exact instantaneous interaction governed by the $\hat{V}_{ee}$ operator (cf. eqs. 2.9 and 2.10) with the sum of one-electron integral operators $\hat{J}_j(1)$

$$\hat{J}(1) = \sum_{j\neq i}\hat{J}_j(1) = \sum_{j\neq i}\int d\mathbf{x}_2\chi_j^*(\mathbf{x}_2)\chi_j(\mathbf{x}_2)r_{12}^{-1} \tag{2.72}$$

which represent the average *local*[25] potential at $\mathbf{x}_1$ arising from the charge distribution[26] $|\chi_j(\mathbf{x}_2)|^2$ of an electron in χ_j. By summing over all $j \neq i$ one obtains the total average potential acting on the electron χ_i arising from the charge distribution of all the other *N-1* electrons in the other spin-orbitals. The exchange operator is a *non-local* operator with form

$$\hat{K}_j(1)\chi_i(\mathbf{x}_1) = \left[\int d\mathbf{x}_2 \chi_j^*(\mathbf{x}_2) r_{12}^{-1} \chi_i(\mathbf{x}_2)\right] \chi_j(\mathbf{x}_1) \tag{2.73}$$

and does not have a classical counterpart[27]. Its effect on the spin-orbital $\chi_i(\mathbf{x}_1)$ is to exchange the variables $\mathbf{x}_1$ and $\mathbf{x}_2$ in the χ_i and χ_j factors and integrate over $\mathbf{x}_2$ by not including the factor $\chi_j(\mathbf{x}_1)$ [30]. This can be better expressed by introducing the permutation operator P_{12} which interchange the electron 1 and 2 so that

$$\hat{K}_j(1)\chi_i(\mathbf{x}_1) = \left[\int d\mathbf{x}_2 \chi_j^*(\mathbf{x}_2) r_{12}^{-1} P_{12} \chi_j(\mathbf{x}_2)\right] \chi_i(\mathbf{x}_1). \tag{2.74}$$

By defining the HF *independent particle* Hamiltonian $\hat{H}_I$ as the sum of one-particle Fock operators over the electrons

$$\hat{H}_I = \sum_i \hat{F}(i) \tag{2.75}$$

the HF variational energy (2.68) can be calculated as

$$E_{HF} = \sum_i \left\{ \langle\chi_i| \hat{h} |\chi_i\rangle + \frac{1}{2}\sum_j \langle\chi_i| \hat{J}_j |\chi_i\rangle - \frac{1}{2}\sum_j \langle\chi_i| \hat{K}_j |\chi_i\rangle \right\} = \sum_i \langle\chi_i| \hat{h} + \frac{1}{2}(\hat{J} - \hat{K}) |\chi_i\rangle \tag{2.76}$$

where the correction factor $\frac{1}{2}$ in front of the algebraic sum of the Coulomb and exchange terms accounts for the double counting of the electron-electron interaction in $\hat{H}_I$ [11].

The spin-orbital solutions of the HF canonical equations (2.69) define the best ground state single configuration wave function for antisymmetric fermionic particles

[25] An operator is *local* if its action $\hat{O}f(x) = g(x)$ at a point $x = x'$ is well defined by simply knowing $f(x)$ in a infinitesimally small neighborhood of x': $\hat{O}(x, x')f(x) = \hat{O}(x)\delta(x - x')f(x)$. An operator is said to be *non-local* if its action at a point $x = x'$ is definied ony by knowing $f(x)$ for all x: $\hat{O}f(x) = \int dx' \hat{O}(x, x')f(x')$, where $\delta(x)$ is the Dirac delta function [31, 11, 9].

[26] The charge distribution is here expressed in electrons per unit volume.

[27] It arises from the antisimmetry nature of the wave function.

which can be written as Slater determinant as

$$|^N\Psi_{HF}>=(N!)^{-\frac{1}{2}}det\,|\chi_1(\mathbf{x}_1)\chi_2(\mathbf{x}_2)\chi_3(\mathbf{x}_3)..\chi_N(\mathbf{x}_N)>\,. \tag{2.77}$$

The orbital energy ϵ_k corresponding to each of the χ_k has a direct physical meaning expressed by the Koopmans' theorem which states that $-\epsilon_k$ can be considered, to a first approximation, as the ionization energy I_k of an *N*-electron ground state determinant $|^N\Psi_{HF}>$ obtained by removing an electron from the corresponding spin-orbital χ_k[28] [11]. Furthermore, the energy difference between an occupied orbital ϵ_k and a *virtual* orbital[29] ϵ_m is a rough estimation of the excitation energy for the electronic transition from the ground state to an excited state in which χ_k is replaced by χ_m [30]. Another important property of the HF single determinant wave functions is expressed by the Brillouin's Theorem which states that a singly excited determinant $|\Psi_k^m>$ will not directly interact with the reference (ground state) HF determinant, i.e. $\langle\Psi_{HF}|\,\hat{H}\,|\Psi_k^m\rangle=0$ [11].

In order to perform actual calculation of the HF wave function the form of the set of spin-orbital basis functions have to be specified.

The *restricted* HF (RHF) method deals with set of spin-orbitals in which each pairs of electrons in a shell are constrained to share the same spatial function while in the *unrestricted* HF (UHF) method the form of the spin-orbital basis set allows electrons with α and β spin to have different spatial functions. Since in this work we are mostly interested in the unrestricted solutions of HF based equations (the Kohn-Sham equations[30], cf. Sect. 2.4.5) we will here describe the UHF method in more details. For the RHF method, which is a special case of the UHF, and its implications cf. [11].

[28]Koopmans IPs are generally not correct due to reorganization of the orbitals after the ionization and correlation effects.

[29]For a *N*-electron system described by a set of spin-orbitals $\{\chi_i\}_{i=1,2...}$, the minimization of the energy of the determinant $|\chi_1,\chi_2,....\chi_i,\chi_j,...,\chi_N\rangle$ lead to the canonical HF eigenvalue equation for the *N* occupied orbitals $\{\chi_i\}_{i=1,2,...N}$. Once these orbitals are known the Fock operator becomes a well-defined Hermitian operator with a finite set of solutions (eigenfunctions). The first *N* solutions correspond to the lowest energy occupied canonical HF orbitals in the ground state wave function while the remaining are defined as virtual or unoccupied spin-orbitals with higher energy.

[30]We will see that the HF theory is a generalization of the density functional theory in which no correlation is considered and the exchange energy is recovered by the functional form of the exchange operator (2.73).

For a given set of unrestricted spin-orbital basis functions

$$\chi_j(\mathrm{x}) = \begin{cases} \psi_j^{\alpha}(\mathrm{r})\alpha(\omega) \\ \psi_j^{\beta}(\mathrm{r})\beta(\omega) \end{cases} \tag{2.78}$$

the canonical HF equations (2.69) transform [11] into two set of spatial integro-differential equations

$$\hat{F}^{\alpha}(1)\psi_j^{\alpha}(1) = \epsilon_j^{\alpha}\psi_j^{\alpha}(1) \tag{2.79}$$

$$\hat{F}^{\beta}(1)\psi_j^{\beta}(1) = \epsilon_j^{\beta}\psi_j^{\beta}(1) \tag{2.80}$$

where $\hat{F}^{\alpha}$ and $\hat{F}^{\beta}$ are the spatial one-particle Fock operators for α and β spin electrons, respectively defined as

$$\hat{F}^{\alpha}(1) = \sum_i^{N^{\alpha}} \hat{h}_i^{\alpha}(1) + \sum_i^{N^{\alpha}} \left[\hat{J}_i^{\alpha}(1) - \hat{K}_i^{\alpha}(1)\right] + \sum_i^{N^{\beta}} \hat{J}_i^{\beta}(1) \tag{2.81}$$

$$\hat{F}^{\beta}(1) = \sum_i^{N^{\beta}} \hat{h}_i^{\beta}(1) + \sum_i^{N^{\beta}} \left[\hat{J}_i^{\beta}(1) - \hat{K}_i^{\beta}(1)\right] + \sum_i^{N^{\alpha}} \hat{J}_i^{\alpha}(1). \tag{2.82}$$

The last terms in both equations arise from the effective interactions between electrons of different spin and show that an α electron would have a Coulomb and exchange interaction with all the other α electrons but only a Coulomb interaction with β electrons. The total energy of the system is expressed as

$$E_{UHF} = \sum_i^{N^{\alpha}} h_{ii}^{\alpha} + \sum_i^{N^{\beta}} h_{ii}^{\beta} + \frac{1}{2}\sum_i^{N^{\alpha}}\sum_j^{N^{\alpha}} \left(J_{ij}^{\alpha\alpha} - K_{ij}^{\alpha\alpha}\right) + \frac{1}{2}\sum_i^{N^{\beta}}\sum_j^{N^{\beta}} \left(J_{ij}^{\beta\beta} - K_{ij}^{\beta\beta}\right) + \sum_i^{N^{\alpha}}\sum_j^{N^{\beta}} J_{ij}^{\alpha\beta} \tag{2.83}$$

where h_{ii}^{α} and h_{ii}^{β} are the (integral) expectation values of the one-electron operator $\hat{h}(1)$ for spin α and β, respectively; $J_{ij}^{\alpha\alpha}$, $J_{ij}^{\beta\beta}$, $K_{ij}^{\alpha\alpha}$ and $K_{ij}^{\beta\beta}$ are the expectation value of the Coulomb and exchange interactions between electrons of the same spin; and $J_{ij}^{\alpha\beta} = J_{ij}^{\beta\alpha}$ are the expectation values of the Coulomb interaction of an electron in ψ_i^{α} with one in ψ_j^{β} [11].

In order to transform the spatial integro-differential UHF equations into a set of algebraic equations which can be handled computationally one introduces a ***finite*** set of atomic atomic basis functions $\{\phi_\mu | \mu = 1, 2, ...K\}$ (cf. Sect. 2.4.2) and expands the unrestricted molecular orbitals ψ_i^{α} and ψ_i^{β} as a linear combination of ϕ_μ functions

(MO-LCAO) as

$$\psi_i^\alpha = \sum_\mu^K C_{\mu i}^\alpha \phi_\mu \qquad i = 1, 2, ..., K \tag{2.84}$$

$$\psi_i^\beta = \sum_\mu^K C_{\mu i}^\beta \phi_\mu \qquad i = 1, 2, ..., K. \tag{2.85}$$

Substituting the expansions (2.84) and (2.85) into the eigenvalue equations (2.79) and (2.80) and integrating one obtains

$$\sum_\nu C_{\nu j}^\alpha F_{\mu\nu}^\alpha = \epsilon_j^\alpha \sum_\nu S_{\mu\nu} C_{\nu j}^\alpha \qquad j = 1, 2, ...K \tag{2.86}$$

$$\sum_\nu C_{\nu j}^\beta F_{\mu\nu}^\beta = \epsilon_j^\beta \sum_\nu S_{\mu\nu} C_{\nu j}^\beta \qquad j = 1, 2, ...K \tag{2.87}$$

or, in matrix notation

$$\mathbf{F}^\alpha \mathbf{C}^\alpha = \mathbf{S}\mathbf{C}^\alpha \epsilon^\alpha \tag{2.88}$$

$$\mathbf{F}^\beta \mathbf{C}^\beta = \mathbf{S}\mathbf{C}^\beta \epsilon^\beta. \tag{2.89}$$

These are the coupled *Pople-Nesbet eigenvalue equations* which have to be solved simultaneously since the *Fock-matrices* $\mathbf{F}^\alpha$ and $\mathbf{F}^\beta$ both depend on matrices of the expansion coefficients for ψ_i^α and ψ_i^β, $\mathbf{C}^\alpha$ and $\mathbf{C}^\beta$[31]. ϵ^α and ϵ^β are the diagonal matrices of the orbital energies. The eigenvectors $\mathbf{C}^\alpha$ and $\mathbf{C}^\beta$ form an orthonormal set and are also irreducible representations of the symmetry group of the multielectron system [11]. The Fock-matrices can be expressed in terms of the matrix elements of the unrestricted density matrices $\mathbf{P}^\alpha$ and $\mathbf{P}^\beta$

$$P_{\mu\nu}^\alpha = \sum_j^{N^\alpha} C_{\mu j}^\alpha (C_{\nu j}^\alpha)^* \tag{2.90}$$

$$P_{\mu\nu}^\beta = \sum_j^{N^\beta} C_{\mu j}^\beta (C_{\nu j}^\beta)^* \tag{2.91}$$

[31]This is due the form of the spatial Fock operators for α and β spin electrons (cf. eq. 2.81 and 2.82) which contain mixed Coulomb terms (cf. also the UHF energy equation 2.83).

and take the form

$$F^{\alpha}_{\mu\nu} = h_{\mu\nu} + \sum_{\lambda}\sum_{\sigma} P^{T}_{\lambda\sigma}(\phi_\mu\phi_\nu|\phi_\lambda\phi_\sigma) - P^{\alpha}_{\lambda\sigma}(\phi_\mu\phi_\nu|\phi_\sigma\phi_\lambda) \quad (2.92)$$

$$F^{\alpha}_{\mu\nu} = h_{\mu\nu} + \sum_{\lambda}\sum_{\sigma} P^{T}_{\lambda\sigma}(\phi_\mu\phi_\nu|\phi_\lambda\phi_\sigma) - P^{\beta}_{\lambda\sigma}(\phi_\mu\phi_\nu|\phi_\sigma\phi_\lambda) \quad (2.93)$$

where $P^{T}_{\lambda\sigma}$ is the matrix element of the total charge density:

$$P^{T}_{\lambda\sigma} = P^{\alpha}_{\lambda\sigma} + P^{\beta}_{\lambda\sigma} \quad (2.94)$$

Because of the functional dependence of the Fock-matrices from the total charge density and thus from the MOs expansion coefficients (cf. eq. (2.84) and (2.85)) the coupled Pople-Nesbet equations must be solved by an iterative procedure, namely the Self Consistent Field (SCF) method. Given a first guess of the charge density matrices $\mathbf{P}^{\alpha}$ and $\mathbf{P}^{\beta}$ one can build up the $\mathbf{F}^{\alpha}$ and $\mathbf{F}^{\beta}$ Fock-matrices[32] and solve the generalized problems (2.88) and (2.89) for $\mathbf{C}^{\alpha}$ and $\mathbf{C}^{\beta}$, form a new approximation to $\mathbf{P}^{\alpha}$ and $\mathbf{P}^{\beta}$ and repeat the procedure until convergence is reached, i.e. until the density matrices at the $(i-1)$th iteration coincide to a prescribed accuracy with those of the ith iteration. Being $N = N^{\alpha}, N^{\beta}$ the number of electrons, for a given basis set of dimension K with $K > N$ the SCF solutions of the coupled Pople-Nesbet equations lead to a set of N^{α} and N^{β} occupied molecular orbitals and to a remaining set of $K - N^{\alpha}$ or $K - N^{\beta}$ unoccupied (virtual) orbitals with higher energy. These orbitals are often used in describing excited states of neutral molecule (cf. Sect. 2.4.4).

The lowest energy molecular orbitals which are solutions of the Pople-Nesbet equations define the best ground state single configuration unrestricted wave function

[32]This is actually the computationally most demanding part of the method, since it requires the calculation of the two electron integrals of the equations (2.86) and (2.87) and their storage in a memory unit. Each integral is a floating point number associated with four indices indicating the basis functions involved in its calculation $(\lambda, \sigma, \mu, \nu)$ and the storage of a double precision floating point number requires 64 bits or 8 bytes. Since in the HF method the number of computed integrals increase proportionally to the fourth power of the number of basis functions, the hard storage memory requirement can be estimates as $\frac{1}{8}M^4 * 8$ bytes, where *M* indicates the size of the basis set. Thus, for a set of ~ 300 basis functions, ~ 64 Gbytes of disk space is needed. Furthermore, these integrals are needed at each SCF iteration which means additional I/O effort and make the disk based SCF methods definitely not practicable. Due to the improvement of the speed of modern electronic computers they have been replaced by the most efficient *Direct SCF methods* in which the integrals are calculated from scratch at each iteration [32].

which can be expressed as an unrestricted Slater determinant of the form

$$\begin{aligned} |\Psi_{UHF}> &= [(N^\alpha + N^\beta)!]^{-\frac{1}{2}} det\, |\psi_1^\alpha(1)\alpha(1)\psi_2^\alpha(2)\alpha(2)...\psi_{N^\alpha}^\alpha(N^\alpha)\alpha(N^\alpha) \\ &\quad \psi_1^\beta(N^\alpha+1)\beta(N^\alpha+1)\psi_1^\beta(N^\alpha+2)\beta(N^\alpha+2)... \\ &\quad \psi_{N^\beta}^\beta(N^\alpha+N^\beta)\beta(N^\alpha+N^\beta)> . \end{aligned} \tag{2.95}$$

It is important to recall that $|\Psi_{UHF}>$ solutions are not eigenfunctions of the $\hat{S}^2$ operator and therefore do not correspond to a pure spin state. Let $|1>$, $|2>$, $|3>$, etc. represent pure singlet doublet, triplet ecc. spin states. It can be demonstrated [32] that the UHF wave function corresponding to a given electronic state $|^M\Psi_{UHF}>$ of multiplicity[33] M of the system, can be written as

$$|^1\Psi> = a_1^1|1> + a_1^3|3> + a_1^5|5> + ... \tag{2.96}$$

$$|^2\Psi> = a_2^2|2> + a_2^4|4> + a_2^6|6> + ... \tag{2.97}$$

$$|^3\Psi> = a_3^3|3> + a_3^5|5> + a_3^7|7> + ... \tag{2.98}$$

which shows that the $|\Psi_{UHF}>$ is in general *contaminated* by higher multiplicity terms of the same parity [11]. Moreover, since the pure spin restricted open shell determinants $|2>$, $|3>$, $|4>$, $|5>$ ecc. are eigenfunctions of the $\hat{S}^2$ spin operator, $|\Psi_{UHF}>$ can be equivalently expressed as multideterminantal expansion in terms of restricted open shell Hartree-Fock (ROHF) determinants. In this sense, $|\Psi_{UHF}>$ accounts, to some extent, correlation effects between electrons with different spin [33]. According to the variational principle this last property guarantees that the energy of the UHF wave function is lower than or equal to the RHF energy. However, spin contamination introduces higher energy spin terms and as their relative weight in the UHF wave function increase[34] the total energy of the system increases as well affecting the true form of the PES [32].

The spin contaminant states can be removed from the UHF wave function by projection technique [34] and the energy of the projected unrestricted wave function (PUHF) is usually lower than that of the contaminated one. Nevertheless, this energy

[33]The word multiplicity comes from spettroscopy and correspond to the number of spectroscopic levels produced by a specific electronic configuration (*term*). It is calculated as $2S_z + 1$ where S_z represent the total spin of the system by $S_z = s_{z1} + s_{z2} + ... + s_{zn}$ and s_{zn} is the spin quantum number associated to the projection of the nth unpaired electron along the z axis [10].

[34]The degree of mixing of higer-order spin contaminant can be determined by the energy difference between the pure states in the multi-determinantal expansion of the true UHF wave function: the smaller is this energy difference, the stronger is the contamination.

is no longer variational and the artificial distortion of the PUHF energy surface is even more pronounced than that of UHF. The amount of spin contamination is given by the expectation value of the $\hat{S}^2$ operator which is usually calculated as

$$< \hat{S}^2 >_{UHF} = < \hat{S}^2 >_{exact} + N^{\beta} - \sum_{i}^{N} \sum_{j}^{N} \left| S_{ij}^{\alpha\beta} \right|^2 \tag{2.99}$$

where $< \hat{S}^2 >_{exact} = S_z(S_z + 1)$ and $S_{ij}^{\alpha\beta}$ is the overlap between all pairs of α and β spin orbitals.

In the case of $N^{\alpha} = N^{\beta}$, the Pople-Nesbet equations can have two independent solutions: the restricted solution in which $\mathbf{P}^{\alpha} = \mathbf{P}^{\beta}$ and the unrestricted solution in which the two charge densities are different. Of course, the restricted solution always exists and in the case of molecular systems close to their equilibrium geometry it is usually accepted as the best one. However, if high-order spin contamination of the wave function plays an important role in computing the variational energy, the restricted solution is not longer correct. This would be the case of the dissociation of a closed shell molecule into two open shell fragments or of a transition states structure in a chemical reaction, in which the unrestricted solution is of significant importance[35] [11].

2.4.2 Basis sets

As discussed in the previous section, the basic approach of the *ab-initio* methods is related with the *Hartree-Fock* approximation which aims at replacing the complex many-electron problem by a series of one-electron problems. In addition the spin orbitals may be expanded as a (finite) linear combination of basis functions (LCAO approximation). The form of the adopted basis function and the size of the basis set have large effect in both the computational costs and the accuracy achieved.

The most simple chemical system for which analytical solutions of the Schrödinger equation are available is the hydrogen atom[36]. The corresponding hydrogenic orbitals

[35] In most of the available computational chemistry codes, the first guess of the density charge matrices P^{α} and P^{β} is usually obtained from low-level computations (i.e. extended-Huckel or semi-empirical methods) of the molecular orbitals or from the sum of the single atomic densities and the HF unrestricted solutions are obtained during the SCF iterations. However, it is not surprising that for highly symmetric closed-shell molecules this procedure lead to the "wrong" restricted HF solution which would affect the final energy value. In these cases one of the best way to overcome the problem would be to run a single-point energy calculation of the corresponding open-shell positive ion and use the resulting molecular orbitals as first guess for computing the starting point for the closed-shell molecule.

[36] The corresponding wave equation has the form

have exponential radial dependence and the simplest set of functions with the same behavior are the *Slater type orbitals* [35] (STO) which have the functional form[37]

$$\chi_{\zeta,n,l,m}(r,\theta,\varphi) = N\mathrm{Y}_{l,m}(\theta,\varphi)r^{n-1}e^{-\zeta r} \tag{2.100}$$

where *n*, *l* and *m* are the quantum numbers[38], $\mathrm{Y}_{l,m}(\theta,\varphi)$ are the usual spherical harmonic functions [9] and *N* is a normalization constant. The exponential form of the Slater type orbitals ensure rapid convergence in the LCAO expansion and the proper description of the cusp of the electronic wave function at the nuclei and its exponential tail for $r \to \infty$ as well. Unfortunately, no efficient methods have been developed for calculating STO many-center two-electron integrals [11] required by the *ab-initio* methods and with the exception of highly symmetric systems such as atoms and diatomic molecules for which high accuracy is required, they have been abandoned altogether in favor of the so-called Gaussian-type orbitals (GTOs)[39].

GTOs have the significant advantage to allow for an efficient evaluation of the molecular integrals [36]. Their form in terms of polar and cartesian coordinates can be written as

$$\chi_{\zeta,n,l,m}(r,\theta,\varphi) = N\mathrm{Y}_{l,m}(\theta,\varphi)r^{2n-2-l}e^{-\zeta r^2} \tag{2.101}$$

$$\chi_{\zeta,l_x,l_y,l_z}(x,y,z) = N x^{l_x} y^{l_y} z^{l_z} e^{-\zeta r^2}, \tag{2.102}$$

respectively. In eq. 2.102 the sum of the l_x, l_y and l_z determines the type of orbital ($l_x + l_y + l_z = l = 0, 1, 2, ...$ for $s,\ p, d, ...$). Notice, that although GTOs seems to be equivalent in the two sets of coordinates, the cartesian form include redundant functions. In particular for $l = 2$ one has 6 GTOs corresponding to 5 d functions and an s function. Similarly, for $l = 3$ one has 10 GTOs which correspond to 7 f functions

---

$$\left(-\frac{1}{2}\nabla^2 - \frac{1}{r}\right)\Psi(r) = E\Psi(r)$$

and its (analitical) solutions are the product of the associated Laguerre radial functions $\mathrm{R}_{nl}(\mathrm{r})$ and the spherical harmonic angular functions $\mathrm{Y}_{lm}(\theta,\varphi)$ [9]. They involve exponential radial dependence of the form e^{-r}.

[37]Here, as in the following description of Gaussian type orbitals, it is assumed that the functions are centred at the nulcei.

[38]From the solution of the Schrödinger equation for the hydrogen atom, *n*, *l* and *m* are the sets of quantum numbers associated with the energy levels, the electronic orbital momentum and its component along the principal axis, respectively [7, 10]

[39]STOs basis sets are also used by those semi-empirical methods in which the many-center two-electron integrals are completely neglected.

and a set of p functions. The r^2 dependence of the exponent of the radial part of the GTOs make them less effective than STOs. In addition, GTOs have zero slope at the nucleus. Thus, in order that the GTOs form a suitable basis set their number must be greater than that of STOs.

Classification of basis sets and contraction schemes

In usual molecular calculations performed using GTOs type functions the basic criterion used in selecting the basis set is just its dimension just its dimension. The *minimal* requirement for a basis set is to include a single set of functions for each atomic shell occupied in the atomic ground state. This corresponds to a single *s*-function for hydrogen and helium; two *s* and one set of *p*-functions for the first row of the periodic table ecc. The next improvement in the basis set is the doubling of the number of all the basis functions, leading to the so-called *Double-Zeta* (DZ) basis set. Similarly, one can define the *Triple-Zeta* (TZ) basis set. Because chemical bonds occur between valence electrons only and the core electrons are essentially independent from the chemical environment, an alternative to DZ and TZ basis sets are the so-called *split-valence*[40] basis sets in which the core shells are described by a single set of function while the number of functions for the valence orbitals are doubled or tripled[41]. Higher order valence electrons basis set as QZ (Quadruple-Zeta), 5Z (Quintuple-Zeta) ecc. are also used.

In the composition of the basis sets described so far only functions of the same symmetry of the occupied atomic orbitals have been considered. However, in molecular calculations higher angular momentum functions named *polarization* functions play an important role. They take into account the distortion from spherical symmetry of an atom when placed in a molecular environment and improve the description of the system in a non uniform electric field. Generally speaking, these functions describe the polarization of the charge distribution in the orbitals involved in a chemical bond and are characterized by angular momentum higher than that of the occupied orbitals[42]. Thus, in order to account for the polarization effects in describing, for instance, the very simple H_2 molecule, the hydrogen *s*-orbitals should be augmented by a set of *p*-

[40]These basis sets have been designed by Pople and coworkers [37, 38, 39] and are also usually named Pople style basis sets.

[41]These basis set are normally reported under the acronymous VDZ and VTZ basis sets.

[42]A orbital described by a function with total angular momentum $L = l_x + l_y + l_z$ results polarized by functions corresponding to empty orbitals with angular momentum $L + i$, $i = 1, 2$, *ecc.*

or even *d*-orbital basis functions[43]. For single determinant wave functions the first set of polarization functions is normally sufficient to account for the polarization effects produced by the atomic environment. However, if correlated methods are used (cf. Sect. 2.4.4), then higher angular momentum functions are essential. Further addition of diffuse functions (i.e. functions with a small exponent) to the basis sets allows a better description of long range properties or electron distribution of negatively charged species. A further requirement in choosing basis sets for molecular calculation concern with their "balance". Of course, the best choice would always be to compute molecular systems in which atoms are described by the same kind of basis sets (i.e. DZ, TZ, ecc.) and the same number and order of polarization functions.

Basis sets are usually derived by carrying out variational HF calculations (cf. Sect. 2.4.1) on atoms with the exponents of the functions as variational parameters; the best set of exponents gives the lowest energy value. The exponents for the polarization functions cannot be obtained by atomic single determinant wave function calculations because such functions are, by definition, not occupied in the ground state. They are usually obtained by performing variational calculations on *ad-hoc chosen* molecular systems[44]. In the variational procedure, the exponents of the basis functions can be optimized independently to each other or by imposing some restrictions. In the latter case the optimization would exhibit reduced convergence problems and the resulting basis sets fall in two different classes, namely the *even tempered* basis sets (the ratio between the exponents of the whole set is kept fixed) and *well tempered* basis sets (the exponents are generated by a suitable parametric formula and only the parameters are optimized for each atom)[45] [40, 36].

A disadvantage of working with energy optimized basis sets is that they mostly depend on the shape of the wave function in the region of the inner shell electrons. By minimizing the energy, the basis set functions will be optimal for the core electrons and less suitable for the valence electrons. Thus, in order to have a good description of the valence electrons the basis set size should be increased by diffuse functions. However, because the computational cost increases as the fourth power (or higher) of the number

[43]Of course, the same argument can be applied to all atoms of the periodic chart.

[44]Indeed, they can be alternatively obtained by means of post Hartree-Fock methods (cf. Sect. 2.4.4) in which the wave function is expressed as a linear combination of slater determinants describing also the occupation of virtual orbitals [32].

[45]Both these procedures have been justified by observing that in a list of energy-optimized Gaussian exponents the ratio of successive exponents held constant by approximatively 1/3 (cf. [40] and references therein).

of the employed atomic basis functions this procedure is very inefficient. Nevertheless, for most of the chemically interesting problems the core electrons are unimportant and can be described by *contracted* Gaussian type orbitals (CGTOs) which are linear combination of a (usually) large number[46] of the primitive functions (PGTOs) of the full set[47]

$$\chi(\text{CGTO}) = \sum_{i=1}^{k} a_i x_i(\text{PGTO}) \tag{2.103}$$

The degree of contraction is the number of PGTOs entering a CGTO.

The specification of a basis set by means of primitive functions is given by the number of PGTOs in parentheses e.g. (10s4p1d/4s1p), where the slash separates the heavy atoms from the hydrogen atoms. The contraction scheme has to be specified and the contracted basis is given in square brackets, i.e. [3s2p1d/2s1p] and gives the size of the final basis set[48]. Split-valence basis set are also indicated by the *k-lnmG* scheme where *k* describe how many PGTOs are used in describing the core electrons and *n, l* and *m* indicate both how many functions the valence orbitals are split into and how many PGTOs are used for their representation. Other basis sets (cf. DZ, TZ, ecc.) are usually given with the specification of the number of primitive and the contraction scheme[49].

It is worth to notice that although the basis sets are suitable for recovering large fractions of the molecular ground state electronic energy, they are not necessarily suited for calculation of other properties as excited states or properties of perturbed systems (i.e. polarizabilities, NMR chemical shifts ecc.). For these purposes, the basis

[46]This is substantially due to the fact that the resulting contracted basis set should allow a good description of the wave function cusp at the nucleus.

[47]There are essentially two ways of treating the GTOs contraction: the general contraction and the segmented contraction [41, 36]. In the general contraction for a given atom all PGTOs with specific angular momentum enter the contracted functions having that angular momentum. Thus, a general contraction scheme would lead to the following set of CGTOs

$$\chi_\mu(\text{CGTO}) = \sum_{i=1}^{k} a_{\mu i} \chi_i(\text{PGTO})$$

where the contraction coefficients are typically determined by atomic natural orbital (ANO) computation. In the segmented contraction each primitive is used in one contracted function and the contraction coefficients are determined by variational atomic SCF computation.

[48]Of course, this notation does not give further information on how the contraction is done.

[49]A typical DZ basis set for the first row elements is usually (9s5p/4s) PGTO to [4s2p/2s] with contraction scheme: 6,1,1,1 for the *s*-function, 4,1 for the *p*-functions and 3,1 for hydrogen [40]

set must be augmented with *ad-hoc* additional functions [40, 36].

2.4.3 Pseudopotentials

One of the primary aim of the computational chemistry is the possibility of modeling to the same accuracy chemical systems including elements from the entire periodic table. From a theoretical point of view this requirement introduces further complications especially when dealing with heavier elements as transition and post-transition metals or lanthanides. In fact, it is well known that relativistic effects such as the contraction of the core electrons toward the nucleus and the consequent enlarged shielding of the nuclear charge felt by the valence electrons, accompanies the increase of the elemental atomic masses with direct consequences on the electronic configuration and chemical properties [42]. Furthermore, compounds containing elements of the *d*- and *f*-block are often characterized by close-lying electronic energy levels which can be appropriately described by correlated methods only (cf. Sec. 2.4.4) and the large number of electrons to be considered easily lead to computationally unmanageable problems. However, from chemical experience it is well known that low-energetic processes such as those involved in chemical reactions, are mostly determined by valence shell electrons. Thus, a theoretical procedure able to focus on the valence electrons only would reduce the computational effort of solving the electronic problem proposed by the equation (2.12) from N^k (where *N* is the number of basis functions and *k* can vary from 4 in the case of the HF method up to 8 for correlated methods) to $(N-Q)^k$ where *Q* denotes the number of (core) orbitals not explicitly treated.

The *ab-initio effective core potential* (ECP) method is a quantum mechanical technique which exploits these facts by replacing the core electrons (i.e. the orbitals which describe them) by a set of operator and potential functions jointly called pseudopotentials [43]. It deals with a further partitioning of the electronic Hamiltonian (2.11) into core and valence terms

$$\hat{H}_{ECP} = V_{NN} + E_{core} + \sum_{v}^{N_v} \left[\hat{h}(v) + \hat{V}^{ECP}(v)\right] + \sum_{v<v'} \frac{1}{r_{vv'}} \tag{2.104}$$

where the index v runs over the valence electron only and the one-electron operator $\hat{V}^{ECP}$ accounts for the neglected core-valence Coulomb and exchange interaction,

otherwise explicitly written as

$$\sum_{c}^{N_{core}} \left(2\hat{J}_c(1) - \hat{K}_c(1)\right), \tag{2.105}$$

and prevents the collapse of the valence orbitals in the core region. Furthermore, it can be shown [44] that in molecular calculations with the effective Hamiltonian (2.104) the term $V_{NN} + E_{core}$ reduces to the Coulomb shielding of the nuclear repulsion energy

$$V_{NN} + E_{core} = \sum_{A>B}^{nucl.} \frac{\left(Z_A - N_A^{core}\right)\left(Z_B - N_B^{core}\right)}{|R_A - R_B|} + const. \tag{2.106}$$

Thus, valence electron calculations can be done by using the effective nuclear charge in V_{NN} and adding the $\hat{V}^{ECP}$ matrix elements to the usual one-electron integrals, all other steps of the calculation being identical to the all electron case.

Derivation of effective core potentials and valence basis sets

Different procedures have been proposed to derive ECPs and the corresponding valence basis sets for atoms. As an example Fig. 2.2 reports the schematic procedure adopted by Stevens, Basch and Krauss [45] whose *relativistic effective core potentials* (RECPs) have been widely used in this work.

The first step in the derivation of a RECP is a highly accurate numerical all electron Dirac-Hartree-Fock (DHF) [42] calculation on an atomic generator state $^{2S+1}\mathrm{M}^{q+}$. This is one of the most important step which implies the choice of the oxidation and spin state of the atom to be computed as the reference state. For the chosen generator state the solution of the DHF equations gives rise to a set of eigenvalues $\epsilon_{n,l,j}$ and (numerical) eigenvectors (spinors) $\phi_{n,l,j}$. The next step consists in generating nodeless *valence* pseudospinors from the all-electron DHF spinors. Stevens and co-workers use a *shape-consistent* procedure [46] in which a normalized valence pseudospinor is generated by splicing together a cubic polynomial and the numerical all electron spinor such that all the $(n - l - 1)$ nodes in the radial distribution function are removed and the shape of the wave function in the valence region[50] results as close as possible to the true one. After having obtained the proper valence pseudospinors the numerical $V_l^{RECP}(r)$ can be generated[51] by *inverting* the Hartree-Fock equations, i.e. by find-

[50]The point in which the spinor and the pseudospinor start to coincide is called match point.

[51]It is perhaps the most difficult step since it primarily deals with the choice of the orbitals to be

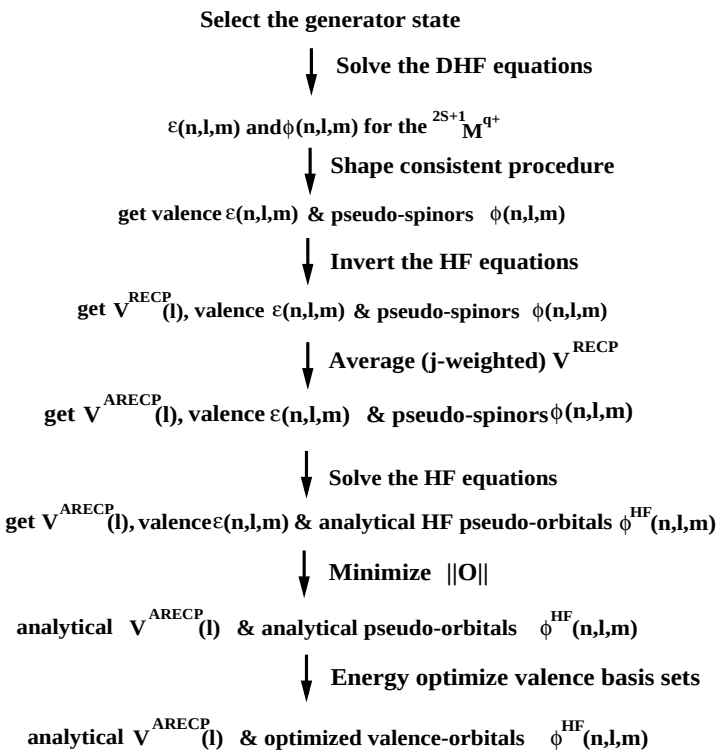

Figure 2.2: The ECP derivation scheme adopted by Stevens and coworkers.

ing the potential which when inserted in the non-relativistic HF Hamiltonian (2.104) allows to reproduce the previously determined wave function and energy of an atom to a satisfactory degree [47]. Of course, these numerical potentials are *j*-dependent[52] and are generated for each particular angular momentum of the core shells by orbital projection techniques [43]. However, in order to remove their *j*-dependence and avoid explicit treatment of the spin-orbit coupling in standard computation [48], they are usually converted into *average relativistic effective core potentials* (ARECPs) by the formula

$$V_l^{ARECP} = \frac{lV_{l,l-\frac{1}{2}}^{RECP}(r) + (l+1)V_{l,l-\frac{1}{2}}^{RECP}(r)}{2l+1}. \tag{2.107}$$

At this point one can use the numerical ARECP and a large gaussian basis set for the valence orbitals to derive *analytical* valence pseudo-orbitals. This can be done by solving the HF equations for atomic orbitals (AOs) expressed as linear combination

included in the core description. From standpoint of chemical reactivity for atoms of the *p*-block all the core electrons are replaced by a pseudopotential (full-core ECPs) while for atoms of the *d*- and *f*-blocks only the innermost core electrons are replaced (semi-core ECPs).

[52]This is of course, due to the fact that the one-electron DHF Hamiltonian is fully relativistic and includes also spin-orbit terms (cf. [48] and references therein).

of gaussian functions in which the exponents are kept fixed and the expansion coefficients are optimized to give the lowest energy[53]. In this respect, the DHF valence pseudospinors are transformed into "exact" HF valence pseudo-orbitals which can be further used to derive analytical forms of pseudopotentials by fitting the numerical ARECP with

$$r^2 V_l^{ARECP}(r) = \sum_k A_{l,k} r^{n_{l,k}} e^{-\zeta_{l,k} r^2} \tag{2.108}$$

where $n_{l,k} = 0, 1, 2$; coefficients and exponents of the gaussian expansion on the right hand side of the eq. 2.108 have to be determined keeping the maximum similarity of $V_l(r)$ with the numerical potential. In this step, the scheme of Stevens and coworkers differ from the standard one [49] which fits the numerical potential with a least-square procedure and a large number of gaussian functions. SBK pseudopotentials are derived using the method proposed by Barthelat et al. [50, 43] based on the definition of the functional

$$\|O\| = [\langle X_l \mid O \mid X_l \rangle]^{1/2} \tag{2.109}$$

$$O = \tilde{\varepsilon} |\tilde{X}_l >< \tilde{X}_l| - \varepsilon_l |X_l >< X_l| \tag{2.110}$$

in which the quantities capped by a tilde are optimized, while the others are the reference quantities to be reproduced [48][54]. Independently of the procedure used to derive the analytical ECP, one proceeds with the optimization of the parameters of the potential with the highest angular momentum (V_{LMAX}^{ARECP}) as first while the potentials with lower angular momentum are successively optimized with V_{LMAX}^{ARECP} subtracted

$$\hat{V}^{ARECP} = V_{LMAX}^{ARECP} - \sum_{l=0}^{LMAX-1} \sum_{m=-l}^{l} \left[V_l^{ARECP} - V_{LMAX}^{ARECP} \right] |lm >< lm|. \tag{2.111}$$

The last step in the procedure is to generate the corresponding optimized basis set for the valence orbitals not replaced by the pseudopotential. This can be done by methods similar to those employed in traditional all electron calculations already described in the Sect. 2.4.2. Usually, the elements of the *p*-block do not require large basis sets whereas the description of properties of molecules including *d*- and *f*-block elements requires large basis sets, augmented by diffuse and polarization functions.

[53] It is worth to emphasize that the atomic HF equations should be solved for the same state (the generator state) defined for the solution of the original DHF equations [48].

[54] This procedure allows to limit the number of gaussians to be used in the analytical expansion (2.108). In this respect the SBK pseudopotentials are called compact ECPs.

It is worth to emphasize, that ECPs obtained on the basis of HF only (with relativistic corrections) calculations, do not guarantee the correct description of the atomic properties. In particular, the ECP results are not expected to compare with experiment when dealing with atomic properties implying change in number of electrons (ionization energies and electron affinities) or excitation energies often affected by change in intrashell correlation. However, if the accurate description of these properties is crucial for the particular chemical problem under consideration it is possible to optimize the coefficients and the exponents of the expansion (2.108) as well as the valence GTOs basis set including experimental values and certain measures of the shape of the pseudo-orbitals such as their radial expectation values in the fitting procedure.

2.4.4 The post Hartree-Fock Methods

The HF solution of the many-electron problem gives rise to reliable total energies for the equilibrium situations. However, large amount of chemical problems cannot be reasonably described by a method which totally neglects the part of the energy arising from the actual instantaneous interaction of the electrons, i.e. the correlation energy[55]. The *post Hartree-Fock* methods improve the HF independent particle approximation by estimating to the best level the correlation energy of a molecular system.

Configuration Interaction

Any *N*-electron antisymmetric eigenfunction of the Hamiltonian (2.9) can be expressed as a linear combination of Slater determinants formed from all possible combinations of one-electron basis functions [51]. Thus, the most obvious way to go beyond the Hartree-Fock approximation is to include in the wave function expansion more than a single configuration in a variational manner.

In the configuration interaction (CI) method the CI wave function is expressed as a linear combination of the *N*-electron functions constructed from the solutions of the HF equations

$$|\Phi_{CI}>= a_0|\Psi_0> + \sum_S a_S|\Psi_S> + \sum_D a_D|\Psi_D> + \sum_T a_T|\Psi_T> + ... + \sum_N a_N|\Psi_N> \tag{2.112}$$

[55]The correlation energy is usually defined as the difference between the energy of the exact (non relativistic) solution of the Schrödinger equation in the framework of the Born-Oppenheimer approximation and the HF energy in the limit of basis set completeness.

where $|\Psi_0>$ is the reference HF ground state and $|\Psi_S>$, $|\Psi_D>$, $|\Psi_T>$, ecc. up to $|\Psi_N>$ correspond to singly, doubly, triply, ecc. up to *N*-tuply excited Slater determinants. By applying the variational principle[56] to (2.112) one obtains the set of CI *secular equations* which in shorthand notation can be written as

$$\mathbf{Ha} = \mathbf{Ea} \tag{2.113}$$

where **H** is the CI matrix [11] and has the triangular form

$$\begin{bmatrix} <\Psi_0|\hat{H}|\Psi_0> & <\Psi_0|\hat{H}|\Psi_S> & <\Psi_0|\hat{H}|\Psi_D> & <\Psi_0|\hat{H}|\Psi_T> & ... \\ & <\Psi_S|\hat{H}|\Psi_S> & <\Psi_S|\hat{H}|\Psi_D> & <\Psi_S|\hat{H}|\Psi_T> & ... \\ & & <\Psi_D|\hat{H}|\Psi_D> & <\Psi_D|\hat{H}|\Psi_T> & ... \\ & & & <\Psi_T|\hat{H}|\Psi_T> & ... \\ & & & & ... \\ ... & ... & ... & ... & ... \end{bmatrix} . \tag{2.114}$$

Solving the CI secular equations is equivalent of diagonalizing the CI matrix. The lowest eigenvalues are the CI energies[57] and the corresponding eigenvectors contains the coefficients of the expansion (2.112). If the CI wave function expansion contains all the possible Slater determinants arising from $|\Psi_0>$ the CI matrix is called *full* CI matrix and the related method full CI. Of course, solving the full CI problem leads to the exact solution of the associated many-electron problem[58] and the difference between the full CI lowest eigenvalue E and the singly determinantal HF energy E_0 is the total correlation energy. The CI matrix elements H_{ij} can be evaluated by expanding each determinant in terms of the corresponding molecular orbitals thus, by computing the corresponding MO integrals. It can be shown [32] that some of these elements are

[56] In the CI theory, the set of Slater determinants arising from the HF molecular orbitals are held fixed and only the coefficients of the CI expansion are optimized to minimize the energy under the constrain of the intermediate normalization $<\Psi_0|\Phi_{CI}>=1$.

[57] Due to the form of the Hamilton operator which contains only one and two electron operators, it can be shown [11] that in the case of reference HF wave function, the CI energy can be completely determined by the coefficients of the double excitations in the intermediate normalized CI wave function. Of course this does not mean that only double excitations need to be included for an exact CI description of the ground state, being these coefficients affected by higher excited configurations.

[58] Indeed, the full CI energy is exact in the subspace spanned by finite size of the one-electron basis set. Thus, also the correlation energy is often called *basis set correlation energy* and is an upper bound of the true value which represents a reference point for all the other approaces for calculation of the correlation energy.

zero[59] and this reduce the computational effort of diagonalizing the matrix. Nevertheless, the number of the excited determinants which enter the expansion (2.112) and determine the size of the matrix (2.114) grows factorially with the size of the basis set[60] and the solution of the full CI problem remains computationally unmanageable also for systems of moderate size.

However, in chemistry one of the main interests is the determination of the relative energy of different molecules and the problem of computing the total correlation energy by a full CI approach can be replaced by the choice of the best approximation which recover the correlation energy of different systems to the same extent. It is in fact well known that the correlation energy behavior is strongly affected by the bonding topology. Its contribution to the total energy of a molecular system tends to remain constant for changes that conserve the number and type of chemical bonds but it can change drastically when bonding change. Truncated CI methods reduce the space of the CI wave function by imposing a limited number of excited determinants to be included in. One of the most used truncated CI scheme is the CISD in which only singly and doubly excited determinants enter the expansion (2.112) and the computational effort of diagonalizing the corresponding CI matrix is strongly reduced. Unfortunately, truncated CI approaches are not *size-extensive*[61] and addition of corrections to the computed energy are needed [52]. Inclusion of triply and quadruple excitations in to the CI wave function expansion (CISDTQ) reduce the size extensivity problem and allows to recover up to 90% of the correlation energy of the system [11]. However, since also for truncated CI approaches the number of excited determinant can become very large, the problem of the computer memory storage for the two electron integrals needed in the evaluation of the CI matrix elements limits the applicability of these methods to

[59] Due to Brillouin theorem all the matrix elements involving the ground state determinant $|\Psi_0>$ and the singly excites determinants are zero. Matrix elements between different spin states as well as between determinants of different symmetry are also zero. Furthermore, states described by excited determinants which are eigenfunctions of the $\hat{S}_z$ but not of the $\hat{S}^2$ spin operator can be spin-adapted [11] to further reduce the number of the non-zero matrix elements to evaluate.

[60] From combinatorial calculus the possible ways of selecting N elements out of K positions is given by the formula $\begin{pmatrix} K \\ N \end{pmatrix}$. Thus, the simple problem of computing the correlation energy of a water molecule with a small split valence 6-31G(d) basis set would involve rougly half a billion determinants and the size of the full CI matrix to be diagonalized would be of the order of the square of this value.

[61] Here and in the following of this work, by size-extensivity is meant that the energy of k non interacting systems (i.e. systems for which the one and two electron integrals common to all the HF and post HF methods vanish if involving MOs belonging to separate subsystems) is a k-multiple of the energy of a single such system. The size-extensivity toghether with the ability to correctly describe the dissociation problem is called *size-consistency*.

relatively small systems[62]. An improvement with respect to the CISD method which also reduces the size-extensivity problem allowing the computation of relatively large systems, is the *multi-reference* SD-CI (MRD-CI) method in which the CI space of singly and doubly excited determinants is constructed by a careful choice of *ad hoc* reference configurations (cf. [53] and references therein).

Also in the framework of truncated CI methods and for systems of moderate size, the CI expansion easily includes an enormous number of terms (of the order of millions) and the full diagonalizing of the CI matrix by standard diagonalizing methods is out of question. Fortunately, often one is interested in the lowest eigenvalue and eigenvector and *direct* CI methods, based on very efficient iterative diagonalizing algorithms [54], can be used.

Moller-Plesset perturbation theory

The Moller-Plesset perturbation theory (MPPT) is a special case of the more general many-body perturbation theory (MBPT) with the aim of calculating the correlation energy of a molecular system by adding corrections to the solutions obtained in the framework of the independent particle approximation. The main assumption of the MBPT is that the problem to be solved slightly differs from that which has been already solved (exactly or approximately). This is mathematically expressed by defining an Hamilton operator $\hat{H}$ as the sum of the reference operator $\hat{H}_0$ and a "small" perturbation operator $\hat{U}$

$$\hat{H} = \hat{H}_0 + \hat{U}. \tag{2.115}$$

The corresponding perturbed Schrödinger equation is

$$\hat{H}|\Psi_n >= W_n|\Psi_n > \qquad n = 0, 1, 2, ... \tag{2.116}$$

and its solutions can be expressed as

$$|\Psi_n > \;=\; |\Psi_n^{(0)} > + |\Psi_n^{(1)} > + |\Psi_n^{(2)} > + |\Psi_n^{(3)} > + ... \tag{2.117}$$

$$W_n \;=\; W_n^{(0)} + W_n^{(1)} + W_n^{(2)} + W_n^{(3)} + ... \tag{2.118}$$

[62] It can be estimated that the number of two electron integrals to be computed in the CISDTQ scheme grows as M^{10} being M the number of basis functions.

where the corrections terms up to the second order are [7, 10]

$$W_n^{(1)} = < \Psi_n^{(0)} | \hat{U} | \Psi_n^{(0)} > \tag{2.119}$$

$$W_n^{(2)} = \sum_{k \neq n} \frac{< \Psi_n^{(0)} | \hat{U} | \Psi_k^{(0)} >< \Psi_k^{(0)} | \hat{U} | \Psi_n^{(0)} >}{\left(E_n^{(0)} - E_k^{(0)} \right)} \tag{2.120}$$

$$| \Psi_n^{(1)} >= \sum_{k \neq n} \frac{< \Psi_k^{(0)} | \hat{U} | \Psi_n^{(0)} >}{\left(E_n^{(0)} - E_k^{(0)} \right)} | \Psi_k^{(0)} > \tag{2.121}$$

$$| \Psi_n^{(2)} >= \sum_j \sum_{k \neq n} \frac{< \Psi_j^{(0)} | \hat{U} | \Psi_k^{(0)} >< \Psi_k^{(0)} | \hat{U} | \Psi_n^{(0)} >}{\left(E_n^{(0)} - E_j^{(0)} \right) \left(E_n^{(0)} - E_k^{(0)} \right)} - \frac{< \Psi_j^{(0)} | \hat{U} | \Psi_n^{(0)} >< \Psi_n^{(0)} | \hat{U} | \Psi_n^{(0)} >}{\left(E_n^{(0)} - E_j^{(0)} \right)^2}. \tag{2.122}$$

In order to use the perturbation theory for calculating the correlation energy of a molecular system, the unperturbed Hamilton operator $\hat{H}_0$ as well has the perturbing operator $\hat{U}$ have to be selected. The Moller-Plesset partitioning of the Hamiltonian consists of using the Fock operator as unperturbed operator

$$\hat{H}_0 = \sum_{i=1}^{N} \hat{F}_i = \sum_{i=1}^{N} \left(\hat{h}_i + \sum_{j=1}^{N} (\hat{J}_{ij} - \hat{K}_{ij}) \right) = \sum_{i=1}^{N} \hat{h}_i + 2 \langle \hat{v}_{HF} \rangle = \sum_{i=1}^{N} \hat{h}_i + \sum_{i=1}^{N} \sum_{j=1}^{N} \langle \hat{g}_{ij} \rangle \tag{2.123}$$

while the perturbation is represented by the exact instantaneous electron-electron interaction operator ($\hat{V}_{ee}$, cf. eq. 2.10) minus twice the expectation value of the Hartree-Fock potential of the eq. (2.71)

$$\hat{U} = \hat{H} - \hat{H}_0 = \hat{V}_{ee} - 2 \langle \hat{v}_{HF} \rangle = \sum_{i=1}^{N} \sum_{j>1}^{N} \hat{g}_{ij} - \sum_{i=1}^{N} \sum_{j=1}^{N} \langle \hat{g}_{ij} \rangle . \tag{2.124}$$

This choice does not really fulfill the basic assumption of the MBPT which requires a small perturbation with respect to the unperturbed Hamiltonian. However, it leads to a very simple size-extensive method in which the solutions of the unperturbed problem are known (cf. Sect. 2.4.1).

For the lowest energy state of the system, the MP zero-order wave function is the HF determinant $| \Psi_0^{(0)} >$ and the corresponding zero-order energy is just the sum of the HF orbital energies. The first-order energy correction (cf. eq. 2.119) is the expectation

value of the perturbation operator over the zero-order HF wave function

$$W_0^{(1)} =< \Psi_0^{(0)}|\hat{U}|\Psi_0^{(0)} >= \left\langle \hat{V}_{ee} \right\rangle - 2\left\langle \hat{V}_{ee} \right\rangle = -\left\langle \hat{V}_{ee} \right\rangle \tag{2.125}$$

which corrects Eq. 2.123 for the overcounting of the electron-electron repulsion due to the use of the Fock-Hamiltonian as unperturbed operator. Thus, the sum of the Moller-Plesset $W_0^{(0)}$ and $W_0^{(1)}$ energy terms is exactly the HF energy of the eq. (2.76). The correlation corrections start to really contribute with the second-order which involves the matrix elements of the perturbation operator between the reference HF ground state wave function and all the possible excited determinants (cf. eq. 2.120). However, because the perturbation is represented by a two-electron operator, all matrix elements involving *triply*, *quadruple*, ecc. excited determinants will be zero. Furthermore, due to the Brillouin theorem also the matrix elements of the form $< \Psi_0|\hat{H}|\Psi_i^a >$ are zero and the second-order correction to W_0 results

$$W_0^{(2)} = \sum_{i<j}^{occ}\sum_{a<b}^{vir} \frac{< \Psi_0^{(0)}|\hat{U}|\Psi_{ij}^{(0)ab} >< \Psi_{ij}^{(0)ab}|\hat{U}|\Psi_0^{(0)} >}{E_0 - E_{ij}^{ab}} \tag{2.126}$$

which expressed in terms of integrals among molecular orbitals and energy difference of Slater determinants lead to the second-order Moller-Plesset energy correction formula

$$E(MP2) = \sum_{i<j}^{occ}\sum_{a<b}^{vir} \frac{(\psi_i\psi_j|\psi_a\psi_b) - (\psi_i\psi_j|\psi_b\psi_a)}{\epsilon_i + \epsilon_j - \epsilon_a - \epsilon_b} \tag{2.127}$$

which allows one to recover up to the 90% of the correlation energy.

The first-order correction to the ground state wave function also depends only from the doubly excited determinants, since the nature of the two electron operator and the Brillouin theorem have the same effects on the matrix elements in the (2.121) as in the (2.120). The knowledge of the first-order wave function allows the calculation up to the third-order energy correction (MP3) by means of the Wigner's *2m+1* rule

$$W_0^{(2m+1)} =< \Psi_0^{(m)}|\hat{U}|\Psi_0^{(m)} > - \sum_{k,l=1}^{m} W_0^{(2m+1-k-l)} < \Psi_0^{(k)}|\Psi_0^{(l)} >$$

from which it is immediately clear that for $m = 1$ only contributions from doubly excited determinants are taken into account.

The formula for the second-order correction in the wave function (2.122) con-

tains the products $< \Psi_j^{(0)}|\hat{U}|\Psi_k^{(0)} >< \Psi_k^{(0)}|\hat{U}|\Psi_0^{(0)} >$ and it is evident that the second term can be non-zero only if $|\Psi_k^{(0)} >$ is a doubly excited determinant with respect to $|\Psi_0^{(0)} >$. Consequently, in order that the first factor differ from zero, $|\Psi_j^{(0)} >$ can only be a singly, doubly, triply or quadruple excited determinant. Thus, from the second-order wave function correction term one can derive the correction up to the fourth-order (MP4) of the energy which contains contributions from singly, doubly, triply and quadruple excited determinants and recover up to the 98% of the correlation energy of the system.

The main limitation of the perturbation methods is the assumption that the solution of the unperturbed problem is a good approximation of the real wave function and that the perturbation operator may have only small effects. In this respect, a HF wave function, when it is intrinsically not reliable because of the characteristics of the system (e.g. transition metal compounds), requires high-order corrections to reach reasonable accuracy in the computation of properties. However, for the description of standard chemical phenomena the use of relatively large atomic basis sets (at least of double- or triple-zeta type plus polarization, cf. Sect. 2.4.2) allows, to a reasonable approximation, to truncate the perturbation expansion (2.118) to the second- (MP2) or fourth- (MP4) order (cf. also Sect. 2.4.6).

In the case of unrestricted reference wave functions, the Moller-Plesset scheme (UMP*n*) is based on the unperturbed Hamiltonian which is the sum of the α and β Fock operators. The UMP*n* method allows a correct description of the dissociation problem. However, to a limited extent, it also suffers from the spin-contamination problems discussed for the UHF wave function [32].

The Coupled-Cluster method

The fundamental idea of the Coupled-Cluster theory is the (intermediate normalized) exponential wave function ansatz

$$\Psi_{CC} = e^T \Phi_0 \tag{2.128}$$

where Φ_0 is considered to be an independent particle reference wave function (i.e. the HF wave function) and $\hat{T}$ is the *cluster* operator which creates excitations from it. The

exponential of (2.128) can be expanded as

$$e^{\hat{T}} = 1 + \hat{T} + \frac{1}{2!}\hat{T}^2 + \frac{1}{3!}\hat{T}^3 + ... + \frac{1}{p!}\hat{T}^p \tag{2.129}$$

where the cluster operator $\hat{T}$ is given by

$$\hat{T} = \hat{T}_1 + \hat{T}_2 + \hat{T}_3 + ... + \hat{T}_N = \sum_{i=1}^{N} \hat{T}_i \tag{2.130}$$

and $\hat{T}_i$ is the excitation operator of order i which, acting on the reference wave function Φ_0, generates *all* the Slater determinants excited at order i. Up to $i = 2$ this can be viewed as

$$\hat{T}_1\Phi_0 = \sum_{i}^{occ}\sum_{a}^{vir} t_i^a \Phi_i^a \tag{2.131}$$

$$\hat{T}_2\Phi_0 = \sum_{i<j}^{occ}\sum_{a<b}^{vir} t_{ij}^{ab} \Phi_{ij}^{ab} \tag{2.132}$$

where Φ_i^a and Φ_{ij}^{ab} indicate single and double excitations of Φ_0, respectively and the t "coefficients" are called *amplitudes*. By means of the eq. (2.130), the exponential operator (2.129) becomes

$$\begin{aligned} e^{\hat{T}} = {} & 1 + \hat{T}_1 + \left(\hat{T}_2 + \tfrac{1}{2}\hat{T}_1^2\right) + \left(\hat{T}_3 + \hat{T}_2\hat{T}_1 + \tfrac{1}{6}\hat{T}_1^3\right) \\ & + \left(\hat{T}_4 + \hat{T}_3\hat{T}_1 + \tfrac{1}{2}\hat{T}_2^2 + \tfrac{1}{2}\hat{T}_2\hat{T}_1^2 + \tfrac{1}{24}\hat{T}_1^4\right) + ... \end{aligned} \tag{2.133}$$

which substituted in eq. (2.128) shows how the various configurations are produced. The first term of (2.133) generates the reference HF state and the second term generates the first excited configurations. The first parenthesis generates all the doubly excited states which can be *connected* ($\hat{T}_2$) or *disconnected*[63] ($\hat{T}_1^2$). All triply excited configurations can be generated by the terms in the third parenthesis and are named *true* ($\hat{T}_3$) or *product* triples. Analogously the quadruple excited configurations can be viewed as composed of five terms, a true quadruple and four product terms.

[63]Connected means that the term is not more decomposable into a product of single excitations. The meaning of the word disconnected follows straigthforwardly.

The Schrödinger equation corresponding to the wave function (2.128) results

$$\hat{H}e^{\hat{T}}\Phi_0 = Ee^{\hat{T}}\Phi_0 \tag{2.134}$$

and the CC ground state energy can be obtained by simply multiplying it from the left by Φ_0^* and integrating

$$E_{cc} =< \Phi_0|\hat{H}e^{\hat{T}}|\Phi_0 > . \tag{2.135}$$

Due to the form of the Hamilton operator which contains only one and two electron operators, it can be shown [55] that in the case that $|\Phi_0 >$ is the reference HF wave function, the CC energy is completely determined by singles and doubles amplitudes and the two electron MO integrals for the double excitations

$$E_{CC} = E_0 + \sum_{i<j}^{occ}\sum_{a<b}^{vir}\left(t_{ij}^{ab} - t_i^a t_j^b - t_i^b t_j^a\right)(< \phi_i\phi_j|\phi_a\phi_b > - < \phi_i\phi_j|\phi_b\phi_a >) . \tag{2.136}$$

Of course, this does not mean that only double excitations need to be created by the cluster operator, being the amplitudes entering the eq. (2.136) dependent on the other excitations[64].

If all the cluster operators up to $\hat{T}_N$ are included in $\hat{T}$, all possible excited determinants are generated and the CC wave function is equivalent to full CI. However, as for the CI method, this leads to an unmanageable computational problem also for moderate size systems. Thus, truncation of the $\hat{T}$ operator need to be considered. In the single-double coupled-cluster (CCSD) method, $\hat{T}$ is restricted to just $\hat{T}_1$ and $\hat{T}_2$ so that the exponential operator (2.129) becomes

$$e^{\hat{T}_1+\hat{T}_2} = 1+\hat{T}_1+\left(\hat{T}_2 + \frac{1}{2}\hat{T}_1^2\right)+\left(\hat{T}_2\hat{T}_1 + \frac{1}{6}\hat{T}_1^3\right)+\left(\frac{1}{2}\hat{T}_2^2 + \frac{1}{2}\hat{T}_2\hat{T}_1^2 + \frac{1}{24}\hat{T}_1^4\right) \tag{2.137}$$

and the corresponding equations for the single and double amplitudes are

$$< \Phi_m^e|\hat{H}e^{\hat{T}_1+\hat{T}_2}|\Phi_0 >= E_{CCSD} < \Phi_m^e|\hat{T}_1\Phi_0 > \tag{2.138}$$

and

$$< \Phi_{mn}^{ef}|\hat{H}e^{\hat{T}_1+\hat{T}_2}|\Phi_0 >= E_{CCSD} < \Phi_{mn}^{ef}|\left(\hat{T}_2 + \frac{1}{2}\hat{T}_1^2\right)\Phi_0 >, \tag{2.139}$$

[64]The procedure of finding the connections among the amplitudes leads to a set of coupled non-linear equations which must be solved iteratively.

respectively. By substituting the expression of the CC energy (2.136) into (2.138) and (2.139) one obtains the coupled non-linear equations for the singles and doubles amplitudes which must be solved iteratively in order to determine the amplitudes and, consequently, the CC energy and wave function.

Comparing the left-hand side of the equations (2.138) and (2.139) with the form of the $e^{\hat{T}_1+\hat{T}_2}$ exponential operator (2.137) it is clear that CCSD method includes excitations of higher order than the order of the truncated cluster operator. Quadruple excited states, for example, are generated by the $\hat{T}_2^2$ operator and they enter the amplitude equations with a weight given by the product of doubles amplitudes [32], [55]. The inclusion of these products of excitations makes the CC theory size-extensive.

CCSD scales as M^6 with the size of the basis set and could be applicable for routine computations. Introduction of triples $\hat{T}_3$ into the cluster operator lead to the CCSDT method which scales as M^8 and is computationally more demanding than CISDT. However, the connections existing between the CC theory and Moller-Plesset perturbation theory [55] make possible the estimation of higher excitation contributions to the CCSD energy by hybrid methods, namely CCSD(T) or CCSD(TQ) in which triples and quadruples contributions are estimated by fourth- and fifth-order perturbation theory calculations respectively [56].

2.4.5 The density functional theory

Let N be the number of electrons of a system and $\rho(r)$ the associated electron density**.** The following definition holds

$$\rho(\mathbf{r}_1) = N \int ... \int \left|\Psi(\mathbf{x}_1, \mathbf{x}_2, ..., \mathbf{x}_N)\right|^2 ds_1 d\mathbf{x}_2 ... d\mathbf{x}_N \tag{2.140}$$

where $\Psi(\mathrm{x}_1, \mathrm{x}_2, ..., \mathrm{x}_N)$ is the electronic wave function of the system and $d\mathbf{x}_i = ds_i d\mathbf{r}_i$ is the spin-space volume element. Notice, that when integrating over the space coordinates it gives the total number of electrons of the system

$$\int \rho(\mathbf{r}) d\mathbf{r} = N. \tag{2.141}$$

In atoms, molecules or solids, at any atomic nucleus the electron density has a finite value $\rho(0)$ and it can be shown [57] that the nuclear cusp condition gives

$$\frac{\partial}{\partial r_\alpha}\overline{\rho}(r_\alpha)|_{r_\alpha=0} = -2Z_\alpha\overline{\rho}(0) \tag{2.142}$$

where $\overline{\rho}(r_\alpha)$ is the spherical average of $\rho(r_\alpha)$. Furthermore, the knowledge of $|\nabla\rho(\mathbf{r})|$ at the nuclei, would give their nuclear charge. Thus, if one knows the exact electron density of a system, the full Schrödinger Hamiltonian would be also known. These simple arguments are the basis of the modern density functional theory which originates from the proof by Hohenberg-Kohn [58] that within the Born-Oppenheimer approximation (cf. Sec. 2.2) the Schrödinger Hamiltonian operator of a molecular system can be written as

$$\hat{H} = \sum_{i=1}^{N}\left(-\frac{1}{2}\nabla_i^2\right) + \sum_{i=1}^{N} v(\mathbf{r}_i) + \sum_{i<j}^{N}\frac{1}{r_{ij}} \tag{2.143}$$

where the external potential acting on the electron i

$$\hat{v}(\mathbf{r}_i) = -\sum_{\alpha}\frac{Z_\alpha}{r_{i\alpha}} \tag{2.144}$$

is univocally determined by the electron density $\rho(r)$. Therefore, the ground state energy can be expressed as a functional of the density as

$$E[\rho] = V_{ne}[\rho] + T[\rho] + V_{ee}[\rho] = \int \rho(\mathbf{r})v(\mathbf{r})d\mathbf{r} + F_{HK}[\rho] \tag{2.145}$$

where

$$F_{HK}[\rho] = T[\rho] + V_{ee}[\rho]\,. \tag{2.146}$$

F_{HK} is expressed in terms of the kinetic energy of interacting electrons and of all possible forms of electron-electron interactions. In particular, $V_{ee}[\rho]$ is the sum of the classical repulsion term

$$J[\rho] = \frac{1}{2}\int\int\frac{1}{r_{12}}\rho(\mathbf{r}_1)\rho(\mathbf{r}_2)d\mathbf{r}_1 d\mathbf{r}_2 \tag{2.147}$$

and of a non-classical term which contains the main part of the exchange-correlation energy of the system. The second Hohenberg-Kohn theorem [58] provides the variational principle for the energy functional $E[\rho]$. Assuming the differentiability of the

terms in (2.145) the ground state electron density[65] is the density which minimizes $E[\rho]$ and hence satisfies the Euler-Lagrange equation

$$\delta E[\rho] - \mu\delta\left[\int \rho(\mathbf{r})d\mathbf{r} - N\right] = 0 \tag{2.148}$$

under the constraint (2.141). In terms of functional derivatives, eq. (2.148) can be written as

$$\mu = v(\mathbf{r}) + \frac{\delta T[\rho]}{\delta\rho(\mathbf{r})} + \frac{\delta V_{ee}[\rho]}{\delta\rho(\mathbf{r})} \tag{2.149}$$

which is an exact equation for $\rho(\mathrm{r})$ only if the functional form of $T[\rho]$ and $V_{ee}[\rho]$ is known.

In order to convert this last equation into a set of working equations Kohn and Sham [59] introduced the idea of considering the determinantal wave function for *N non-interacting* electrons in *N* orbitals ψ_i in such a way that the true ground state kinetic energy and the electron density can be computed to a good approximation as

$$T_s[\rho] = \sum_i^N \left\langle \psi_i \left| -\frac{1}{2}\nabla^2 \right| \psi_i \right\rangle \tag{2.150}$$

$$\rho(\mathbf{r}) = \sum_i \sum_s |\psi_i(\mathbf{r}, s)|^2 \tag{2.151}$$

The orbitals obey an equation of the form

$$\left[-\frac{1}{2}\nabla^2 + v_s(\mathbf{r})\right]\psi_i = \epsilon_i\psi_i \tag{2.152}$$

where $v_s(\mathbf{r})$ is an external potential in which the non-interacting electrons move. Therefore, the energy of the system is given by

$$E[\rho] = T_s[\rho] + \int v_s(\mathbf{r})\rho(\mathbf{r})d\mathbf{r} \tag{2.153}$$

in which there are no electron-electron interaction terms. Returning to the problem of

[65] More rigorously the second HK theorem is valid only if the electron density is *v*-representable, i.e. if it is the density associated with the antisymmetric ground state wave funtion of a Hamiltonian of the form (2.143) being $v(\mathrm{r})$ some external potential [31].

interacting electrons one can write the total energy as

$$\begin{aligned} E[\rho] &= \int v_s(\mathbf{r})\rho(\mathbf{r})d\mathbf{r} + T[\rho] + V_{ee}[\rho] \\ &= \int v_s(\mathbf{r})\rho(\mathbf{r})d\mathbf{r} + T_s[\rho] + J[\rho] \\ &+ (T[\rho] - T_s[\rho]) + V_{ee}[\rho] - J[\rho] \\ &= \int v_s(\mathbf{r})\rho(\mathbf{r})d\mathbf{r} + T_s[\rho] + J[\rho] + E^{XC}[\rho] \\ &= \int v_s(\mathbf{r})\rho(\mathbf{r})d\mathbf{r} + \int \epsilon^{XC}(\mathbf{r})\rho(\mathbf{r})d\mathbf{r} + T_s[\rho] + J[\rho] \end{aligned} \tag{2.154}$$

in which the first line is from eq. (2.145), the second line inserts and removes the non-interacting kinetic energy (2.150) and the Coulomb energy (2.147), the next lines introduce the exchange-correlation energy functional and the exchange-correlation potential ϵ^{XC} which is related to the functional derivatives of v^{XC} as follow

$$E^{XC} = T[\rho] - T_s[\rho] + V_{ee}[\rho] - J[\rho] \tag{2.155}$$

$$\begin{aligned} v^{XC}(\mathbf{r}) &= \tfrac{\delta E^{XC}[\rho]}{\delta\rho(\mathbf{r})} \\ &= \epsilon^{XC}(\mathbf{r}) + \rho(\mathbf{r})\tfrac{\delta\epsilon^{XC}[\rho]}{\delta\rho(\mathbf{r})} \end{aligned} \tag{2.156}$$

By comparing the equations (2.153), (2.155) and (2.156) one can deduce that the problem is now recast into the one involving non-interacting electrons in *N* orbitals which obey the equations

$$\left[\frac{1}{2}\nabla^2 + v(\mathbf{r}) + \int \frac{\rho(\mathbf{r}')}{|\mathbf{r}-\mathbf{r}'|}d\mathbf{r}'\right] + v^{XC}(\mathbf{r})\psi_i(\mathbf{r}) = \epsilon_i\psi_i(\mathbf{r}) \tag{2.157}$$

which are the Kohn-Sham (KS) equations for the KS orbitals ψ_i [31]. Notice, that the KS equations are SCF equations and can be solved within a finite basis set representation in which the KS orbitals are expanded in terms of atomic basis functions (cf. Sect. 2.4.2).

The above derivation of the *spin-compensated* Kohn-Sham equations assumes the absence of a vector potential due to the presence of a magnetic field in the Hamiltonian (2.143). If such a vector potential is added, a spin-polarized formalism which consider both the ρ^α and ρ^β densities as basic variables is necessary. The key idea of the spin-unrestricted density functional theory is to introduce a reference system of non-interacting electrons in an effective field with electron density equal to the one of

the real system. Therefore, the density can be decomposed into one electron functions ψ^{α} and ψ^{β} (the unrestricted Kohn-Sham orbitals) as

$$\rho^{\alpha} = \sum_{i=1}^{N_{\alpha}} \left|\psi_i^{\alpha}\right|^2, \qquad \rho^{\beta} = \sum_{j=1}^{N_{\beta}} \left|\psi_j^{\beta}\right|^2 \tag{2.158}$$

in which the orbitals obey the usual orthonormality conditions and guarantee that the density integrates as

$$\int \rho^{\sigma}(\mathbf{r}) d\mathbf{r} = N^{\sigma}. \tag{2.159}$$

The functional of the total energy in terms of Kohn-Sham orbitals ψ_i^{σ} can now be written as[66]

$$\begin{aligned} E\left[\rho^{\alpha},\rho^{\beta}\right] &= \textstyle\sum_{i\sigma} \int d\mathbf{r} \psi_i^{\sigma}(\mathbf{r}) \left(-\frac{1}{2}\nabla^2\right) \psi_i^{\sigma}(\mathbf{r}) + J\left[\rho^{\alpha},\rho^{\beta}\right] \\ &+ E^{XC}\left[\rho^{\alpha},\rho^{\beta}\right] + \int d\mathbf{r}\left[v(\mathbf{r})(\rho^{\alpha}+\rho^{\beta})\right] \end{aligned} \tag{2.160}$$

and the corresponding unrestricted Kohn-Sham (UKS) equations are obtained by variational minimizing of $E\left[\rho^{\alpha},\rho^{\beta}\right]$ subject to the normalization constraint of the orbitals

$$\begin{aligned} \left[-\tfrac{1}{2}\nabla^2 + v_{eff}^{\alpha}(\mathbf{r})\right]\psi_i^{\alpha} &= \epsilon_i^{\alpha}\psi_i^{\alpha}, \qquad i = 1,2,...N_{\alpha} \\ \left[-\tfrac{1}{2}\nabla^2 + v_{eff}^{\beta}(\mathbf{r})\right]\psi_j^{\beta} &= \epsilon_j^{\beta}\psi_j^{\beta}, \qquad j = 1,2,...N_{\beta} \end{aligned} \tag{2.161}$$

where the spin dependent effective potentials read as

$$\begin{aligned} v_{eff}^{\alpha}(\mathbf{r}) &= v(\mathbf{r}) + \int \frac{\rho^{\alpha}(\mathbf{r}')+\rho^{\beta}(\mathbf{r}')}{\left|\mathbf{r}-\mathbf{r}'\right|} d\mathbf{r}' + \frac{\delta E^{XC}\left[\rho^{\alpha},\rho^{\beta}\right]}{\delta\rho^{\alpha}(\mathbf{r})} \\ v_{eff}^{\beta}(\mathbf{r}) &= v(\mathbf{r}) + \int \frac{\rho^{\alpha}(\mathbf{r}')+\rho^{\beta}(\mathbf{r}')}{\left|\mathbf{r}-\mathbf{r}'\right|} d\mathbf{r}' + \frac{\delta E^{XC}\left[\rho^{\alpha},\rho^{\beta}\right]}{\delta\rho^{\beta}(\mathbf{r})}. \end{aligned} \tag{2.162}$$

From eq. (2.154) to (2.162) it is clear that if the exact $E^{XC}[\rho]$ or $E^{XC}\left[\rho^{\alpha},\rho^{\beta}\right]$ functionals and their derivatives were known, DFT would provide the exact total energy of a system including the correlation energy. DFT methods, therefore, have the

[66] For a sake of semplicity the vector potential arising from the presence of a magnetic field is not considered.

potential of including the computationally difficult part in wave mechanics, the correlation energy, at a computational effort similar to that for determining the uncorrelated HF energy[67]. Although it is possible to prove that the the exchange-correlation potential v^{XC} is a unique functional valid for all systems, an explicit functional form of this potential is not known and one has to deal with approximations. Furthermore, there is no straightforward way in which E^{XC} functionals can be systematically improved, unlike other quantum chemistry methods[68].

Local density methods

The way how to proceed in DFT is to start from a model for which there is an exact solution. This model assumes that the density can be locally treated as a uniform electron gas [31] and gives rise to the local density approximation (LDA) in which the exchange energy of the exchange-correlation functional may be calculated by the Dirac formula for a uniform electron gas as

$$E^X_{LDA}[\rho] = -C_x \int \rho^{4/3}(\mathrm{r}) d\mathrm{r} \tag{2.163}$$

whose corresponding exchange potential is

$$\varepsilon^X_{LDA}[\rho] = -\left(\frac{3}{\pi}\rho(\mathrm{r})\right)^{1/3} \tag{2.164}$$

with $C_x = \frac{3}{4}\left(\frac{3}{\pi}\right)^{1/3}$.

In the more general case of different α and β densities, LDA transforms to local spin density approximation (LSDA) in which the exchange energy functional and its potential can be expressed as

$$\begin{aligned} E^X_{LSDA}\left[\rho^\alpha, \rho^\beta\right] &= -2^{1/3} C_x \int \left[\rho_\alpha^{4/3}(\mathbf{r}) + \rho_\beta^{4/3}(\mathbf{r})\right] d\mathbf{r} \\ \varepsilon^X_{LSDA}\left[\rho^\alpha, \rho^\beta\right] &= -2^{1/3} C_x \left[\rho_\alpha^{1/3}(\mathbf{r}) + \rho_\beta^{1/3}(\mathbf{r})\right], \end{aligned} \tag{2.165}$$

[67] This statement holds true for the known approximations to E_{xc}. It may infact well be that the exact exchange-correlation functional is so complicated that the computational effort of solving the KS equations will be similar to that required for solving the Schrödinger equation exactly with a wave mechanics approach.

[68] In quantum chemistry the wave function computed with SCF methods can in principle be improved to unlimited accuracy through configuration interaction or perturbation theory (cf. Sect. 2.4.1 and 2.4.4.

respectively. The correlation potential of a uniform electron gas has been determined by Monte Carlo methods for a number of different densities and it has been translated into a suitable analytical interpolation formula by Vosko, Wilk and Nursair [60] and by Perdew and Wang [61] as will be reported in the next sections.

The LSDA approximation in general underestimates the exchange energy by $\sim 10\%$, thereby creating errors which are much larger than the whole correlation energy. Electron correlation is furthermore overestimated, often by a factor of two and bond strengths are as a consequence also overestimated [31].

Gradient corrected methods

Improvements of the LSDA approach are possible only by considering the non-uniform electron gas. A step in this direction is to make the exchange and correlation energies dependent not only on the electron density but also on the derivatives of the density. However, a straightforward Taylor expansion of the density around a coordinate does not lead to an improvement of the LSDA approximation [31] and an alternative method named generalized gradient approximation (GGA) has been developed. GGA methods are sometime referred as *non-local* methods. Nevertheless, as reported in footnote 25 a non local operator is usually defined as an operator, the expectation value of which depends on the space volume and not only on the density and its derivatives at a given point [62]. Thus, exchange and correlation functionals derived in the framework of the GGA approximation are better defined as local gradient corrected functionals which can be written as the expectation values of a one-electron operator.

GGA functionals are based on the modification of the LSDA approximation to the expression of the exchange potential proposed by Perdew and Wang [63]

$$\epsilon_x^{PW86} = \epsilon_{LDA}^X \left(1 + ax_\sigma^2 + bx_\sigma^4 + cx_\sigma^6\right)^{1/15} \tag{2.166}$$

in which x_σ is a dimensionless gradient variable

$$x_\sigma = \frac{|\nabla\rho|}{\rho^{4/3}} \tag{2.167}$$

and *a*, *b* and *c* are suitable constants. However, GGA functionals can be defined in a

more general way in the form

$$E^{XC} = \int f(\rho_\alpha, \rho_\beta, \gamma_{\alpha\alpha}, \gamma_{\beta\beta}, \gamma_{\alpha\beta}) d\mathrm{r} \tag{2.168}$$

where

$$\gamma_{\alpha\alpha} = |\nabla\rho_\alpha|^2, \quad \gamma_{\beta\beta} = |\nabla\rho_\beta|^2, \quad \gamma_{\alpha\beta} = \nabla\rho_\alpha \cdot \nabla\rho_\beta \tag{2.169}$$

and f is a function of the local ρ_α and ρ_β densities and their gradient invariants [62]. In this respect, the one electron potentials corresponding to (2.168) can be obtained by the calculus of variations as following

$$\begin{aligned} V_\alpha^{XC} &= \tfrac{\partial f}{d\rho_\alpha} - 2\nabla \cdot \left(\tfrac{\partial f}{\partial\gamma_{\alpha\alpha}}\nabla\rho_\alpha\right) - \nabla \cdot \left(\tfrac{\partial f}{\partial\gamma_{\alpha\beta}}\nabla\rho_\beta\right) \\ V_\beta^{XC} &= \tfrac{\partial f}{d\rho_\beta} - 2\nabla \cdot \left(\tfrac{\partial f}{\partial\gamma_{\beta\beta}}\nabla\rho_\beta\right) - \nabla \cdot \left(\tfrac{\partial f}{\partial\gamma_{\alpha\beta}}\nabla\rho_\alpha\right). \end{aligned} \tag{2.170}$$

In the framework of the KS formalism, by expressing the orbitals as finite expansion in a basis set ϕ_μ, $(\mu = 1, 2, ...N)$

$$\psi_i^\beta = \sum_\mu c_{\mu i}^\alpha \phi_\mu, \qquad \psi_i^\beta = \sum_\mu c_{\mu i}^\beta \phi_\mu \tag{2.171}$$

so that

$$\rho_\alpha = \sum_\mu^N \sum_\nu^N \sum^N (c_{\mu i}^\alpha)^* c_{\nu i}^\alpha \phi_\mu \phi_\nu = \sum_{\mu\nu} P_{\mu\nu}^\alpha \phi_\mu \phi_\nu \tag{2.172}$$

$$\rho_\beta = \sum_\mu^N \sum_\nu^N \sum^N (c_{\mu i}^\beta)^* c_{\nu i}^\beta \phi_\mu \phi_\nu = \sum_{\mu\nu} P_{\mu\nu}^\beta \phi_\mu \phi_\nu \tag{2.173}$$

and

$$\nabla\rho_\alpha = \sum_{\mu\nu} P_{\mu\nu}^\alpha \nabla(\phi_\mu \phi_\nu) \tag{2.174}$$

$$\nabla\rho_\beta = \sum_{\mu\nu} P_{\mu\nu}^\beta \nabla(\phi_\mu \phi_\nu) \tag{2.175}$$

one obtains a finite set of algebraic equations for canonical orbitals

$$\sum_\nu^N \left(F_{\mu\nu}^\alpha - \epsilon_i^\alpha S_{\mu\nu}\right) c_{\nu i}^\alpha = 0 \tag{2.176}$$

$$\sum_\nu^N \left(F_{\mu\nu}^\beta - \epsilon_i^\beta S_{\mu\nu}\right) c_{\nu i}^\beta = 0 \tag{2.177}$$

in which $F^{\alpha}_{\mu\nu}$ and $F^{\beta}_{\mu\nu}$ are the Fock-like matrices

$$F^{\alpha}_{\mu\nu} = H^{core}_{\mu\nu} + J_{\mu\nu} + F^{XC\alpha}_{\mu\nu} \tag{2.178}$$

$$F^{\beta}_{\mu\nu} = H^{core}_{\mu\nu} + J_{\mu\nu} + F^{XC\beta}_{\mu\nu}. \tag{2.179}$$

Here $S_{\mu\nu}$ and $H^{core}_{\mu\nu}$ are the overlap and bare-nucleus Hamiltonian matrices, respectively and $J_{\mu\nu}$ is the Coulomb matrix with form

$$J_{\mu\nu} = \sum_{\lambda\sigma} P_{\lambda\sigma}(\mu\nu|\lambda\sigma) \tag{2.180}$$

where $P_{\lambda\sigma}$ is the total density matrix given by the sum of $P^{\alpha}_{\lambda\sigma}$ and $P^{\beta}_{\lambda\sigma}$. The GGA exchange-correlation parts of the Fock matrices are given by

$$F^{XC\alpha}_{\mu\nu} = \int \left[\frac{\partial f}{\partial \rho_{\alpha}} \phi_{\mu}\phi_{\nu} + \left(2\frac{\partial f}{\partial \gamma_{\alpha\alpha}} \nabla\rho_{\alpha} + \frac{\partial f}{\partial \gamma_{\alpha\beta}} \nabla\rho_{\beta} \right) \nabla(\phi_{\mu}\phi_{\nu}) \right] d\mathrm{r} \tag{2.181}$$

and

$$F^{XC\beta}_{\mu\nu} = \int \left[\frac{\partial f}{\partial \rho_{\beta}} \phi_{\mu}\phi_{\nu} + \left(2\frac{\partial f}{\partial \gamma_{\beta\beta}} \nabla\rho_{\beta} + \frac{\partial f}{\partial \gamma_{\alpha\beta}} \nabla\rho_{\alpha} \right) \nabla(\phi_{\mu}\phi_{\nu}) \right] d\mathrm{r}. \tag{2.182}$$

The equations (2.176) and (2.177) are very similar to the Pople-Nesbet equations (2.86) and (2.87) and can be solved by iterative procedure, the only difference being that the usual exchange matrix is replaced by the GGA exchange-correlation potentials (2.181) and (2.182). Furthermore, the Fock-like matrix elements (2.178) and (2.179) contain the integrals arising from the exchange-correlation terms (cf. (2.181) and (2.182)) which cannot be expressed in a closed analytical form and numerical quadrature techniques have to be employed [64]. The resulting Kohn-Sham energy is

$$E = \sum_{\mu\nu} P_{\mu\nu} H^{core}_{\mu\nu} + \frac{1}{2} \sum_{\mu\nu\lambda\sigma} P_{\mu\nu} P_{\lambda\sigma} \left(\mu\nu|\lambda\sigma\right) + E^{XC}, \tag{2.183}$$

where E^{XC} is given by eq. (2.168).

The Becke-Lee-Yang-Parr (BLYP) functional

Among the wide variety of functionals proposed in the literature, one of the most reliable is the exchange-correlation functional worked out by Becke-Lee-Yang-Parr (BLYP). The functional is composed of an exchange part proposed by Becke [65], which is a corrected local density approximation functional with the right asymptotic behavior of both the exchange-energy density

$$\lim_{r\to\infty} \varepsilon_\sigma^X = -\frac{1}{r} \tag{2.184}$$

and the spin density ρ_σ

$$\lim_{r\to\infty} \rho_\sigma = e^{-a_\sigma r} \tag{2.185}$$

where a_σ is a constant related to the ionization potential of the system. The B88 exchange functional has the form

$$E^X = E^X_{LDA} - \beta \sum_\sigma \int \rho_\sigma^{4/3} \frac{x_\sigma^2}{\left(1 + 6\beta x_\sigma \sinh^{-1} x_\sigma\right)} d\mathrm{r} \tag{2.186}$$

where x_σ is the usual dimensionless reduced density variable defined in (2.167) and the parameter β has been determined by least square fitting of the functional to the exact HF exchange energy of the noble gases helium trough radon and takes the value of $\beta = 0.0042$ [65, 66].

Based on the work of Colle and Salvetti [67, 68] who derived an approximate correlation energy formula in which the correlation energy is expressed in terms of the electron density and the Laplacian of the second-order HF density matrix, Lee, Yang and Parr [69], proposed a correlation energy density functional involving the density and the local kinetic-energy density only. For open shell cases it has the form

$$\begin{aligned} E^C \quad = \quad & -a \int \tfrac{\gamma(\mathbf{r})}{1+d\rho^{-1/3}} \times \\ & \{\rho + 2b\rho^{-5/3}[2^{2/3} C_F \rho_\alpha^{8/3} + 2^{2/3} C_F \rho_\beta^{8/3} - \rho t_W + \\ & \tfrac{1}{9}(\rho_\alpha t_W^\alpha + \rho_\beta t_W^\beta) + \tfrac{1}{18}(\rho_\alpha \nabla^2 \rho_\alpha + \rho_\beta \nabla^2 \rho_\beta] e^{-c\rho^{-1/3}} \} d\mathrm{r} \end{aligned} \tag{2.187}$$

where *a*, *b*, *c* and *d* are parameters determined by fitting data for the helium atom. γ is

a factor expressed as

$$\gamma(\mathbf{r}) = 2\left[1 - \frac{\rho_\alpha^2(\mathbf{r}) + \rho_\beta^2(\mathbf{r})}{\rho^2(\mathbf{r})}\right] \tag{2.188}$$

and the t_W^σ term is the local Weizsäcker kinetic energy density functional [31] which reads as

$$t_W^\sigma = \frac{1}{8}\left[\frac{|\nabla\rho_\sigma(\mathbf{r})|^2}{\rho_\sigma(\mathbf{r})} - \nabla^2\rho_\sigma(\mathbf{r})\right]. \tag{2.189}$$

It is worth to emphasize that due to the explicit presence of the γ term, the LYP functional does not predict any parallel spin correlation energy. In their original paper Lee, Yang and Parr reported the correlation energies for some atoms and molecules computed with the LYP functional in comparison with the original Colle-Salvetti formula and other correlation energy functionals, namely VWN [60] and P86 [70, 63] emphasizing the reliability of their approximation in predicting correlation energy.

Since their publication, the B-LYP functionals have been widely tested in the framework of the G2-method in reproducing atomic and molecular properties, i.e. ionization potential, electron affinity and enthalpies of formation [71, 72]. Furthermore, due to the excellent performances of the functionals in describing heavy metal compounds, they have been successfully used in many studies of chemical reactivity (cf. for example [73] and [74]).

Hybrid HF/KS methods and the B97 functional

From the Hamiltonian (2.143) and the definition of the exchange-correlation energy of eq. (2.155) an exact connection can be made between E^{XC} and the corresponding potential connecting the non-interacting reference system and the actual system. The resulting equation is the *adiabatic connection formula* [75] which in the KS-DFT formalism can be conveniently formulated as [76]

$$E^{XC} = \int_0^1 U_\lambda^{XC}(\lambda)d\lambda \tag{2.190}$$

where λ is an electronic coupling-strength parameter which switches on the Coulomb repulsion between electrons and U_λ^{XC} is the potential of the exchange-correlation energy at intermediate coupling strength. As pointed out by Becke this formula connects the non-interacting Kohn-Sham reference system (defined by $\lambda = 0$) to the fully interacting real system through a continuum of partially interacting systems ($0 \leq \lambda \leq 1$) all of which share a common density ρ, i.e. the density of the real, fully interacting

system (see also [31]). Thus, the exchange-correlation potential energy U_0^{XC} is the pure exchange energy of the Slater determinant of the KS orbitals, with no dynamical correlation whatsoever. At the other extreme, U_1^{XC} can be estimated by local spin density approximation.

The adiabatic connection formula, bridges the density functional theory expressed by the formalism of the KS equations, to the HF theory [31] and allows to include some fraction of the *HF*-exact[69] exchange (E_{exact}^X) in building up density functionals for the exchange-correlation energy E^{XC}. Accordingly, Becke proposed different exchange-correlation approximations, the most popular and widely used one is the so called *Becke 3 parameter functional* [76] which has the following general form

$$E_{B3}^{XC} = (1 - a_0)E_{LSDA}^X + a_0 E_{exact}^X + a_X \Delta E_{B88}^X + E_C^{LSDA} + a_C \Delta E_C^{GGA} \quad (2.191)$$

where a_0, a_X and a_C are empirical coefficients which have been determined by fitting the heats of formation of standard set of molecules and the ΔE_C^{GGA} can be alternatively the local spin density PW91 functional [61] or the gradient corrected LYP correlation functional [69].

Indeed, the B3 approximation has been recently improved by Becke who has shown that a careful parameterization of hybrid HF/KS functionals leads to an improved prediction of thermochemical data. The Becke 97 (B97) family of functionals is defined in terms of α and β spin densities by the following general form

$$E^{XC} = E_{GGA}^{X\alpha\alpha} + E_{GGA}^{X\beta\beta} + E_{GGA}^{C\alpha\alpha} + E_{GGA}^{C\beta\beta} + E_{GGA}^{C\alpha\beta} + c_X E_{exact}^X \quad (2.192)$$

namely a sum of terms for exchange, parallel-spin dynamical correlation and opposite-spin dynamical correlation. Furthermore, the exact HF exchange is considered in the functional expansion. Starting from suitable LSD approximation each contribution in eq. (2.192) is expressed as a power series

$$E = \int e_{LSDA}(\rho) \sum_i c_i u^i d\mathrm{r} \quad (2.193)$$

in terms of the finite variable

$$u = \frac{\gamma s^2}{(1 + \gamma s^2)} \quad (2.194)$$

[69]Of course, exact, here means that the exchange energy is computed by the *nonlocal* two-electron *K* operator as defined in (2.74) by using the Kohn-Sham orbitals instead the HF orbitals [76].

where s is the reduced spin density gradient

$$s = \frac{|\nabla\rho|}{\rho^{4/3}} \tag{2.195}$$

so that $0 \leq u \leq 1$. In more details, the exchange part of the functional is the GGA correction of the Dirac exchange formula (2.163) which can be obtained by substituting eq. (2.195) and (2.194) into the (2.193) and has the form

$$E^X_{GGA} = -\frac{3}{2}\left(\frac{3}{4\pi}\right)^{1/3} \sum_\sigma \int \rho^{4/3} \sum_{i=0}^{m} c_{_iX\sigma} \left[\left(\frac{\gamma_{X\sigma}\left|\nabla\rho_\sigma\right|^2}{\rho_\sigma^{8/3} + \left|\nabla\rho_\sigma\right|^2}\right)\right]^i d\mathrm{r} \tag{2.196}$$

where $c_{X\sigma}$ are the linear exchange coefficients and $\gamma_{X\sigma}$ is a non linear parameter determined from atomic computations (see Ref. 12 in [77]). The dynamical correlation partner of the B97 exchange functional treats parallel and opposite spins separately. In particular, the parallel spin correlation energy functional is written as

$$E^{C\sigma\sigma}_{GGA} = \int e^{C\sigma\sigma}_{LSDA}(\rho_\sigma) \sum_{i=0}^{m} c_{iC\sigma\sigma} \left[\frac{\gamma_{C\sigma\sigma}\left|\nabla\rho_\sigma\right|^2}{\rho_\sigma^{8/3} + \left|\nabla\rho_\sigma\right|^2}\right]^i d\mathrm{r} \tag{2.197}$$

while the anti-parallel correlation results

$$E^{C\alpha\beta}_{GGA} = \int e^{C\alpha\beta}_{LSDA}(\rho_\alpha,\rho_\beta) \sum_{i=0}^{m} c_{iC\alpha\beta} \left\{\frac{\gamma_{C\alpha\beta}\frac{1}{2}\left[\rho_\beta^{8/3}\left|\nabla\rho_\alpha\right|^2 + \rho_\alpha^{8/3}\left|\nabla\rho_\beta\right|^2\right]}{\rho_\alpha^{8/3}\rho_\beta^{8/3} + \gamma_{C\alpha\beta}\left[\rho_\beta\left|\nabla\rho_\alpha\right|^2 + \rho_\alpha\left|\nabla\rho_\beta\right|^2\right]}\right\}^i d\mathrm{r} \tag{2.198}$$

in which the average value $s^2_{avg} = \frac{1}{2}\left[s^2_\alpha + s^2_\beta\right]$ is used instead of s^2_σ in eq. (2.194). In eq. (2.197) and (2.198) the the terms $e^{C\sigma\sigma}_{LSDA}$ and $e^{C\sigma\sigma}_{LSDA}$ refer to parallel and opposite spin uniform electron gas correlation energy densities per unit volume and have the form [78, 61, 77]

$$e^{C\sigma\sigma}_{LSDA}(\rho_\sigma) = e^C_{LSDA}(\rho_\sigma, 0) = \rho_\sigma \xi^C(r_s, 1) \tag{2.199}$$

and

$$\begin{aligned} e^{C\alpha\beta}_{LSDA}(\rho_\alpha,\rho_\beta) &= e^C_{LSDA}(\rho_\alpha,\rho_\beta) - e^C_{LSDA}(\rho_\alpha,0) - e^C_{LSDA}(\rho_\beta,0) \\ &= \rho\xi^C(r_s,\zeta) \end{aligned} \tag{2.200}$$

in which

$$\begin{aligned} \xi^C(r_s,\zeta) &= \xi^C(r_s,0) + \alpha^C(r_s)\frac{f(\zeta)}{f''(\zeta)}(1-\zeta^4) \\ &+ \left[\xi(r_s,1) - \xi(r_s,0)\right] f(\zeta)\zeta^4 \end{aligned} \tag{2.201}$$

$$f(\zeta) = \frac{\left[(1+\zeta)^{4/3} + (1-\zeta)^{4/3} - 2\right]}{(2^{4/3}-2)} \tag{2.202}$$

$$\zeta = \frac{\rho_\alpha - \rho_\beta}{\rho_\alpha + \rho_\beta} \tag{2.203}$$

$$r_s = \left(\frac{3}{4\pi\rho}\right)^{1/3} \tag{2.204}$$

where $\xi^C(r_s,1)$, $\xi^C(r_s,0)$ and $\alpha^C(r_s)$ are expressed by different parameterization of the following analytical function (for further details, cf. [61])

$$\begin{aligned} G(r_s,A,a_1,b_1,b_2,b_3,b_4,p) &= -2A(1+a_1 r_s) \\ & ln\left[1 + \frac{1}{2A\left(b_1 r_s^{1/2} + b_2 r_s + b_3 r_s^{3/2} + b_4 r_s^2\right)}\right]. \end{aligned} \tag{2.205}$$

Of course, the total correlation energy is the sum of the parallel and opposite spin contributions, eq. (2.197) and (2.198).

The functional (2.192) has been parametrized by Becke using a basis set free methodology [79] by a fitting procedure with reference to the thermochemical data of the so called G1 and G2 set of molecules (cf. Sect. 2.4.6). Of course, due to the large number of coefficients involved in the optimization, different sets of parameters have been obtained [77, 80] all giving a remarkable improvement with respect to the other available density functionals in predicting atomic ionization potentials and electron affinities as well as atomisation energies. in connection with the development of an exchange-correlation density functional with a similar form to that proposed by Becke[70], Handy and co-workers [81] have re-optimized the parameters of the B97 functional in the framework of a finite gaussian basis set approach obtaining only a modest improvement with respect to the set of parameters obtained by the numerical

[70]Indeed, the functional proposed by Handy and co-worker does not include any exact HF exchange contribution.

procedure of Becke.

During the study in the framework of this thesis, we have coded the B97 functional in different quantum chemistry packages, namely CADPAC [82], TURBOMOLE [83] and Gaussian 98 [84]. Furthermore, for the first time, we have developed the code for the second derivatives of the functional, which introduced in the Gaussian 98 program allows to compute analytic frequencies of systems also involving pseudopotentials. The whole code has been written with the help of the Mathematica [85] program and several tests including numerical first and second derivative calculation have been performed in order to check correctness of the various implementations.

The performances of the B97 functional in its different parameterization have been examined and verified in the framework of the finite basis set solution of the HF/KS equations for different chemical applications. Concerning thermochemical data, its superiority over the other currently available functionals is well documented in the original papers of Becke [77, 80]. Further analysis of its performance in computing molecular structures, harmonic frequencies, dipole moments and polarisabilities and NMR absolute isotropic shielding constants can be found in [86], [81] and [87].

Performances of density functional methods

The specification of a DFT method, requires the selection of a suitable form of the exchange and correlation energy functionals. Although one may in principle select a LSDA approach for the exchange energy and a gradient corrected form for the correlation (or viceversa) this procedure is not so consistent. Gradient corrected methods usually perform better than LSDA. In general, it has been found that GGA methods often give geometries and vibrational frequencies for stable molecules of the same quality (or better) than MP2, at a computational cost similar to HF and hybrid HF/KS methods performs almost as well as the elaborate G2 model for test cases [88].

Due to the inclusion of electron correlation in a single determinantal wave function, DF methods in the spin unrestricted form Kohn-Sham formalism do not suffer from the spin contamination problem (cf. Sect. 2.4.1): indeed, $\langle S^2 \rangle$ is normally very close to the pure spin value. However, *spin contamination* is not well defined in DFT and the expectation value of S^2 should not be equal to $S_z(S_z + 1)$ [89]. This is primarily due to the fact that real systems display *spin polarization* effects [34], i.e. for open shell systems there are points in space in which ρ_β is larger than ρ_α, a fact which is very important in investigating magnetic properties of high spin systems as transition

metal compounds and clusters (cf. Chapter 3).

In solving the Kohn-Sham equations in the framework of a finite basis set approximation, the number of the two-electron integrals to be evaluated increases as M^4, due to the Coulomb integrals in eq. (2.180). Furthermore, the computational effort for the evaluation of the numerical integrals in eqn. (2.178) and (2.179) shows a cubic dependence on the system size [64]. However, the two-electron coulomb (and exchange) integrals can be now calculated with an effort which scales as M^1 by using fast multipole methods and the numerical integration required for the exchange-correlation functionals may also be reduced to a computational cost which scales linearly with the system size [90]. Thus, modern DFT techniques can be considered as true linear scaling methods and can be used to perform accurate calculations also on systems containing thousands atoms.

2.4.6 The Gaussian-2 (G2) approach

The Gaussian-2 approach [91] is a general theoretical procedure based on ab-initio molecular orbital theory computations of the total energy of molecules at their equilibrium geometry. It was developed with the objective of finding a general predictive procedure routinely applicable to any molecular system in an unambiguous manner able to reproduce known experimental energy data to a prescribed accuracy of about ± 2 Kcal mol^{-1}. It is a further improvement of the previously developed Gaussian-1 (G1) theory in which the energy of a molecular system was calculated by several steps involving HF/6-31G* geometry optimization and zero-point energy evaluation, MP2(Full)/6-31G* geometry optimization and higher order corrections to the MP2(full) energy, namely MP4SDTQ(Frozen-Core)/6311G**, MP4/6-311G**(2df) and Quadratic CISD(T)/6-311G** [92], [93].

The G2 theory corrects the deficiencies of the G1 theory which concern the non additivity of the separate basis set extensions and add a third *d* function to non hydrogen atoms and a second *p* function to the hydrogens [91]. Thus, the total energy of a molecular system in the G2 procedure is

$$E_0(G2) = E_0(G1) + \Delta + 1.14n\text{pair}, \tag{2.206}$$

where the $E_0(G1)$ is a value obtained by the G1 theory [92] and Δ is a sum of the

following terms

$$\begin{aligned} \Delta \;=\; \Delta_1 + \Delta_2 \;=\; & E\left[MP2/6-311+G(3df,2p)\right] \\ & -E\left[MP2/6-311G(2df,p)\right] \\ & -E\left[MP2/6-311+G(d,p)\right] \\ & +E\left[MP2/6-311G(d,p)\right] \end{aligned} \tag{2.207}$$

The High Level Correlation energy correction factor 1.14*n*pair (in millihartrees) refers to the number of valence electron pairs of the molecular system and has been determined to give the zero mean deviation from experiment of calculated atomisation energies of an extensive set of molecules having well-established experimental values. It is the only empirical parameter included in the theory [92].

The G2 approach has been widely applied for compounds of first- second- and third-row elements (cf. [88], [72], [94]) and is normally accepted as the reference method in determining reliable molecular energetic properties. Our interest in the G2 theory concerns the development of density functional theory in which new parametric exchange-correlation functional forms have been optimized and tested on the G2 set of chemical systems, as has been discussed in section 2.4.5.

Chapter 3

Structural, electronic and chemical properties of $\mathbf{Ni}_4^q$ ($q = 0, \pm 1$) and its carbonyl derivatives

3.1 Motivation and introduction

The electronic and geometrical structure of transition metal (TM) clusters, is still a largely unexplored area of the cluster chemistry, due to the well-known methodological and computational difficulties connected with the d electron elements. In order to elucidate the electronic properties responsible for the cluster stability, the following basic questions should be answered: (i) which role do the d electrons play in the metal-metal bond formation; (ii) to which extent are the d states localized on atoms; (iii) which mechanism gives rise to the appearance of magnetism in TM clusters?

In this section the Ni_4 cluster which is a very interesting prototype of magnetic clusters will be considered in detail. In addition, the electronic structure of the derivatives $Ni_4(CO)_X$ x $= (1, 2)$ will be discussed in order to show whether the presence of a few ligands is sufficient to quench partially or totally the cluster magnetism. The stability of the Ni_4 cluster depends only on the strength of the metal-metal bond, which may be qualitatively described as follows. The Ni atom, being at the end of the first transition series, is characterized by a large effective nuclear charge and, therefore, by localized 3d states and relatively diffuse 4s orbitals. In fact, maxima in the radial functions for 3d and 4s orbitals occur at 0.33 and 1.2 Å, respectively [95]. Therefore, in small clusters, the two-center overlap between 3d orbitals is expected to be small while

the 4s-4s interaction may play a dominant role in the metal-metal bond formation. The d^9s^1 electronic configuration is the most suitable one for promoting s-s interaction. This means that on each nickel atom taking part into the formation of a Ni_n cluster does exist a localized d-electron hole, responsible for the appearance of the magnetic moment which is expected to be close to $S = n/2$. The theoretical studies on nickel clusters so far reported in the literature [96] do not give unambiguous answers to the above questions. In particular the lack of a complete characterization of Ni_4 is mainly due to the fact that no systematic analysis has been carried out on possible spin states and isomeric forms.

The aim of the work presented in this section is to contribute to a better understanding of the electronic structures of the nickel tetramer on the basis of results of density functional theory calculations on Ni_4 and on its partially carbonylated forms.

3.2 Computational details

The electronic and geometrical structure of Ni_4^q $(q = 0, \pm 1)$ and $Ni_4(CO)_x$ $(x = 1, 2)$ has been investigated by means of DFT calculations, based on the non-local exchange and correlation energy functionals proposed by Becke and Lee, Yang and Parr (cf. Sect. 2.4.5 pag. 66). For Ni atoms the effective core potential (ECP, 18 valence electrons) proposed by Hay and Wadt [49] has been adopted together with the associated basis set, used with the contraction scheme $[2111/41/311]$ (basis set A). On carbon and oxygen atoms, the ECPs and the $(31/31)$ basis sets of [45] have been adopted. The electronic structure of Ni_4 has been first studied using the basis set A while the contraction $[2111/41/41]$ has been introduced (basis set B) for nickel atoms to reduce the computational demand for studying the carbonylated forms. However, it has been carefully checked that the two basis sets A and B give equal energy ordering of the Ni_4 forms as well as cluster stability and equilibrium geometry.

As well known, the ECP operators of [49] for Ni atoms have been derived in the context of the Hartree-Fock model. The same ECP has been tested in the framework of DFT by the carrying out BLYP calculations on low-lying states of the nickel atom (cf. Table 3.1). When compared with the experimental data [97] the DFT results appear to be much better than the corresponding HF results. In particular, the energy sequence $E(^3D) < E(^3F) < E(^1S)$ is correctly described at the BLYP level, while the HF method gives a wrong ordering of the states, predicting the ^3F state with d^8s^2

Table 3.1: Atomic properties of Ni atom.

Config.	Term symbol	Exp.	HF	DFT-BLYP
d^9s^1	^3D	0.00	1.41	0.00
d^8s^2	^3F	0.03	0.00	0.11
d^{10}	^1S	1.73	4.79	2.65
IP$^{(a)}$		7.62	9.00	7.98
EA$^{(b)}$		1.16		0.88

$^{(a)}$The IP values are computed for the process Ni (d^9s^1, ^3D)$\rightarrow$ Ni^+ (d^9,^2D).
$^{(b)}$The EA values are computed for the process Ni (d^9s^1, ^3D) $\rightarrow$ Ni (d^9s^2,^3D).

configuration, to be 1.4 eV lower in energy than the ^3D state, which is the ground state. The d^{10}, ^1S state lies too high in energy both at the HF and BLYP levels, although the latter yields considerably smaller error (about 0.9 eV) than the former (3.0 eV). The correct ordering of the low-lying configurations is an important tool, especially for the study of metal-metal bond formation. In this respect, the HF method is inadequate, because the coupling of the s electrons of the d^9s^1 configuration leading to the Ni-Ni bond is a process possible only after promotion to an excited state. In contrast such an energy demand is absent in the DFT description.

The ground state geometries of Ni_4 isomers have been determined by gradient based energy minimization in the framework of spin-polarized DFT. Special attention has been payed that self-consistent solutions belong exactly to an irreducible representation of the cluster point group. This requirement is necessary, since we wish also to address electronic and geometrical relaxations due to the occurrence of static Jahn-Teller instabilities. The stability of the Ni_4 clusters will be discussed in terms of binding energy per atom, defined as

$$\frac{BE}{n} = -\frac{E(\mathrm{Ni}_n) - nE(\mathrm{Ni})}{n}, \tag{3.1}$$

while the stability of the carbonylated derivatives is defined according to

$$\frac{BE}{x} = -\frac{E(\mathrm{Ni}_4(\mathrm{CO})_x) - E(\mathrm{Ni}_4) - xE(\mathrm{CO})}{x}, \tag{3.2}$$

where $E(\mathrm{Ni}_4)$ and $E(\mathrm{CO})$ are the energies of the most stable nickel tetramer and of the free CO ligand, respectively and x is the number of coordinated carbonyl groups.

Table 3.2: Ground state properties of Ni_4, Ni_4^+ and Ni_4^- clusters.

Cluster	State			$BE/n^{(a)}$	$IP_v^{(b)}/VDE^{(c)}$	$IP_a^{(b)}/EA^{(c)}$
Ni_4	D_{2d}	$a_2e^2b_2$	$^5A_2$	1.574	5.66	5.57
Ni_4	C_{2v}	$a_2b_2b_1b_2$	$^5B_2$	1.566		
Ni_4	C_{3v}	e^2e^2	$^5A_1$	1.552		
Ni_4	T_d	$t_2^3t_2$	$^5T_2$	1.543		
Ni_4	D_{4h}	$e^2e^2b_{1g}b_{1u}$	$^7A_{1u}$	1.527		
Ni_4^+	T_d	t_2^3	$^4A_1$	2.177		
Ni_4^-	D_{2d}	$e\ e\ a_2e\ e$	$^6A_2$	1.673	1.77	1.27
Ni_4^-	C_{3v}	$e\ e\ a_2e\ e$	$^6A_2$	1.651		
Ni_4^-	C_{2v}	$b_1a_2b_1$	$^4A_2$	1.593		
Ni_4^-	D_{2d}	$e\ e\ a_2$	$^4B_1$	1.560		

$^{(a)}$ BE/n is the binding energy per atom (eV) as expressed by the eq. 3.1.

$^{(b)}$ Vertical (IP_v) and adiabatic (IP_a) ionization potential (eV) for Ni_4.
$^{(c)}$Vertical detachment energy (VDE) and electron affinity (EA) for Ni_4^-.

3.3 Ni_4^q $(q = 0, \pm 1)$ clusters ground state properties.

The most compact form of Ni_4 is the tetrahedron. The DFT geometry optimization carried out by imposing the T_d symmetry constraint gives a form characterized by a $BE/n = 1.543$ eV and by an equilibrium distance $r^e_{\text{Ni–Ni}} = 2.39$ Å. However, the associated electronic state $^5T_2$ $(t_2^3t_2^1)$ is Jahn-Teller unstable thus, distortions along non-totally symmetric normal modes can give rise to different cluster isomers (cf. Fig. 3.1). A distortion along the C_3 axis of the tetrahedron lowers the symmetry to C_{3v} and, after the geometry optimization, a stable isomer is found with a ground state $^5A_1$ (e^2e^2). The computed symmetry independent $r^e_{\text{Ni–Ni}}$ distances are 2.44 and 2.34 Å (average value 2.39 Å) while the value of BE/n is 1.552 eV. When the distortion of the tetrahedron is applied along a C_2 axis a cluster of D_{2d} symmetry is generated. Its optimized geometry corresponds to a Jahn-Teller stable configuration of type $a_2^1e^2b_2^1$ with the two independent $r^e_{\text{Ni–Ni}}$ distances of 2.39 and 2.45 Å (average value 2.42 Å) and a BE/n of 1.574 eV (cf. Table 3.2). As expected, the geometrical rearrangement (measured in terms of variation of the average $\text{Ni} - \text{Ni}$ distances) and the energy stabilization caused by Jahn-Teller distortions are very small. Another Ni_4 isomer has been identified characterized by a lower symmetry (C_{2v}), which can be obtained by allowing a double distortion along two orthogonal twofold axis of the tetrahedron. The C_{2v} form has stability similar to all other forms $(BE/n = 1.566$ eV, cf. Table 3.2

and Fig. 3.1) but lies slightly higher in energy with respect to the D_{2d} form which is therefore the most stable Ni_4 isomer. Notice, that the transformation $T_d \rightarrow C_{2v}$ is not a spontaneous Jahn-Teller distortion. Finally, we have considered also the square arrangement (D_{4h}) which can be obtained from the stable structure D_{2d} (or the unstable structure T_d), by allowing the shift of a pair of Ni atoms along a C_2 axis. In the case of the Ni_4 (D_{4h}) cluster we found that the quintuplet state lies higher in energy than the S=3 state; in fact, the most stable square planar isomer has electronic configuration $^7A_1$ $(e_u^2 e_u^2 b_{1g}^1 b_{1u}^1)$ and shows BE/n of 1.527 eV which is significantly lower than that of all other structures including the Jahn-Teller unstable T_d form.

The removal of an electron occupying the highest t_2 orbital in Ni_4 (T_d) leads to the stable cation of T_d symmetry of Fig. 3.1. An optimum $r^e_{\text{Ni-Ni}}$ value of 2.38 Å has been computed for the Ni_4^+ species $(^4A_1,\ t_2^3\ )$, which has been used as reference structure to obtain the value for adiabatic ionization potential IP_a of the neutral tetramer which is 5.66 eV. On the contrary, the electron attachment process to the nickel tetramer leads to a much more complicated many-fold of states and isomers. Of course, both sextet and quartet states of the Ni_4^- T_d structure are Jahn-Teller unstable. However, distortions along the C_2 axis, lead to isomers in which the JT instability is not present. The resulting high spin stable isomers (cf. Fig. 3.2a and 3.2b) have D_{2d} and C_{3v} symmetry with electronic states $^6A_2$ $(e^1e^1a_2^1e^1e^1)$ and $^6A_2$ $(e^1e^1a_2^1e^1e^1)$ and BE/n of 1.673 and 1.655 eV, respectively. Both forms are characterized by the presence of four unpaired electrons in d shells plus one unpaired electron which occupies a more diffuse molecular orbital of s type. Low spin isomers are less stable (cf. Fig. 3.2c and 3.2d). They belong to the C_{2v} $(^4A_2)$ and D_{2d} $(^4B_1)$ symmetry groups and are characterized by a BE/n of 1.593 and 1.560 eV, respectively. This fact, confirms that the nickel tetramer has a strong tendency to keep at least one unpaired electron per atom in d-shells. Furthermore, for Ni_4^- clusters a VDE experimental value of ~ 1.55 eV has been measured by Ganteför [98]. This is consistent with the computed VDE of the sextet structure of Fig. 3.2a reported in Table 3.2 and is a further confirmation of the tendency of bare nickel tetramers to retain the highest possible electronic spin configuration in the ground state.

For the Ni_4^q $(q = 0, \pm 1)$, the analysis of the electron distribution has been carried out according to the standard Mulliken's scheme (cf. Table 3.3). Such a procedure is known to be based on a quite arbitrary partitioning of the electronic charge [99] and it is used here just to show in a qualitative way that the metal-metal bond in the nickel

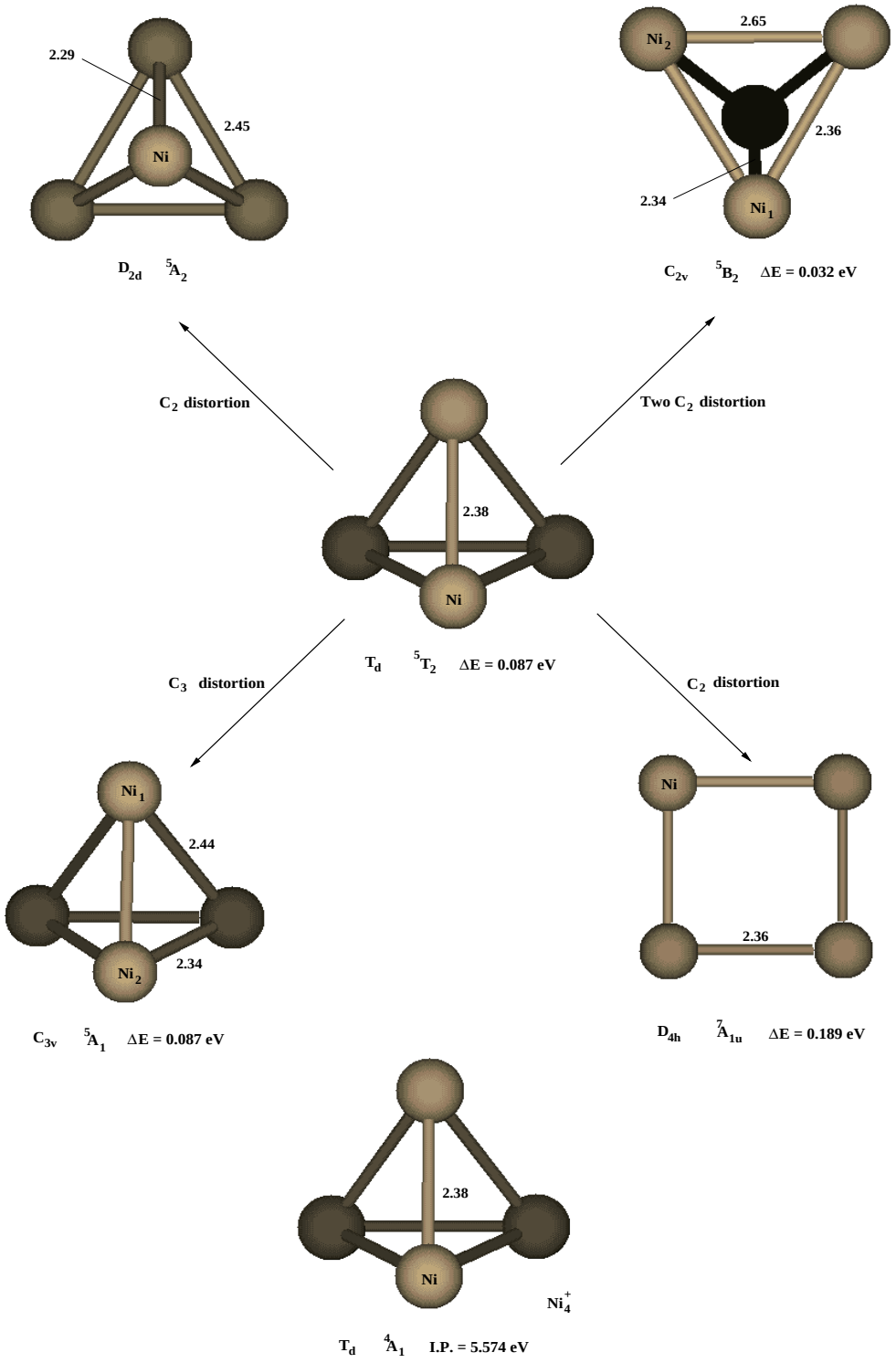

Figure 3.1: Schematic structure of the isomers of the neutral Ni_4 clusters, as derived by the distortion of the Jahn-Teller unstable T_d form. Data for the cationic Ni_4^+ are also reported.

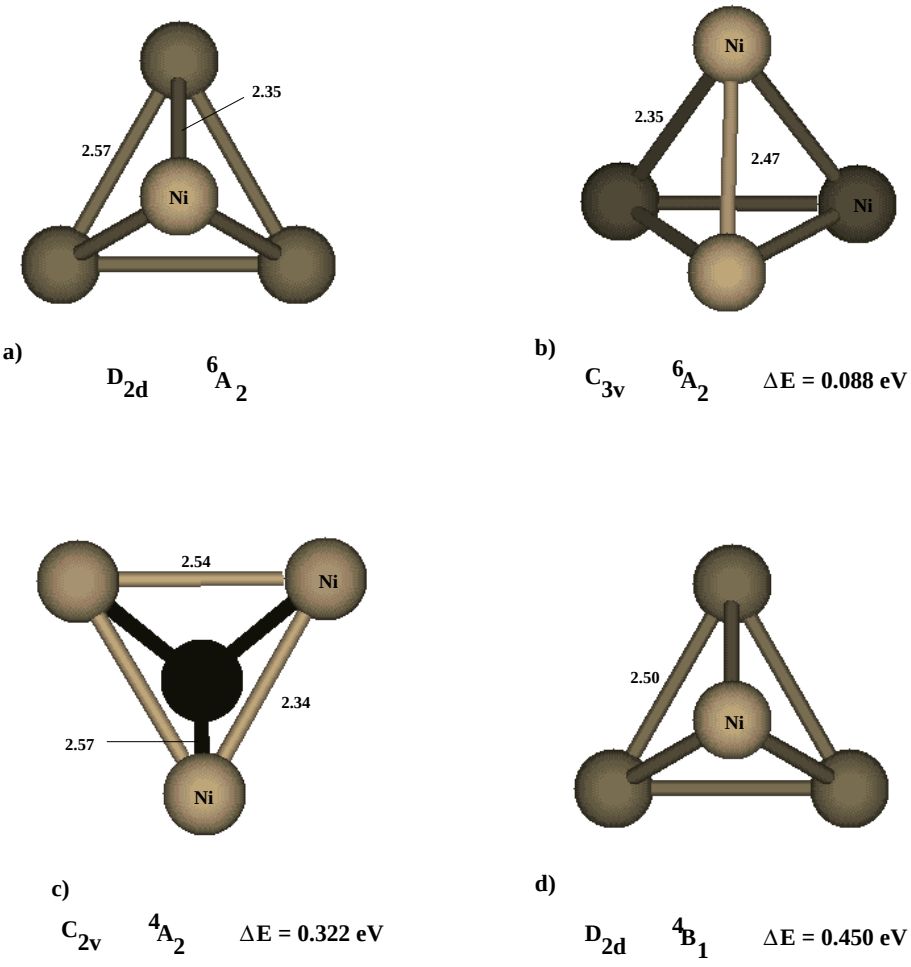

Figure 3.2: Schematic structure of the isomers of the Ni_4^- clusters, as derived by the distortion of the Jahn-Teller unstable T_d form.

Table 3.3: Electron and spin distribution in Ni_4, Ni_4^+ and Ni_4^- species[(a)]

Cluster	State	Atom	*s*	*p*	*d*
Ni_4	D_{2d}, $^5A_2$	Ni	3.006	6.019	8.975
			0.097	0.010	0.893
		Ni_1	2.822	6.047	9.037
Ni_4	C_{2v}, $^5B_2$		-0.146	0.034	0.841
		Ni_2	3.188	5.995	8.909
			0.329	-0.012	0.953
		Ni_1	3.378	5.965	8.837
Ni_4	C_{3v}, $^5A_1$		0.612	-0.048	1.015
		Ni_2	2.882	6.040	9.020
			-0.079	0.034	0.852
Ni_4	T_d, $^5T_2$	Ni	3.006	6.017	8.976
			0.014	0.010	0.886
Ni_4	D_{4h}, $^7B_{1g}$	Ni	3.162	6.005	8.783
			0.324	0.004	1.172
Ni_4^+	T_d, $^1A_1$	Ni	2.730	6.007	9.012
			-0.092	0.004	0.837
Ni_4^-	D_{2d}, $^6A_2$	Ni	3.182	6.136	8.932
			0.198	0.098	0.954
		Ni_1	2.898	6.182	9.042
Ni_4^-	C_{3v}, $^6A_2$		-0.196	0.115	0.853
		Ni_2	3.268	6.127	8.895
			0.324	0.106	0.978
		Ni_1	3.076	6.211	8.989
Ni_4^-	C_{2v}, $^4A_2$		-0.384	-0.114	0.811
		Ni_2	3.177	6.102	8.944
			0.202	0.089	0.896
Ni_4^-	D_{2d}, $^4B_1$	Ni	3.121	6.174	8.954
			-0.116	-0.020	0.887

[(a)] The atoms are labelled as in the corresponding Fig. 3.1 and 3.2. For each atom the total electron population and the spin density are reported as first and second entry, respectively

tetramer actually occurs according to the simple scheme already commented in Sect. 3.1. In fact, all the nickel atoms have a valence electron configuration very close to the $3d^9 4s^1$, with a very small occupancy of the $4p$ orbitals. In the case of the Ni_4 C_{3v} and C_{2v} forms, the symmetry independent pairs of nickel atoms have occupancy of the $4s$ orbitals slightly higher and lower than 1, respectively, but the average configuration is again very close to $3d^9 4s^1$. Is is also important to note that in Ni_4^+ and Ni_4^- the occupancy of the $3d$ orbitals remains almost unchanged and that the ionized electron in Ni_4^+ is of s character while the extra electron in the high spin anions is mainly distributed among s and p orbitals. This suggests that the nine d electrons are localized at atoms and do not contribute to bonding but play the major role in determining the magnetism of the clusters. This is further confirmed by the analysis of the electron spin distribution (cf. Table 3.3) which shows that in the neutral cluster the largest part (about 90%) of the unpaired electrons is associated with the $3d$ orbitals. Only in the case of the C_{3v} and C_{2v} forms one can note a small spin transfer between symmetry non equivalent atoms, accompanied also by a spin polarization process.

3.4 Carbonylation of the clusters: reactivity and quenching of the magnetism

The first carbonylation reaction of the nickel tetramer leads to the species $Ni_4(CO)$ in which the CO group can occupy a terminal (μ_1), or a side-bridge (μ_2) or a face-bridge (μ_3) position. The coordination of a $\mu_1 - CO$ ligand has been found to be quite unfavorable from an energetic point of view, and it will not be discussed further. When the carbonyl group occupies a μ_2 position, the symmetry of the cluster cannot be higher than C_{2v} (cf. Fig. 3.3a-d). The two more stable electronic states have high $(^5A_1)$ and lower $(^3B_2)$ spin character, and their BE/x energy is equal to 2.098 and 2.064 eV, respectively (cf. Table 3.3). Therefore, the quintet state is more stable than the triplet by about 0.033 eV and this proves that the perturbation of the electronic structure of the bare Ni_4 cluster caused by the μ_2 coordination of a single CO group is not sufficiently large to modify its ground state magnetism. In the case of the $Ni_4(\mu_3 - CO)$ species in the C_{3v} symmetry (cf. Fig. 3.3c and 3.3d), the stability order of the quintet and triplet states is reversed with respect to the μ_2 coordination (cf. Table 3.4). The $\mu_3\ ^5B_2$ quintet state is unfavorable and moreover the $\mu_3\ ^3E$ triplet state lies 0.30 eV above the $\mu_2\ ^5A_1$ state. The wavefunctions of the $Ni_4(CO)$ systems have been projected along

Table 3.4: Reaction energy and charge rearrangements due to the coordination of CO groups to the Ni_4 clusters[(a)].

Cluster	BE/x	State	Q_{Ni_4}	Q_{CO_σ}	Q_{CO_π}
$Ni_4(\mu_2-CO)$	2.098	$C_{2v},\ ^5A_1,\ \mu_2$	0.492	0.215	0.707
$Ni_4(\mu_2-CO)$	2.064	$C_{2v},\ ^3B_2,\ \mu_2$	0.506	0.214	0.720
$Ni_4(\mu_3-CO)$	1.791	$C_{3v},\ ^3E,\ \mu_3$	0.693	0.215	0.908
$Ni_4(\mu_3-CO)$	1.190	$C_{3v},\ ^5A_1,\ \mu_3$	0.746	0.321	1.068
$Ni_4(\mu_2-CO)_2$	2.123	$D_{2d},\ ^1A_1,\ \mu_2$	0.928	0.261	0.725
$Ni_4(\mu_2-CO)_2$[(b)]	1.912	$C_{2v},\ ^3B_2,\ \mu_2$	0.965	0.230	0.706
				0.224	0.713
$Ni_4(\mu_2-CO)_2$	1.826	$D_{2d},\ ^5A_2,\ \mu_2$	1.091	0.241	0.786
$Ni_4(\mu_3-CO)_2$	2.049	$C_{2v},\ ^3B_2,\ \mu_3$	1.378	0.196	0.885
$Ni_4(\mu_3-CO)_2$	2.026	$C_{2v},\ ^1A_1,\ \mu_3$	1.335	0.194	0.856
$Ni_4(\mu_3-CO)_2$	1.853	$C_{2v},\ ^5A_1,\ \mu_3$	1.302	0.256	0.906
$Ni_4(\mu_2-CO)_4$	2.254	$D_{4h},\ ^1A_1,\ \mu_2$	1.304	0.225	0.914
$Ni_4(\mu_2-CO)_4$	2.077	$D_{4h},\ ^3A_1,\ \mu_2$	1.201	0.210	0.956
$Ni_4(\mu_2-CO)_6$	1.838	$T_d,\ ^1A_1,\ \mu_2$	1.097	0.197	0.933
$Ni_4(\mu_2-CO)_6$	1.726	$D_{2d},\ ^3A_2,\ \mu_2$	1.125	0.214	0.904

[(a)] The reaction energy is the BE/x quantity (cf. eq. 3.2 of the text). $Q_{Ni_4} = q^0_{Ni_4} - q_{Ni_4}$, where $q^0_{Ni_4}$ is the total electron population on the lowest energy Ni_4 form and q_{Ni_4} is the total electron population on the Ni_4 framework in the $Ni_4(CO)_x$ system. $Q_{CO_{\sigma,\pi}} = q_{CO_{\sigma,\pi}} - q_{CO_{\sigma,\pi}}$ where $q^0_{CO_{\sigma,\pi}}$ and $q_{CO_{\sigma,\pi}}$ are the populations on free and coordinated CO, respectively.

[(b)] The population on the two symmetry independent CO groups (cf. Fig. 3.3) are reported in first and second entry, respectively.

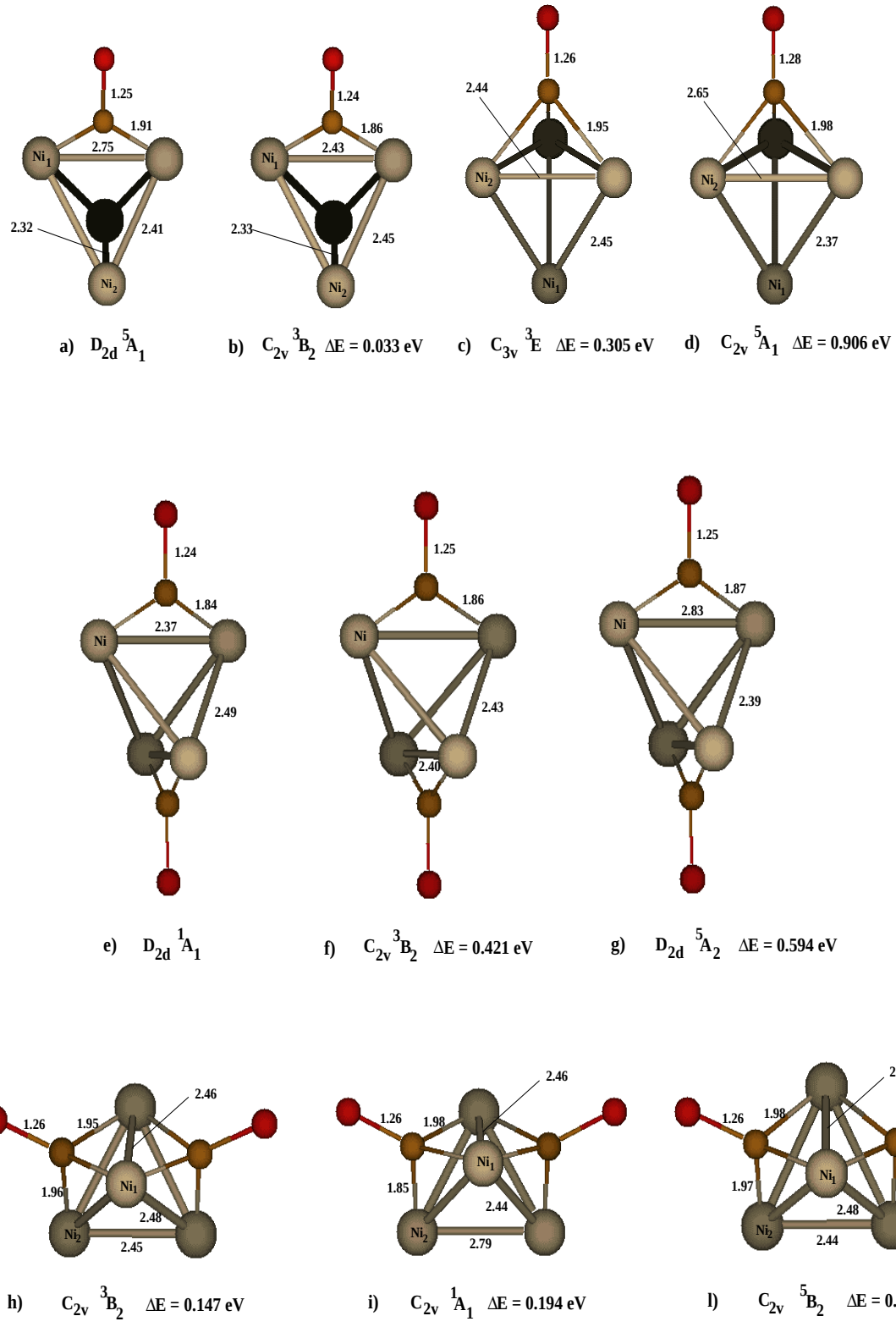

Figure 3.3: Schematic structures of $Ni_4(CO)$ and $Ni_4(CO)_2$ clusters. The monocarbonyl forms are characterized by a μ_2 (a, b) and μ_3 (c, d) coordination. The dicarbonyl derivatives have either a μ_2-μ_2 coordination (e-g) or a μ_3-μ_3 coordination (h-l).

the σ and π local components of the carbonyl group, in order to compute the amount of σ CO $\rightarrow cluster$ donation and the π $cluster \rightarrow$ CO back-donation. This leads to the Mulliken type analysis, reported in Table 3.4. In the case of the μ_2 coordination of the CO ligand, no appreciable differences can be found between the cluster-CO bonding mode in the quintet or triplet state. In both cases, the CO ligand acts, as expected, better as a π acceptor (about 0.7 electrons) than as a σ donor (about 0.2 electrons). In the case of the μ_3 coordination, the triplet and quintet states slightly differs concerning the σ and π contributions. The π back-bonding is always larger for the μ_3 than for the μ_2 coordination. This is consistent with the expectations based on qualitative arguments [100, 101]. However the present calculations show that an enhanced π back donation does not necessarily lead to a stronger cluster-CO bond.

When a second carbonyl group is added to the nickel tetramer, two different stable geometrical arrangements are obtained as reported schematically in Fig. 3.3e-l. Also in this case only the forms with both CO groups in a μ_2 or in a μ_3 coordination will be discussed, since the μ_1 coordinated carbonyls are energetically very unstable. Table 3.4 shows that in the case of the μ_2 coordination (cf. Fig. 3.3e-g) the three states $^1A_1$ (D_{2d}), $^3B_2$ (C_{2v}) and $^5A_2$ (D_{2d}) are characterized by BE/x values equal to 2.123, 1.912 and 1.826 eV, respectively. The strength of the cluster-CO bond is therefore very similar for the first and the second ligand but the perturbation of the cluster electronic structure is now so pronounced that the magnetism of the nickel tetramer is quenched. The triplet state, the lowest energy paramagnetic form, lies about 0.4 eV higher in energy than the diamagnetic form. The efficiency of the second CO ligand in quenching the Ni_4 magnetism is very evident also in the case of the μ_3 coordination. In fact, the three states $^3B_2$ (C_{2v}), $^1A_1$ (C_{2v}) and $^5B_2$ (C_{2v}) (cf. Fig. 3.3h-l) are characterized by BE/x values equal to 2.049, 2.026 and 1.853 eV, respectively. These results show that the μ_3 coordination is slightly less favorable than the μ_2 one also in the case of two coordinated carbonyls and that among the μ_3 isomers, the triplet state is the most stable one although it is almost degenerate with the singlet one while the quintet state lies much higher in energy (about 0.4 eV). This confirms that the coordination of a second CO ligand is really effective in quenching completely the paramagnetism of the nickel tetramer. The data of Table 3.4 show that the extent of σ-donation and π-back-donation present in the cluster-CO bonds in the $Ni_4(CO)_2$ species is very similar to that already discussed for the mono-carbonyl derivatives.

The addition of four and six carbonyl groups to the Ni_4 cage leads to the $Ni_4(CO)_X$

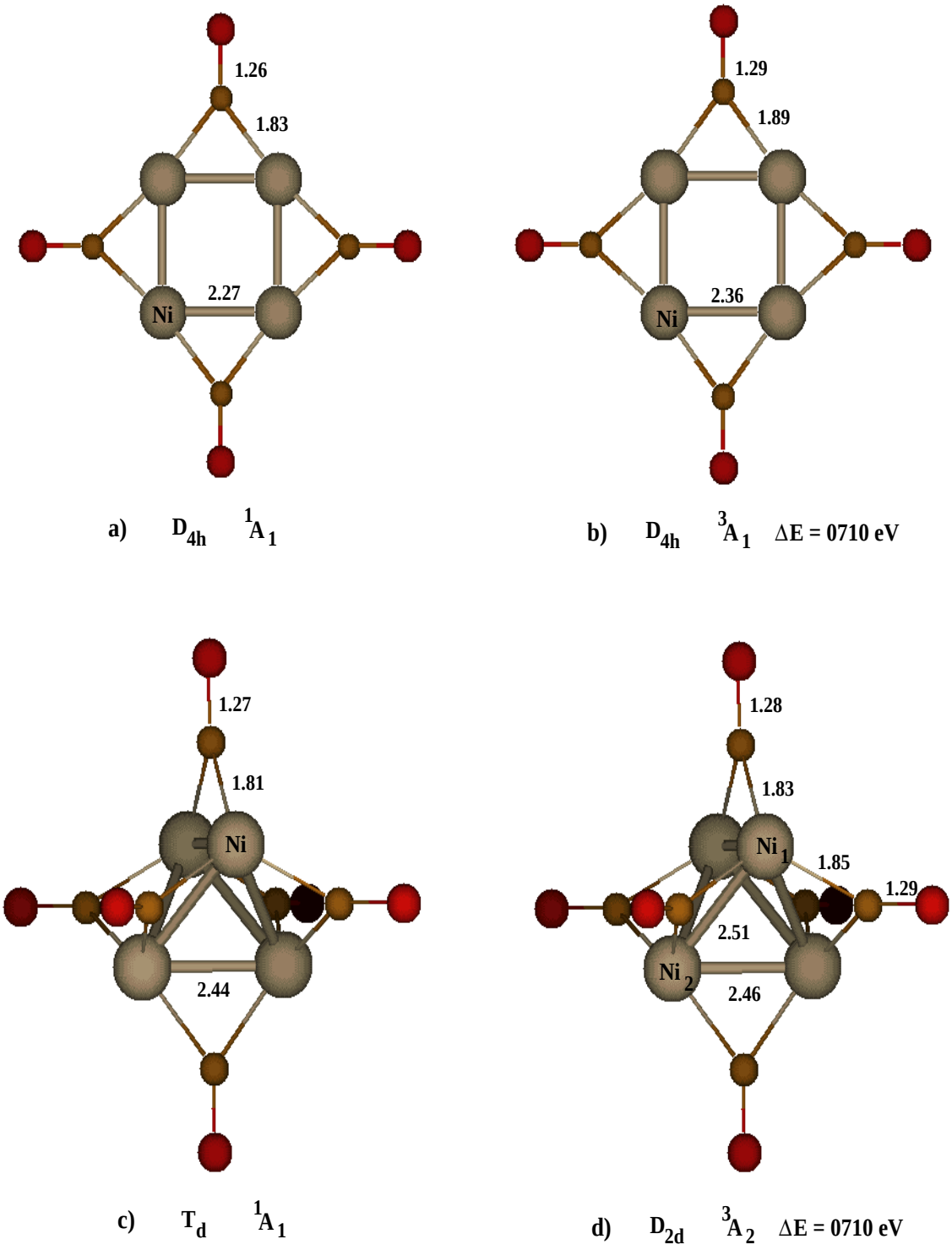

Figure 3.4: Schematic structures of $Ni_4(CO)_4$ and $Ni_4(CO)_6$ clusters. All the carbonyl derivatives are characterized by a μ_2 coordination.

$(\mathrm{x} = 4, 6)$ clusters shown in Fig. 3.4. The most stable structure of the $Ni_4(CO)_4$ is paramagnetic and belongs to the D_{4h} symmetry group in which the four carbonyl groups bridge the edge of a square planar Ni_4 framework (cf. Fig. 3.4a). This species shows the strongest binding energy per CO group (2.254 eV) among the whole series of the computed $Ni_4(CO)_X$ $(\mathrm{x} = 1 - 6)$ species (cf. Table 3.4). The corresponding triplet structure is reported in Fig. 3.4b and lies 0.710 eV higher in energy with a reduced BE/x value (2.077 eV). By comparison of the energy differences between the carbonylated nickel tetramers it becomes apparent that the higher is the number of carbonyl groups bound to the Ni_4 cage the largest is the energy gap between the (stable) diamagnetic forms and the related paramagnetic structures. This is also confirmed by the energy difference between the diamagnetic and paramagnetic $Ni_4(CO)_6$ species reported in Fig. 3.4c and 3.4d. In this case the $\Delta E = 0.672$ eV is smaller than that of the $Ni_4(CO)_4$ clusters probably due to steric effects arising from the high coverage of the Ni_4 cage by CO groups.

3.5 Summary and conclusions

On the basis of the results of DFT-BLYP calculations, on Ni_4 and $Ni_4(CO)_X$ (x=1-6) species, we have drawn the following conclusions. i) Due to the contraction of the d orbitals, the Ni $-$ Ni bond is largely dominated by s-s electron interaction. The first ionization process involves only s electrons and the d electron remains almost unmodified and strongly localized in a core-like shell, where all the unpaired spins are present. ii) The coordination of a single CO ligand to the nickel tetramer does not introduces an appreciable change in the global electron distribution and in particular does not promote any spin coupling. Thus, the spin multiplicity of the mono-carbonyl derivatives remains equal to 2, with the four unpaired electrons again localized in the 3d metal atom shells. iii) By addition of a second CO group the magnetism of the $Ni_4(CO)_2$ species is completely quenched in the case of a $\mu_2 - \mu_2$ coordination, whereas in the case of a $\mu_3 - \mu_3$ coordination, an almost complete quenching of the magnetism occurs giving rise to nearly degenerated singlet and triplet states.

Chapter 4

Structural and energetic properties of bismuth oxide clusters and their role in the oxidation reaction of alkene

4.1 Motivation and introduction

Bismuth oxides in combination with different transition metal (TM) oxides (vanadium, iron, molybdenium) [102], [103], [104] have been widely studied as catalysts in hydrocarbon oxidation processes [105]. Attempts to define a possible reaction mechanism by studying deuterated alkenes forms interacting with ^{17}O-enriched catalysts led to a model based on the assumption that the hydrocarbon oxidation proceeds via the transfer of one oxygen atom bound to the transition metal whereas another oxygen atom bound to bismuth favors the abstraction of hydrogen from the alkenes [106]. According to this model, the activated oxygen could bridge two metal atoms (Bi-O-M) [105] or bind to the transition metal with terminal bond (M=O): in both cases the TM center plays a key role in the oxygen transfer reaction. Swift et al. [107] showed that pure solid Bi_2O_3 under suitable reaction conditions could be catalytically active; in addition it was proposed that only terminal oxygen may react with the unsaturated substrate [108], [109].

Gas phase mass selected experiments carried out on bismuth oxide clusters by Kinne et al. [110] have evidenced that peaks of stable species deplete in the presence of propene. The experiments have been carried out by scattering a mixture of stable bismuth clusters with general stoichiometry $\left[BiO^{+}(Bi_2O_3)_n\right]$ in a reaction cell

fed with propene at different partial pressures both under canonical and single collision conditions (cf. Ref. [110] and [111] for details). By comparing the extent of the depletion of the bismuth oxide mass peaks in presence of the hydrocarbon with the depletion of the same peaks in presence of inert gases a conclusion has been drawn that these clusters should be studied as models for catalysts in oxidation processes of unsaturated hydrocarbons [110]. However, the experimental set-up did not allow for a characterization of the reaction products. Our first theoretical findings pointed out that the Bi-O bonds in the clusters are too strong in order to be broken to produce oxidized species and that moleculat oxygen must be present in order to promote interaction with alkenes. These results stimulated Fielicke and Rademann. (cf. [112]) to carry out experiments on the same species with the aim to determine the reaction products (cf. Fig. 4.1). They have found that the cluster with stoichiometry $Bi_3O_4^+$ forms stable complexes when interacting with alkenes, but also in this case ethene and propene oxides as neutral products have not been identified. However, a novel finding of these experiments is that the stable bismuth oxide cluster series with stoichiometry $(Bi_2O_3)_n^+$ $(n \geq 2)$ yields particularly high reactive cross sections when interacting with alkenes. Moreover, direct evidence of oxidative properties of these clusters with respect to ethene and propene via activation of molecular oxygen has been observed.

Since bismuth oxide clusters might serve as model systems for oxidation catalysts, we carried out first a systematic theoretical study of the ground state properties of the stoichiometric $Bi_3O_4^+$ and $Bi_4O_6^+$ species and their oxygenated forms. In addition, their chemical behavior in presence of ethene and molecular oxygen and propene and molecular oxygen has been investigated by following different reaction paths including: i) direct oxygen transfer reactions from the cluster to the alkenes π bond; ii) formation of stable intermediates between the clusters and the unsaturated hydrocarbons; iii) activation of molecular oxygen by the cluster and oxygen transfer reactions to the alkenes; iv) chain reactions of radical species supported on the cluster subunit. The aim of the present work is to gain a better understanding of the general chemical behavior of oxygenated Bi clusters by the identification and energetic characterization of the different chemical species involved in the reactive process.

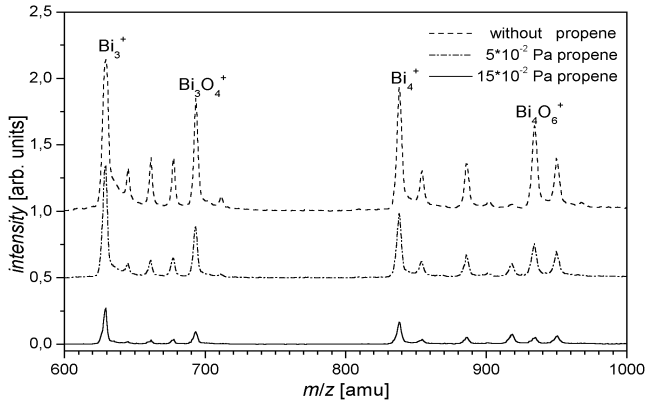

a)

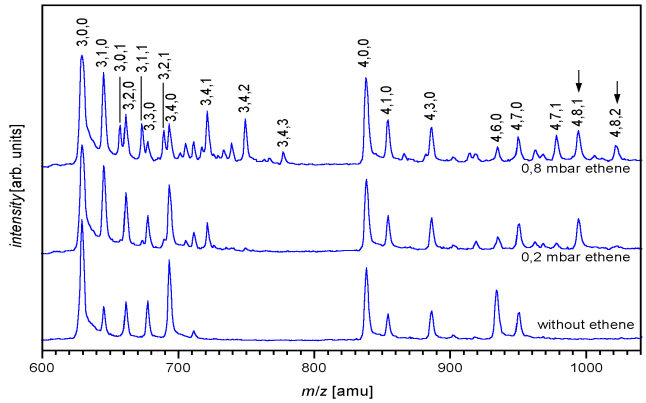

b)

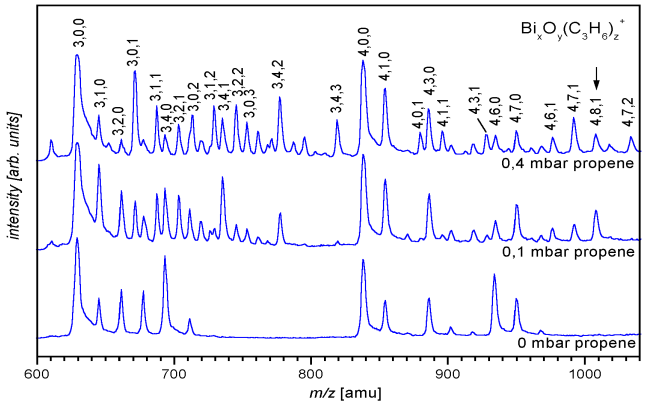

c)

Figure 4.1: **a)** Mass spectra evidencing the depletion of the cationic bismuth and bismuth oxide cluster peaks in the presence of propene as carrier gas. **b)** and **c)** Abundance spectra of the reaction products for the interaction of cationic bismuth oxide clusters and ethene and propene, respectively. The triples *x*,*y*,*z* at the top of the peaks indicate the number of bismuth, oxygen and hydrocarbon group as composition of each detached ion, respectively. (Reproduced with permission, [112]).

4.2 Computational details

All the ground state (GS) structural and electronic properties of the oxide clusters as well as the structures of the transition states (TS) along the different investigated reaction paths, has been computed by means of spin polarized density functional theory (DFT) based on the non local exchange and correlation functionals proposed by Becke (B97) [77]. As already reported in Sec. 2.4.5, the reliability of these new functionals has been tested on the G2 thermochemical data set, and in the framework of the hybrid functionals an improvement with respect to the commonly used three-parameter B3LYP functional has been achieved for calculation of atomisation energy and molecular geometries as well as vibrational frequencies. In order to reduce the computational effort, the effects of the core electrons have been represented by the effective core potentials proposed by Stevens et al. [113] for Bi atom and by Basch et al. [45] for oxygen and carbon atoms. For the valence orbitals of the Bi atom the double-zeta ECP-AO basis set of Ref. [113] augmented by a d polarization function with exponent 0.200 has been used. For oxygen and carbon atoms, we adopted the associated basis set of Ref. [45] of double-zeta type which has been augmented by sp diffuse functions (with exponents 0.0438 and 0.0845, respectively) and by a d polarization function (with exponents 0.750 and 0.800, respectively). The computed ground state properties of Bi_2, BiO^+ and BiO are in excellent agreement with experimental data [114] as shown in Table 4.1 giving us the confidence about accuracy of the chosen functionals, ECPs and AO basis set.

Critical points on the Born-Oppenheimer potential Potential Energy Surface (PES) associated with stable reactants, intermediates and products, have been determined by gradient based energy minimization methods (cf. Ref. 2.2.1) using the Gaussian 98 (G98) quantum chemistry package [84]. Transition state (TS) structures have been obtained using the Synchronous Transit Guided Quasi-Newton (STQN) Method developed by Schlegel [13] as implemented in the Gaussian 98 code.

The relative stability of the computed cluster structures is discussed in terms of binding energy (BE) per atom defined as

$$\frac{\mathrm{BE}}{(x+y)} = \frac{\mathrm{E(Bi}_x\mathrm{O}_y^+) - \mathrm{E(Bi}^+) - (x-1)\mathrm{E(Bi)} - y\mathrm{E(O)}}{(x+y)}$$

At each critical point on the PES (obtained with the convergence criteria 10^{-4} for gradients) analytical forces have been computed and vibrational frequency analysis

Table 4.1: Comparison of calculated and experimental[(a)] properties of Bi atom, Bi_2, BiO and BiO^+ dimers.

		IP (eV)	EA (eV)
Bi			
	this work	7.580	0.557
	exp$t$.[(a)]	7.285	0.910
		R_oÅ	D_o kcal mol^{-1}
Bi_2			
	this work	2.906	48.00
	expt[(a)]		47.89
BiO			
	this work	1.905	79.90
	expt.[(a)]	1.934	80.55
BiO^+			
	this work	1.792	100.21

[(a)] Experimental data for ionization potential (IP), electron affinity (EA), bond distances (R_o) and dissociation enthalpies (D_o) at 298 K from [114].

has been carried out. These quantities have been used in addition to the total energy of the system to obtain the thermodynamic properties (cf. Sec. 2.3.1) of the investigated species in order to describe the chemical processes in terms of a canonical ensemble of interacting particles in the framework of the Generalized Transition State Theory (GTST) (cf. Ref. 2.3.2). All reactions have been considered as bimolecular reactions and no tunneling effects as well as vibrational anharmonicities along the reaction path have been taken into account. Of course, this approach can lead to significant errors being the Eyring equation (cf. eq. 2.51) an exponential law. However, the purpose of this work is to give a qualitative picture of the mechanisms which are responsible for chemical oxidation reactions characterized either by relatively high reaction barrier (of the order of several kcal mol^{-1} due to the breaking of strongly covalent bonds) or by no barrier at all (due to the formation of bonds involving radical species) and tunneling as well as dynamical quantum effects in the region of the transition state can be neglected without affecting the proposed reaction models. Furthermore, we mainly deal with reactions involving relatively large compounds and heavy atoms for which more sophisticated approaches to the TS theory (cf. Variational Transition State Theory [26]) would be computationally too expensive. Nevertheless, care has been devoted to the location of the TS structures by imposing severe convergence criteria

(10^{-8} for the electronic density) and the influence of the coupling of the real vibrational normal modes of the TS complex to the imaginary reaction path mode (which is treated classically in the GTST) has been avoided by the projection technique proposed by Baboul and Schlegel [115]. In order to avoid artificial distortions of the PES it was carefully checked that the spin contamination of the wave function (density matrix) inherent to the UHF/KS method remains low also during breaking of chemical bonds (cf. Sec. 2.4.1). Charge population analysis based on the Natural Atomic Orbital (NAO) scheme (cf. Ref. [116] and references therein) has been preferred to the classical Mulliken scheme [99] due to several recognized deficiencies of the latter [117].

4.3 The $Bi_3O_X^+$ clusters; Structures and energetics

According to experimental findings [110, 118, 111] the $Bi_3O_4^+$(cf. [112]) cluster play an important role in reactions with alkenes. Therefore we first address ground state properties of $Bi_3O_X^+$ clusters and their derivatives in the context of the role they might play in oxidation processes of unsaturated hydrocarbons.

The ground state of $Bi_3O_4^+$ assumes a closed shell electronic configuration. The computed most stable structure with C_{3v} symmetry shown in Fig. 4.2a has been also previously reported as the most stable isomer of this species by MP2/6-311G* calculations [110]. The second isomer with the C_{2v} symmetry (Fig. 4.2b) lies relatively close in energy to the C_{3v} structure. The enthalpy difference between the two isomers computed at 298 K is 6.6 kcal mol^{-1} with an isomerization barrier of 7.6 kcal mol^{-1} indicating their possible coexistence as dynamical equilibrium also at room temperature. A Bi-O-Bi binding sub-unit with an average Bi-O distance of 2.08 Å characterizes both isomers, but in the C_{3v} isomer (4.2a) the μ_3 (capping) oxygen has longer distance (2.25 Å) than the μ_2 (bridging) oxygens in the C_{2v} isomer (1.94 Å) (4.2b). These values compare well with the bond distances in the BiO and BiO^+ dimers (see Table 4.1). Further analysis of geometrical data yields average O-O distance of 2.80 Å revealing pronounced compactness of these species and the absence of di-oxygen bonds. The binding energies per atoms given in Table 4.2 also compare well with the corresponding BiO and BiO^+ dissociation energies reported in Table 4.1, reflecting a very high cluster stability due to the absence of metal-metal bonds and to the presence of very stable Bi-O covalent bonds. Furthermore, according to NAO charge popula-

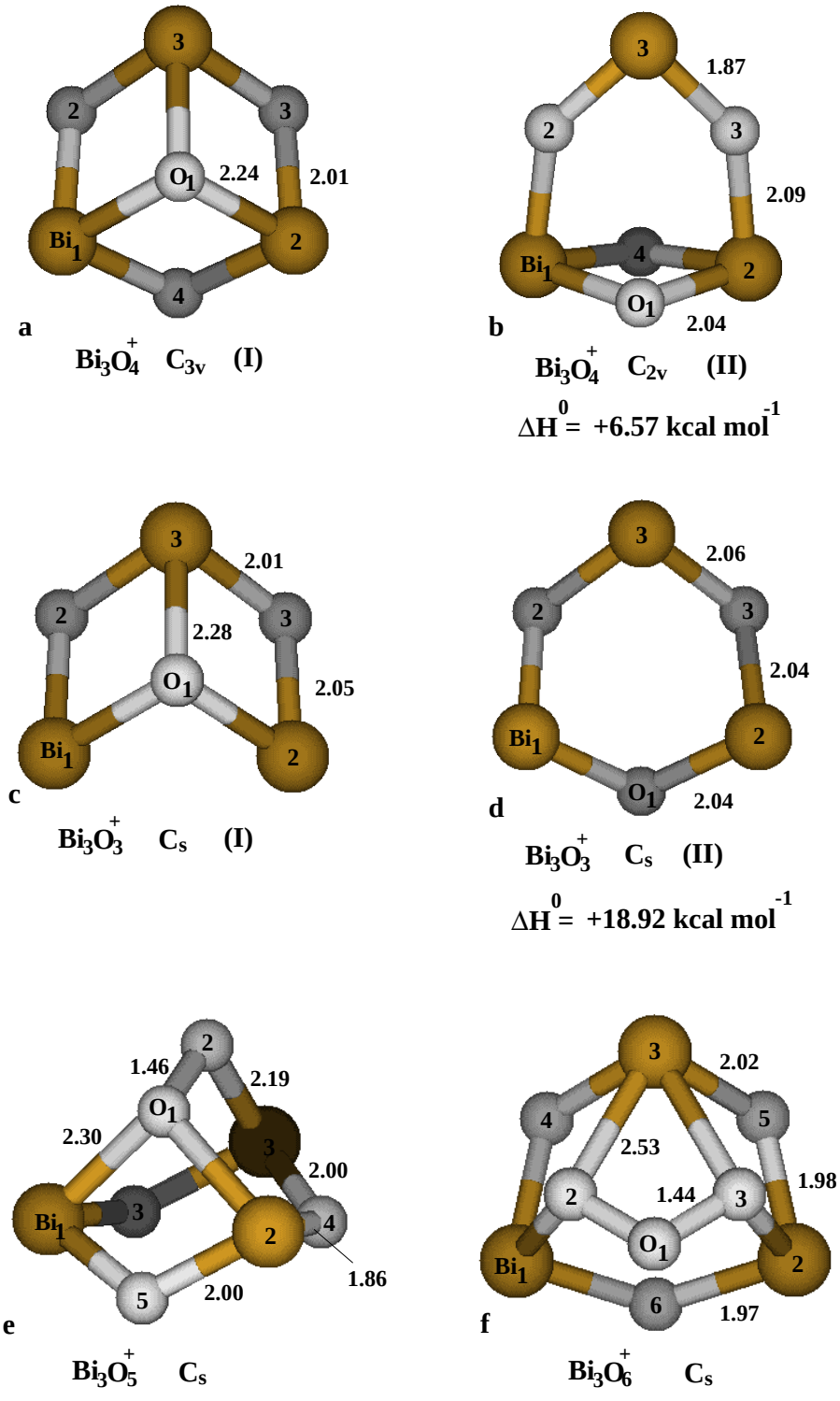

Figure 4.2: The most stable structures with symmetry labels of the $Bi_3O_y^+$ $(y = 3-6)$ clusters (isomers I). For $Bi_3O_4^+$ and $Bi_3O_3^+$, isomers II (with symmetry labels are also displayed with the corresponding enthalpy differences ΔH^o in kcal mol^{-1} (cf. Table 4.3). Bond lengths are given in angstroms (Å) in all figures.

Table 4.2: Ground state energy and properties of $Bi_3O_y^+$ $(y = 3, 4, 5, 6)$ clusters.

Cluster[(a)]	Sym.	E_{DFT} (au)	$H_{DFT}^{o(b)}$ (au)	$\Delta H^{o(c)}$ (kcal mol^{-1})	$BE/(x+y)^{(d)}$ (kcal mol^{-1})
$Bi_3O_4^+$ (I)	C_{3v}	-79.823 589	-79.802 654		86.56
$Bi_3O_4^+$ (II)	C_{2v}	-79.813 062	-79.792 179	6.57	85.61
$Bi_3O_3^+$ (I)	C_s	-63.790 459	-63.773 254		78.28
$Bi_3O_3^+$ (II)	C_s	-63.760 060	-63.743 084	18.92	75.10
$Bi_3O_5^+$ (I)	C_s	-95.728 845	-95.703 750		82.73
$Bi_3O_6^+$ (I)	C_s	-111.624 036	-111.594 488		79.05

[(a)] For geometries of clusters cf. Fig. 4.2; I and II label the isomers according to the energy ordering.
[(b)] The H_{DFT}^o is the sum of DFT electronic energy and thermal correction to enthalpy at 298 K.
[(c)] The DFT enthalpy difference between isomers.
[(d)] Binding energy per atom (cf. Sec. 4.2). The total energies of the composing atoms within the basis set and ECP approximation used (cf. Sec. 4.2) are: $E(\mathrm{Bi}) = -5.290\,762$ au; $E(\mathrm{Bi}^+) = -5.012\,182$ au; $E(\mathrm{O}) = -15.816\,088$ au.

tion analysis (cf. Table 4.3) the average partial charge of Bi atom is ~2.2 charge units which differs substantially from the formal oxidation state (+3) of the metal in ionic compounds emphasizing the covalent character of the Bi-O bonds in clusters. Other isomers with terminally bound oxygen or with higher multiplicity have considerably higher energies with respect to the isomers 4.2a and 4.2b (cf. Ref. [110]) and have not been considered further in the present study.

The removal of the μ_3 oxygen from the isomer 4.2a of the $Bi_3O_4^+$ cluster gives rise to the $Bi_3O_3^+$ species (Fig. 4.2c) with singlet ground state. The second isomer of $Bi_3O_3^+$ (Fig. 4.2d) with the ring structure has considerably higher enthalpy $(18.92$ kcal mol$^{-1})$. The calculated BE per atom of the stable $Bi_3O_3^+$ structure is 78.3 kcal mol^{-1} (cf. Table 4.2). However, this cluster can be considered as unstable toward oxidation, since an energy of $+136.1$ kcal mol^{-1} is needed for the extraction of one of the oxygens from the $Bi_3O_4^+$ cluster, whereas the $Bi_3O_3^+$ oxidation by molecular oxygen results in an extremely exoergic process $(-72.7$ kcal mol$^{-1})$ since the reaction energy barrier has not been located.

The structure of the oxygenated cluster of stoichiometry $Bi_3O_5^+$ shown in Fig. 4.2e exhibits very interesting properties. In fact, some reactions on metal oxides investigated in connection with oxidation catalysts are induced also by dioxygen species [119, 6, 120]. The computed structure of this cluster has a molecular subunit similar to the $Bi_3O_4^+$ C_{2v} cluster with an additional oxygen bound to a metal atom and to an-

Table 4.3: NAO Charge population analysis of the most stable structures of $Bi_3O_y^+$ $(y = 3, 4, 5, 6)$ and $Bi_4O_6^+$ clusters.

atoms	$Bi_3O_4^{+(a)}$	$Bi_3O_3^{+(a)}$	$Bi_3O_5^{+(a)}$	$Bi_3O_6^{+(a)}$	$Bi_4O_6^{+(b)}$
O_1	-1.44	-1.40	-0.75	-0.07	-1.42
Bi_1	2.19	1.47	2.20	2.21	2.23
O_2	-1.38	-1.35	-0.63	-0.68	-1.42
Bi_2	2.19	1.47	2.20	2.21	2.21
O_3	-1.38	-1.35	-1.40	-0.68	-1.43
Bi_3	2.19	2.18	2.17	2.21	2.21
O_4	-1.38		-1.40	-1.39	-1.42
O_5			-1.39	-1.39	-1.42
Bi_4					2.23
O_6				-1.43	-0.76

$^{(a,b)}$For structures and atom labels of the clusters cf. Fig. 4.2 and 4.3.

other oxygen atom with distances 2.02 Å and 1.46 Å, respectively. By comparing the dioxygen bond length in the cluster with the experimental value of the free molecular oxygen in its electronic ground state ^3P (1.21 Å) [114] and with the computed bond distance of the O_2^{2-} peroxide adsorbed on metals (1.49 Å) [119, 6, 120], the conclusion can be drawn that this cluster strongly supports an activated dioxygen species. In fact, the computed vibrational frequency of 928.4 cm^{-1} associated with the stretching of the O_2 group in the $Bi_3O_5^+$ cluster compares well to the experimental v(O-O) vibrational energy $(700 - 900$ cm$^{-1})$ of peroxide groups on different metal complexes [6]. However, the NAO charge distribution analysis of Table 4.3 shows that the excess of negative charge on the dioxygen group is smaller (-1.38 charge units) than in the free peroxo anion. This confirms that the elongation of the O-O distance in the bismuth oxide is not necessarily caused by a large negative charge on the dioxygen group itself and therefore its classification as peroxide should be considered as very approximate.

The ground state structure of the $Bi_3O_6^+$ cluster contains an ozonide-like group (cf. Fig. 4.2f) and according to thermochemical analysis it can be considered as a thermodynamically unstable compound exhibiting only kinetic stability (cf. Table 4.2). $Bi_3O_6^+$ can be produced by direct oxidation of $Bi_3O_4^+$ with a reaction enthalpy of $+11.4$ kcal mol^{-1} and an activation barrier of $+32.9$ kcal mol^{-1}. The key role of this compound will be pointed out in connection with the role of bismuth oxide clusters in alkenes oxidation processes (cf. Sect. 4.5).

Table 4.4: Ground state energy and properties of $Bi_4O_y^+$ $(y = 6, 7)$ clusters.

Cluster[a]	Sym.	E_{DFT} (au)	$H^{o(b)}_{DFT}$ (au)	$\Delta H^{o(c)}$ (kcal mol^{-1})	$BE/(x+y)^{(d)}$ (kcal mol^{-1})
$Bi_4O_6^+$ (I)	C_s	-117.166 494	-117.135 976		86.94
$Bi_4O_6^+$ (II)	C_s	-117.117 387	-117.086 719	30.91	83.86
$Bi_4O_6^+$ (III)	C_s	-117.087 749	-117.056 473	49.89	82.00
$Bi_4O_6^+$ (IV)	C_{2v}	-117.047 366	-117.015 687	75.48	79.47
$Bi_4O_7^+$ (I)	C_s	-133.074 809	-133.040 041		84.30
$Bi_4O_7^+$ (II)	C_s	-132.946 195	-132.912 880	79.80	76.96

[a] For geometries of clusters cf. Fig. 4.3; I to IV label the isomers according to the energy ordering.
[b] The H^o_{DFT} is the sum of DFT electronic energy and thermal correction to enthalpy at 298 K.
[c] The DFT enthalpy difference between isomers.
[d] Binding energy per atom (cf. Sec. 4.2). The total energies of the composing atoms within the basis set and ECP approximation used (cf. Sec. 4.2) are: $E(\text{Bi}) = -5.290\,762$ au; $E(\text{Bi}^+) = -5.012\,182$ au; $E(\text{O}) = -15.816\,088$ au.

4.4 The $Bi_4O_6^+$ cluster and its oxygenated derivatives

The computed most stable structure of the $Bi_4O_6^+$ cluster with C_s symmetry arises from the Jahn-Teller distortion of the most symmetric C_{3v} structure and is shown in Fig. 4.3a. It has an open shell GS electronic configuration and exhibits a very compact molecular skeleton, which maximizes the number of Bi-O bonds avoiding any Bi-Bi and O-O bonds. Notice, that this structure closely resembles the well known P_4O_6 and As_4O_6 species. The second isomer with compact structure as well as other two isomers containing O-O bonds and terminal oxygen atoms are shown in Fig. 4.3b-d. They lie more than 30 kcal mol^{-1} higher in energy with respect to the isomer 4.3a (cf. Table 4.4) and have not been considered further as important species in the present study. In the isomer I of $Bi_4O_6^+$ (Fig. 4.3a) the unpaired electron is localized on the mostly exposed bridging oxygen atom. The corresponding electronic configuration gives rise to the pronounced charge distribution on this atom as reported in Table 4.3 which allows us to consider the cluster as a radical species.

The most stable structure of the $Bi_4O_7^+$ cluster shown in Fig. 4.3e contains a dioxygen form and the unpaired electron is shared by both oxygen atoms with different weights. Similarly as in the case of $Bi_4O_6^+$ the second isomer of $Bi_4O_7^+$ lies more than 30.0 kcal mol^{-1} higher in energy with respect to the most stable one (cf. Fig. 4.3f and Table 4.4) and therefore will be not further considered.

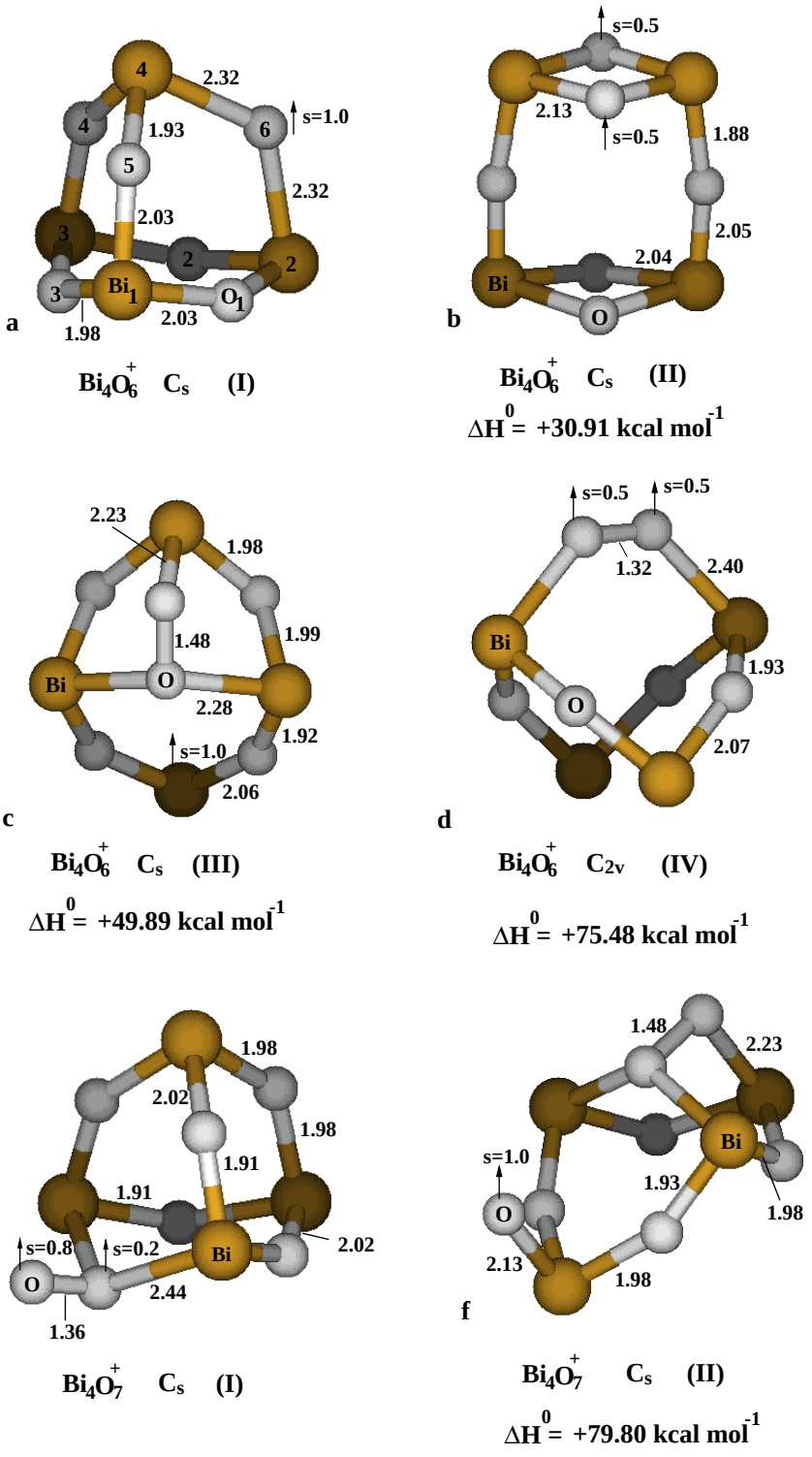

Figure 4.3: The most stable structures of Bi_4O_y $(y = 6, 7)$ (isomers I) as well as isomeric forms with higher energies, with symmetry labels and the corresponding enthalpy differences ΔH^o in kcal mol^{-1}. The spin population of the unpaired electron has been assigned to the corresponding atom.

Highly oxygenated cluster forms, such as $Bi_4O_8^+$ species are not stable, being characterized by a positive formation enthalpy in agreement with the experimental findings of Fielicke and Rademann [112].

4.5 $\mathbf{Bi_xO_y^+}$ $(\mathbf{x} = 3, 4;\ \mathbf{y} = 3 - 6)$ clusters and their interaction with ethylene

As presented in the previous sections, the chemistry of the bismuth oxide clusters is mainly dominated by the presence of strong covalent Bi-O bonds in which the formal oxidation state of the metal atom is +3. The aim of this section is to investigate the mechanisms under which the metal oxide clusters $Bi_xO_y^+$ $(x = 3, 4;\ y = 3 - 6)$ can invoke transfer of oxygen atoms to unsaturated organic substrates leading to oxygenated compounds. It will be shown that the oxidation process of π bonds involving the breaking of Bi-O bonds in the $Bi_3O_4^+$ species and the transfer of oxygen from the cluster framework to the alkene is very unfavorable and that the presence of molecular oxygen is necessary to provoke the reactivity of the cluster by involving a complex several step reaction mechanism. The role of the $Bi_4O_6^+$ clusters in promoting self propagating chain reactions involving radical species such as $(\cdot OC_2H_4)$ will be also presented in the contest of discussing model systems for catalysis.

Due to its simple form and compact size, the ethylene molecule has been chosen as reference π system. However, it will be shown that other non-conjugated unsaturated hydrocarbons such has propene do not influence significantly the energetics of the investigated reactions (cf. Sec. 4.6). Reaction channels for oxygen transfer have been intuitively selected. However, the transition state structures have been located without any constraints to geometrical parameters and molecular symmetry.

4.5.1 Oxide clusters reactions with ethylene

The oxygen transfer reaction from the stoichiometric $Bi_3O_4^+$ cluster (in both C_{3v} and C_{2v} isomeric forms) to ethene involving oxirane as oxidized product[1] is an unfavorable process from both thermodynamic and kinetic point of view. The enthalpy for the reaction

$$Bi_3O_4^+ + C_2H_4 \rightleftharpoons Bi_3O_3^+ + OC_2H_4 \tag{4.1}$$

calculated at 298 K and involving the isomer I of $Bi_3O_4^+$ (cf. Fig. 4.2a) is +52.5 kcal mol^{-1} with an activation barrier of +60.5 kcal mol^{-1}. This is mainly due to the fact that the process involves the breaking of a strong Bi-O bond and that the reduced $Bi_3O_3^+$ cluster has lower stability than its oxygenated homologous (cf. Sect. 4.3). The same oxidation process involving the isomer II of $Bi_3O_4^+$ (cf. Fig. 4.2b) yields a reaction enthalpy of +45.9 kcal mol^{-1} with an activation barrier of +53.89 kcal mol^{-1}. The lower barrier in the latter case is due to the energy difference between the two isomers (cf. Table 4.5). In fact, starting the reaction path from both isomers the same TS structure has been located implying the involvement of the isomerization of the $Bi_3O_4^+$ clusters in the oxygen transfer process. The scheme of the reaction together with its energetics and the plot of the computed values of the equilibrium constant against the temperature[2] is reported in Fig. 4.4. As expected the equilibrium constant values increase with the temperature. Nevertheless, these values are very small and allow to conclude that the reaction would not take place under standard conditions. The NAO charge population analysis of the TS structure reported in Table 4.6 compared with the values of the free clusters of Table 4.3, evidences that during the reactive process a strong charge rearrangement occurs both at atoms belonging to the cluster as well as at carbon atoms of ethene.

It is worth to emphasize that the $Bi_3O_4^+$ cluster interacts with ethene by forming stable complexes as shown in Fig. 4.5a and 4.5b. This is probably due to the fact that in the free cluster (cf. Table 4.3) the positive charge is mostly localized on metal centers associating the cluster with a Lewis acid. In both isomers of Fig. 4.5, the π character

[1] We investigated the production of oxirane as first oxidized intermediate in the oxidation of ethene. This relatively stable species could however further transform to other more stable oxides (e.g. acetaldehyde). Since the present study addresses the energetics of oxygen transfer reactions involving bismuth oxide clusters, we focused on oxirane as product.

[2] According to the transition state theory, the equilibrium constant as a function of the temperature of a chemical reaction may be computed as the ratio between the forward (reactants to TS) and backward (products to TS) reaction rate constants evaluated as in the eq. 2.63, pag. 30.

Figure 4.4: Structures of reactants, TS and products as well as the computed energetics and the plot of the equilibrium constant values as a function of the temperature for the reaction 4.1.

Table 4.5: Ground and transition state (TS) energies of $Bi_3O_y^+$ $(y = 4, 5, 6)$ clusters interacting with ethylene.

Structures	E_{DFT} (au)	H^0_{DFT} (au)
$(Bi_3O_4^+)C_2H_4$ (I)$^{(a)}$	-93.506 793	-93.428 894
$(Bi_3O_4^+)C_2H_4$ (I)$^{(a)}$	-93.486 241	-93.408 694
$(Bi_3O_4^+)C_2H_4$ (TS)$^{(a)}$	-93.475 263	-93.398 676
$(Bi_3O_4^+)C_2H_4$ (TS)$^{(b)}$	-93.385 643	-93.308 132
$(Bi_3O_5^+)C_2H_4$ (TS)$^{(c)}$	-109.366 685	-109.286 238
$(Bi_3O_6^+)C_2H_4$ (TS)$^{(d)}$	-125.247 975	-125.163 216
$O_2^{(e)}$	-31.817 039	-31.809 969
$C_2H_4^{(f)}$	-13.656 457	-13.601 838
$OC_2H_4^{(g)}$	-29.608 472	-29.547 570

$^{(a)}$For geometries of clusters cf. Fig. 4.5; I and II label isomers according to the energy ordering; TS labels the structure of the activated complex for the formation of the most stable isomer I.
$^{(b,c,d)}$For the geometry of the activated complex cf. Fig 4.4, Fig. 4.5 and Fig. 4.6, respectively.
$^{(e,f,g)}$Energies and enthalpies for ground state structures of molecular oxygen (^3P), ethene $(^1A_1)$ and oxirane $(^1A_1)$.

of the carbon-carbon bond is lost and one of the cluster oxygen forms an alcohol-like bond whereas the metal atom acts as acid site. The energy difference between the two isomers (cf. Fig. 4.5a and Fig. 4.5b) is +12.7 kcal mol^{-1} with an isomerization barrier of +13.7 kcal mol^{-1} due to the breaking of a strong Bi-O bond. Notice, that the structural sub-unit of the pseudo ethyl alcohol in the framework of the isomer 4.5b is closer associated to the most stable conformation of the free alcohol, than in the case of the isomer 4.5a. The TS structure for the formation of the isomer 4.5a is shown in Fig. 4.5c. The reaction is exoergic by 16.5 kcal mol^{-1} and the energy barrier has been computed as +3.7 kcal mol^{-1} (cf. Table 4.5). Furthermore, the values of NAO charge population analysis for isomer 4.5a and 4.5b and for the TS of the $(Bi_3O_4^+)C_2H_4$ reported in Table 4.6, evidence that the hydrocarbon looses its π character already in the activated complex.

The ethene oxidation reaction involving the $Bi_3O_5^+$ cluster is a thermodynamically favorable process and the relatively low reaction energy barrier offers also accessible kinetics. In fact, the reaction enthalpy of the process

$$Bi_3O_5^+ + C_2H_4 \rightleftharpoons Bi_3O_4^+ + OC_2H_4 \tag{4.2}$$

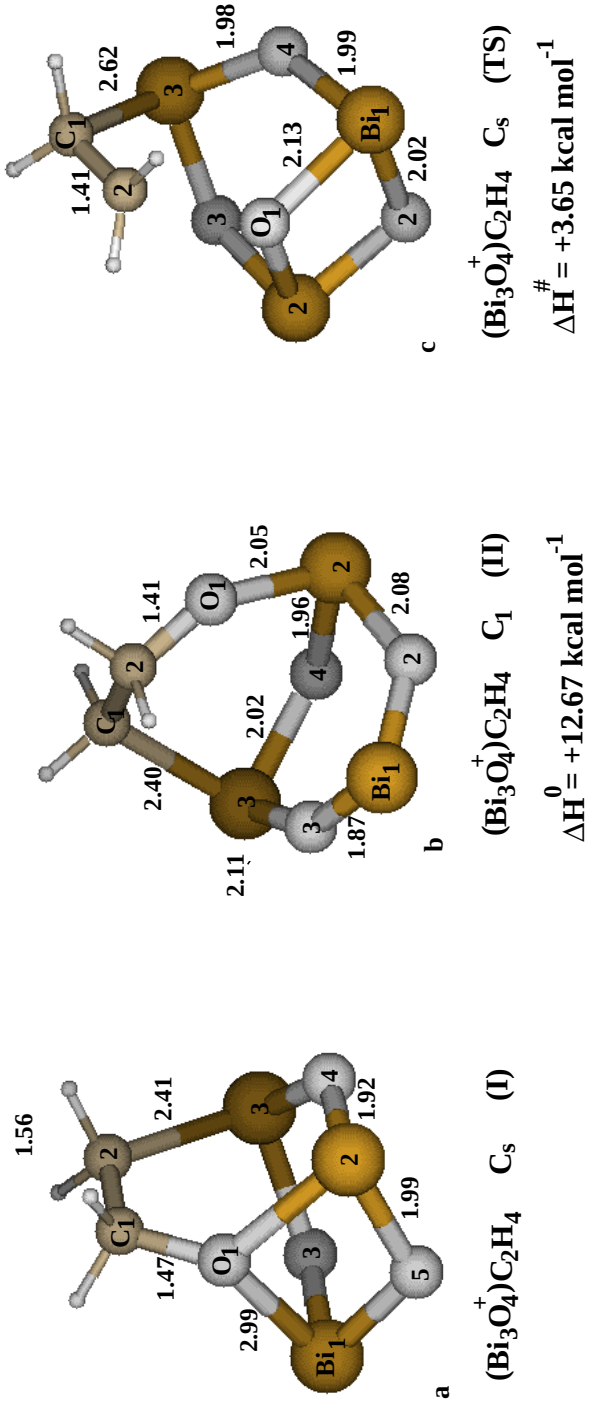

$(Bi_3O_4^+)C_2H_4$ C_s (I)

$(Bi_3O_4^+)C_2H_4$ C_1 (II)

$(Bi_3O_4^+)C_2H_4$ C_s (TS)

ΔH^0 = +12.67 kcal mol^{-1}

$\Delta H^{\#}$ = +3.65 kcal mol^{-1}

Figure 4.5: Structures of isomers I and II of the $(Bi_3O_4^+)C_2H_4$ complex together with the TS and the corresponding enthalpy differences ΔH^o expressed in kcal mol^{-1} (cf. also Table 4.5.

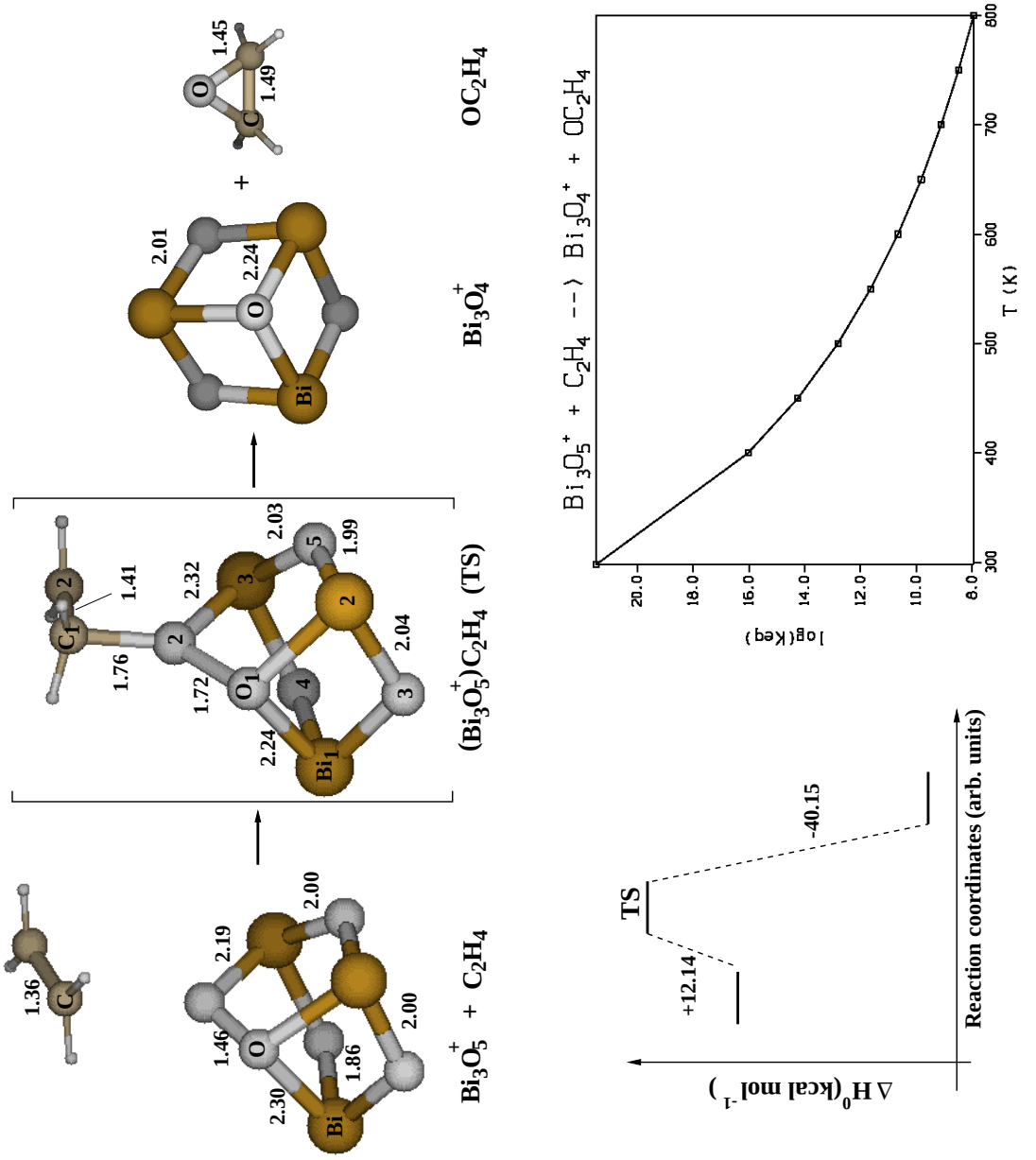

Figure 4.6: Structures of reactants, TS and products as well as the energetics and the plot of the equilibrium constant values as a function of the temperature for the reaction 4.2.

Table 4.6: NAO charge population analysis of the transition state structures of $Bi_3O_y^+$ $(y = 4 - 6)$ clusters interacting with ethylene.

Atoms	$(Bi_3O_4^+)C_2H_4$ (I)$^{(a)}$	$(Bi_3O_4^+)C_2H_4$ (TS)$^{(a)}$	$(Bi_3O_4^+)C_2H_4$ (TS)$^{(b)}$	$(Bi_3O_5^+)C_2H_4$ (TS)$^{(c)}$	$(Bi_3O_6^+)C_2H_4$ (TS)$^{(d)}$
O_1	-1.01	-1.34	-0.84	-0.96	-0.32
Bi_1	2.21	2.19	2.12	2.20	2.20
O_2	-1.38	-1.37	-1.39	-0.68	-0.68
Bi_2	2.21	2.19	1.74	2.20	2.21
O_3	-1.40	-1.41	-1.40	-1.38	-0.69
Bi_3	2.02	2.14	1.54	2.20	2.22
O_4	-1.40	-1.41	-1.38	-1.41	-1.39
O_5				-1.41	-1.39
O_6					-1.39
C_1	-0.98	-0.85	-0.12	-0.18	-0.25
C_2	-0.08	-0.11	-0.18	-0.52	-0.40

$^{(a)}$For structures and atom label of the clusters cf. Fig. 4.4.
$^{(b,c,d)}$For structures and atom label of the clusters cf. Fig. 4.4, Fig. 4.5 and Fig. 4.6, respectively.

amounts to 28.0 kcal mol^{-1} with an activation barrier of +12.1 kcal mol^{-1} (cf. Fig. 4.5 and Table 4.5). In Fig. 4.5 the plot of the equilibrium constant of the reaction as a function of the temperature is also reported. Of course, due the exoergicity of the reaction it shows an exponential decay by increasing the temperature. However, the predicted values of K_{eq} is large enough to ensure that reactive collisions would lead to products with a probability close to unity. The reactive interaction gives rise to more pronounced charge redistributions on both carbon atoms than in the other cases (cf. Table 4.6). Furthermore, the TS structure closely resembles the geometry of reactants, in agreement with the prediction of the Hammond postulate for exoergic reactions.

According to results of Section 4.3, the $Bi_3O_6^+$ oxide is thermodynamically unstable but kinetically stable; analogous behavior of the free O_3 suggested us to investigate the thermochemistry of the following reaction:

$$Bi_3O_6^+ + C_2H_4 \rightleftharpoons Bi_3O_5^+ + OC_2H_4 \tag{4.3}$$

This reaction is exoergic by 34.5 kcal mol^{-1} and has to overcome a barrier of +20.8 kcal mol^{-1} in order to take place (cf. Fig. 4.6 and Table 4.5). Of course, due to the strong exoergicity of the process, the plot of the equilibrium constant for the reaction

4.3 as function of the temperature reported in Fig. 4.7 is typical of a favorable process. However, this process plays an important role in defining a possible catalytic cycle involving bismuth oxide clusters and molecular oxygen and the relatively high reaction energy barrier requires a more extensive investigation of its kinetics. In Fig. 4.8a and 4.8b we present the plots of the activation enthalpy and entropy for the bimolecular reaction 4.3 computed from the partition functions of the reactants and TS structures, respectively (cf. Sec. 2.3). Due to the temperature dependence of the various translational, rotational and vibrational contributions to the thermodynamics functions (cf. Tab. 2.1 pag. 26), the absolute values of ΔH_{att} and $T\Delta S_{att}$ increase with the temperature. Nevertheless, from eqs. 2.63 to 2.66 it follows that, mainly due to the rate of the molecular collisions measured by the pre-exponential factor A (cf. Fig 4.8d), the plot of the rate constant for the forward reaction

$$Bi_3O_6^+ + C_2H_4 \rightarrow Bi_3O_5^+ + OC_2H_4$$

as function of the temperature (cf. Fig. 4.8e) identifies a favorable process. Fig. 4.8f shows the rate constant of the backward reaction

$$Bi_3O_5^+ + OC_2H_4 \rightarrow Bi_3O_6^+ + C_2H_4$$

which has been used to define the equilibrium constant of the whole process reported in Fig. 4.7.

4.5.2 Oxygen transfer reactions; The activation of molecular oxygen by the $Bi_3O_4^+$ cluster

As mentioned in the introduction to this chapter, Kinne et al. [110] proposed that the $Bi_3O_4^+$ cluster can be used as a model system to study catalytic properties of bismuth oxides in oxidation processes of alkenes. The global gas phase oxidation reaction of ethene (or π bonds in general) involving the $Bi_3O_4^+$ species proceeds according to the following chemical equation to form oxirane:

$$Bi_3O_4^+ + 2C_2H_4 + O_2 \rightleftharpoons Bi_3O_4^+ + 2OC_2H_4$$

with a reaction enthalpy of $\Delta H^o_{298} = -51.1$ kcal mol^{-1} which is a thermodynamically favorable process. As pointed out in Section 4.5 the transfer of oxygen from the $Bi_3O_4^+$

Figure 4.7: Structures of reactants, TS and products as well as the energetics and the plot of the equilibrium constant values as a function of the temperature for the reaction 4.3.

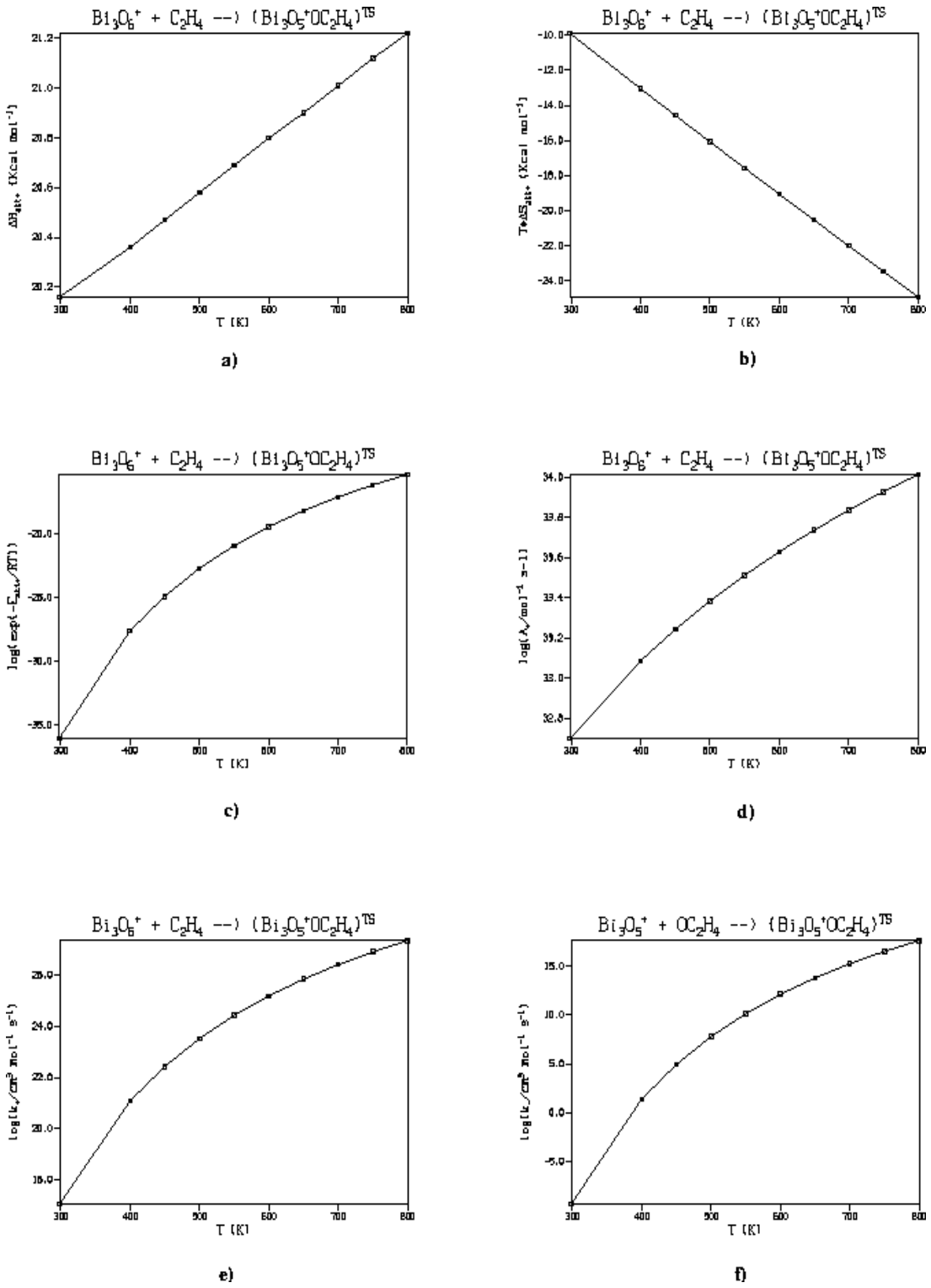

Figure 4.8: Various thermodynamics and kinetics contributions for the reactive process 4.3, Fig. 4.7.

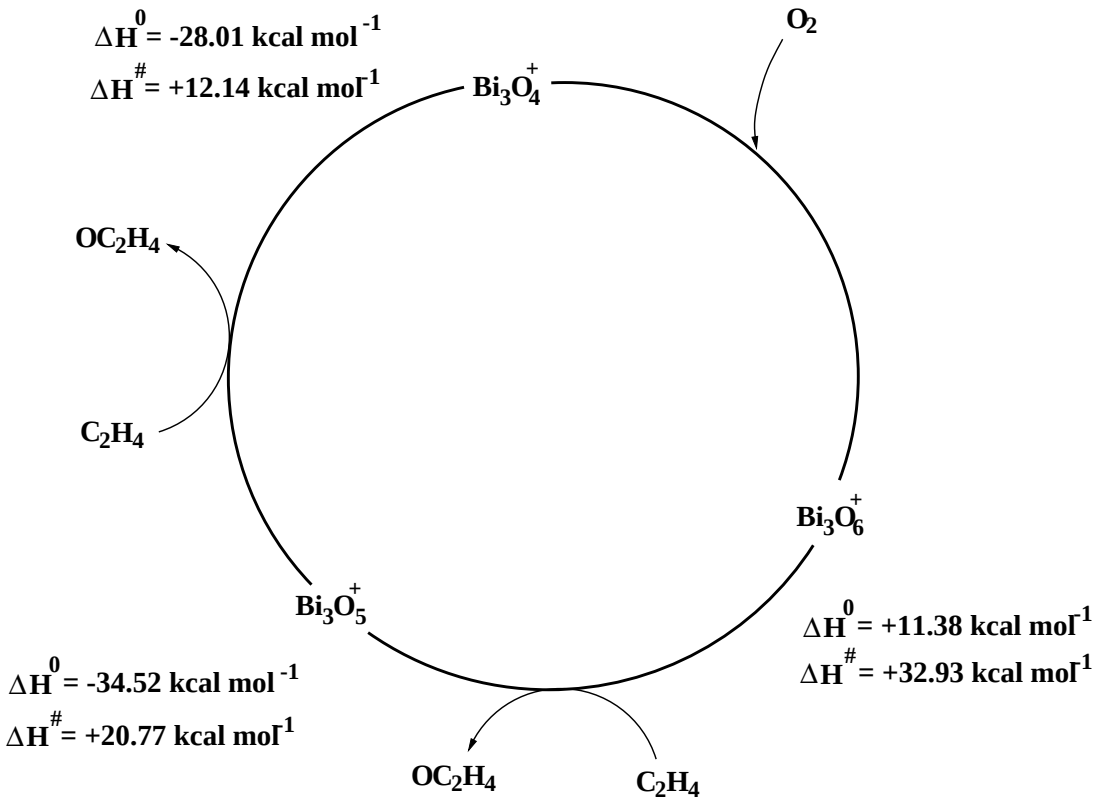

Figure 4.9: Scheme of the proposed catalytic cycle involving the $Bi_3O_4^+$ species and its oxygenated derivatives.

cluster to the alkene requires a large amount of energy (cf. eq. 4.1). Thus, in an oxidative catalytic cycle the cluster alone cannot act as catalyst by transferring its own oxygen atoms. On the other hand, the oxidation of ethene involving the $Bi_3O_5^+$ cluster (cf. eq. 4.2) shows a favorable thermodynamics and kinetics as well. Moreover, once the $Bi_3O_6^+$ has been formed, it reacts easily further to form oxirane and $Bi_3O_5^+$ as products (cf. eq. 4.3 and Fig. 4.7). Based on these results, a three step oxidation process according to the global thermodynamic cycle shown in Fig. 4.9 can be proposed.

FIRST STEP:

$$Bi_3O_4^+ + O_2 \rightleftharpoons Bi_3O_6^+$$

$\Delta^1 H^o_{298} = +11.4$ kcal mol^{-1}; $\quad \Delta^1 H^{\#}_{298} = +32.9$ kcal mol^{-1}

SECOND STEP:

$$Bi_3O_6^+ + C_2H_4 \rightleftharpoons Bi_3O_5^+ + OC_2H_4$$

$\Delta^2 H^o_{298} = +-35.4$ kcal mol^{-1}; $\quad \Delta^2 H^{\#}_{298} = +20.8$ kcal mol^{-1}

THIRD STEP:

$$Bi_3O_5^+ + C_2H_4 \rightleftharpoons Bi_3O_4^+ + OC_2H_4$$

$\Delta^3 H^o_{298} = +-28.0$ kcal mol^{-1}; $\quad \Delta^3 H^{\#}_{298} = +12.1$ kcal mol^{-1}

The thermodynamics energy balance of the process is $\Delta^1 H^o_{298} + \Delta^2 H^o_{298} + \Delta^3 H^o_{298} = -51.1$ kcal mol^{-1} corresponding to the energetics of the stoichiometric reaction

$$2C_2H_4 + O_2 \rightleftharpoons 2OC_2H_4.$$

Furthermore, the high exoergicity of the second and third step compared to the activation enthalpy at each step suggests that once the first reaction has been activated the cycle will self propagate.

The above discussed cycle can in principle exist. However, according to the findings of the Section 4.5, which have been confirmed by the experimental results of Fielicke and Rademann (cf. Fig. 4.1a,b), the $Bi_3O_4^+$ cluster interacting with π systems has a strong tendency to form stable complexes. Thus, the cycle of Fig. 4.9 would be very difficult to realize. Nevertheless, it shows that the presence of molecular oxygen is necessary to provoke the reactivity of the clusters as will be discussed in the next Sections.

4.5.3 The $Bi_4O_6^+$ cluster as a promoter of chain reactions involving ethylene

The most stable structure of the $Bi_4O_6^+$ cluster has been characterized as a radical species in section 4.4. According to the experimental observation [112] this species exhibits particularly large reactive cross section when interacting with a mixture of alkene and molecular oxygen, leading to the formation of compounds with identified masses corresponding to stoichiometry $Bi_4O_8^+(C_2H_4)_z$ $(z = 1, 2)$. However, from both experimental evidence and theoretical prediction the $Bi_4O_8^+$ free species is expected to be unstable (cf. Sec. 4.4. This fact suggested us to investigate the gas-phase reactivity of the $Bi_4O_6^+$ cluster in stepwise reactions involving ethene as first reactant. The results are summarized in Fig. 4.10 and Table 4.7, which will be used for further

Table 4.7: Energies of the most stable structures of the $Bi_4O_6^+O_y(C_2H_4)_z$ ($y = 0-3$; $z = 1, 2$) complexes.

structures	E_{DFT} (au)	H^o_{DFT} (au)
$(Bi_4O_6^+)C_2H_4^{(a)}$ (b)	-130.876 892	-130.789 983
$(Bi_4O_6^+)C_2H_4O_2^{(a)}$ (c)	-162.748 185	-162.648 492
$(Bi_4O_6^+)C_2H_4O_2C_2H_4^{(a)}$(d)	-176.417 722	-176.261 679
$(Bi_4O_6^+)C_2H_4O^{(a)}$(e)	-146.843 400	-146.750 800
$(Bi_4O_6^+)C_2H_4OC_2H_4^{(a)}$(f)	-160.541 062	-160.389 285
$(Bi_4O_6^+)C_2H_4OC_2H_4O_2^{(b)}$(k)	-192.413 183	
$(Bi_4O_6^+)C_2H_4OC_2H_4O_2C_2H_4^{(b)}$(l)	-206.084 347	
$THF^{(c)}$	-43.342 689	-43.221 853

$^{(a)}$For geometries of clusters cf. Fig. 4.10b-f.
$^{(b)}$Complexes involved in path V of Figure 4.11.
$^{(c)}$Tetrahydrofuran (path II of Fig. 4.11).

discussion.

Fielicke and Rademann (cf. 4.1b and [112]) evidenced by experiments that the bismuth oxide clusters can easily bind one or more ethene molecules. This is also the case of the $Bi_4O_6^+$ species, which forms a stable complex $(Bi_4O_6^+)C_2H_4$ (adduct (b) of Fig. 4.10) by a strongly exoergic process (-32.7 kcal mol^{-1}). The resulting complex exhibits a radical nature with the unpaired electron being localized on the terminal carbon atom. Furthermore, it is important to emphasize that all attempts to locate a TS structure along the specified reaction coordinates failed both in constrained and unconstrained PES-TS optimization. This can be considered as an indication that the reaction might occur also due to very favorable kinetics. The complex $(Bi_4O_6^+)C_2H_4$ (cf. Fig. 4.10b) with the radical center has been identified in experiments as well. However, we considered it as reactive intermediate which can further react with molecular oxygen by following the idea that O_2 will attack the organic substrate of the complex and the product will retain its radical character. In fact, it has been found (step (b) to (c) of Fig. 4.10) that the addition of O_2 is a very exoergic process ($\Delta H^o_{298} = -30.4$ kcal mol^{-1}) leading to superoxide species $(Bi_4O_6^+)C_2H_4O_2$ (cf. adduct (c) of Fig. 4.10). Also in this case, a TS structure could not be located probably due to the high reactivity of radical species such as $(Bi_4O_6^+)C_2H_4$[3].

[3]This hypotesis has been also confirmed by the experimental mass spectra findings of Fielicke et al. who found that small complexes easily react further to produce high masses products of stoichiometry $(Bi_4O_6^+)O_y(C_2H_4)_z$ (cf. [112]).

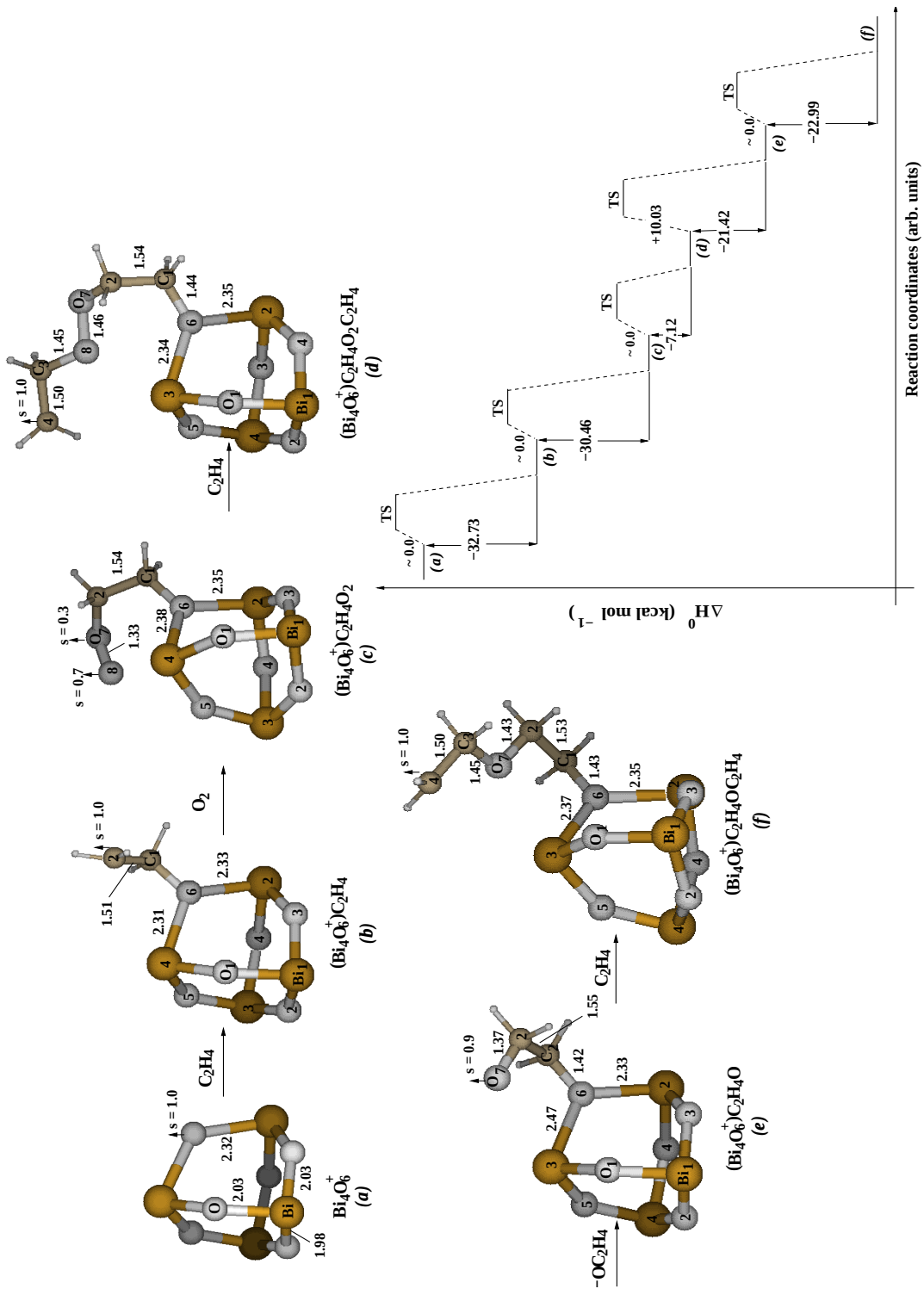

Figure 4.10: Structures and energetics of complexes with the $Bi_4O_6^+$ cluster obtained by adding oxygen and ethene (b-d) and releasing oxirane (e) and adding ethene (f).

Stimulated by this result and by the experimental findings, we investigated the possibility that the radical reactions could proceed via addition of another ethene forming an C-C-O-O-C-C pattern attached to the cluster until dissociation of some species might occur. Accordingly, reaction of the superoxide species $(Bi_4O_6^+)C_2H_4O_2$ with an ethene gives rise to an exoergic process (step (c) to (d) of Fig. 4.10) with the energy gain of 7.1 kcal mol^{-1}, which is considerably smaller than those of the previous steps. Also the reaction leading to $(Bi_4O_6^+)C_2H_4O_2C_2H_4$ is characterized by nearly zero energy barrier. Notice, that the adduct (d) of Fig. 4.10 closely resembles a peroxide species, with an extremely activated O-O bond (1.46 Å) which can be considered as a precursor for bond breaking producing oxirane. Indeed, such a dissociation occurs easily from an energetic point of view: the computed reaction energy is $\Delta H^o_{298} = -21.4$ kcal mol^{-1} with an activation energy barrier of $+10.0$ kcal mol^{-1}. This is schematically shown in Fig. 4.10 for the step (d) to (e) in which an oxirane molecule is released and a radical species of stoichiometry $(Bi_4O_6^+)C_2H_4O$ is formed (the TS structure is not reported in the Figure). The latter species can, in principle, react following different paths: i) to dissociate a second OC_2H_4 molecule and restore the $Bi_4O_6^+$ cluster; ii) to react with molecular oxygen leading to an ozonide-like species or, iii) to react further with an additional ethene molecule. The path i) requires the dissociation of a bond between the C atom and of the C_2H_4O group and an oxygen atom belonging to the cluster frame. For this process a reaction enthalpy $\Delta H^o_{298} = +42.2$ kcal mol^{-1} is needed and even higher reaction barrier might be present. Therefore it can be considered as an unfavorable reaction path. For the second path ii) neither theoretical nor experimental evidence has been found. Finally the path iii) which corresponds to the step (e) to (f) of Fig. 4.10 is thermodynamically favorable by an extent of 23.0 kcal mol^{-1} and seems to occur in the absence of activation energy. This confirms all our theoretical findings for bi-molecular reactions involving radical species. Notice that the adduct (f) of Fig. 4.10 closely resembles a radical ether.

The above discussed chain process certainly involves unusual chemical species which actually have been so far identified by quantum chemical calculation only. However, all these species have been detected experimentally and a particularly high reactive cross section for $Bi_4O_6^+$ due to reactive collisions has been observed (cf. [112]). Furthermore, in the presence of a mixture of ethene and molecular oxygen only a small quantity of $(Bi_4O_6^+)C_2H_4$ (adduct (b) of Fig. 4.10) has been formed whereas other

species have been identified with molecular masses corresponding to $(Bi_4O_6^+)C_2H_4O_2$ (adduct (c)) and $(Bi_4O_6^+)C_2H_4O_2C_2H_4$ (adduct (d)) as well as $(Bi_4O_6^+)C_2H_4O$ (adduct (e)) and $(Bi_4O_6^+)C_2H_4OC_2H_4$ (adduct (f)). Of course, the claim cannot be made that the reaction mechanism based on our theoretical investigation represents the only way that reactions can proceed. However, our mechanism seems to be realistic under the assumption that no more than one ethene molecule can be attached directly to $Bi_4O_6^+$. This has been confirmed by the fact that no experimental evidence has been obtained for the existence of species such as $C_2H_4(Bi_4O_6^+)C_2H_4$ as well as $O_2C_2H_4(Bi_4O_6^+)C_2H_4O_2$.

Based on the determined reactive properties of the $Bi_4O_6^+$ cluster, a complete thermodynamic cycle can be designed. As well known, oxidation processes involving heterogeneous catalysts usually occur via adsorption and activation of molecular oxygen. In the case of transition metal homogeneous catalysts [119], the activation of O_2 usually requires that the metal is in a low oxidation state [101]. The chemistry of bismuth [100, 101] is dominated by compounds (cf. Bi_2O_3) with the metal atoms in (+3) formal oxidation state. Mainly due to relativistic effects, and inert pair effects of s electrons, compounds with the metal atoms in lower or higher oxidation states do exist only under very special conditions [101]. Therefore, forms like $Bi_4O_6^+$ are expected to be particularly stable since the transfer of oxygen atoms to substrate would change the oxidation state of the metal. This observation has been considered as the key assumption in proposing a reaction mechanism involving the activation of molecular oxygen acting as primary oxidant and leaving the cluster intact.

A stable compound with stoichiometry $(Bi_4O_6^+)C_2H_4OC_2H_4$ has been identified experimentally and theoretically. A proposed reaction mechanism for the formation of these products involves reactions with C_2H_4, O_2 and $Bi_4O_6^+$ species, where the bismuth oxide plays a crucial role in the indirect activation of molecular oxygen leading to the formation of hydrocarbon peroxide species and oxidized ethene by exoergic processes (cf. Table 4.7).

The question can be raised whether a catalytic cycle can be designed based on the computed properties. The attempt has been made in Fig. 4.11. The right part of the figure (step (a) to (f)) summarizes our findings presented in Fig. 4.10 showing that the $Bi_4O_6^+$ cluster easily reacts with ethene and molecular oxygen to form stable adducts which can be considered as intermediates (species (b), (c), (d), (e) and (f)) or products (OC_2H_4). Here we wish to address the role of (f) and (e) adducts. Starting from (e) the cycle can be closed by following the path IV of Fig. 4.11 in which the adduct (e) would

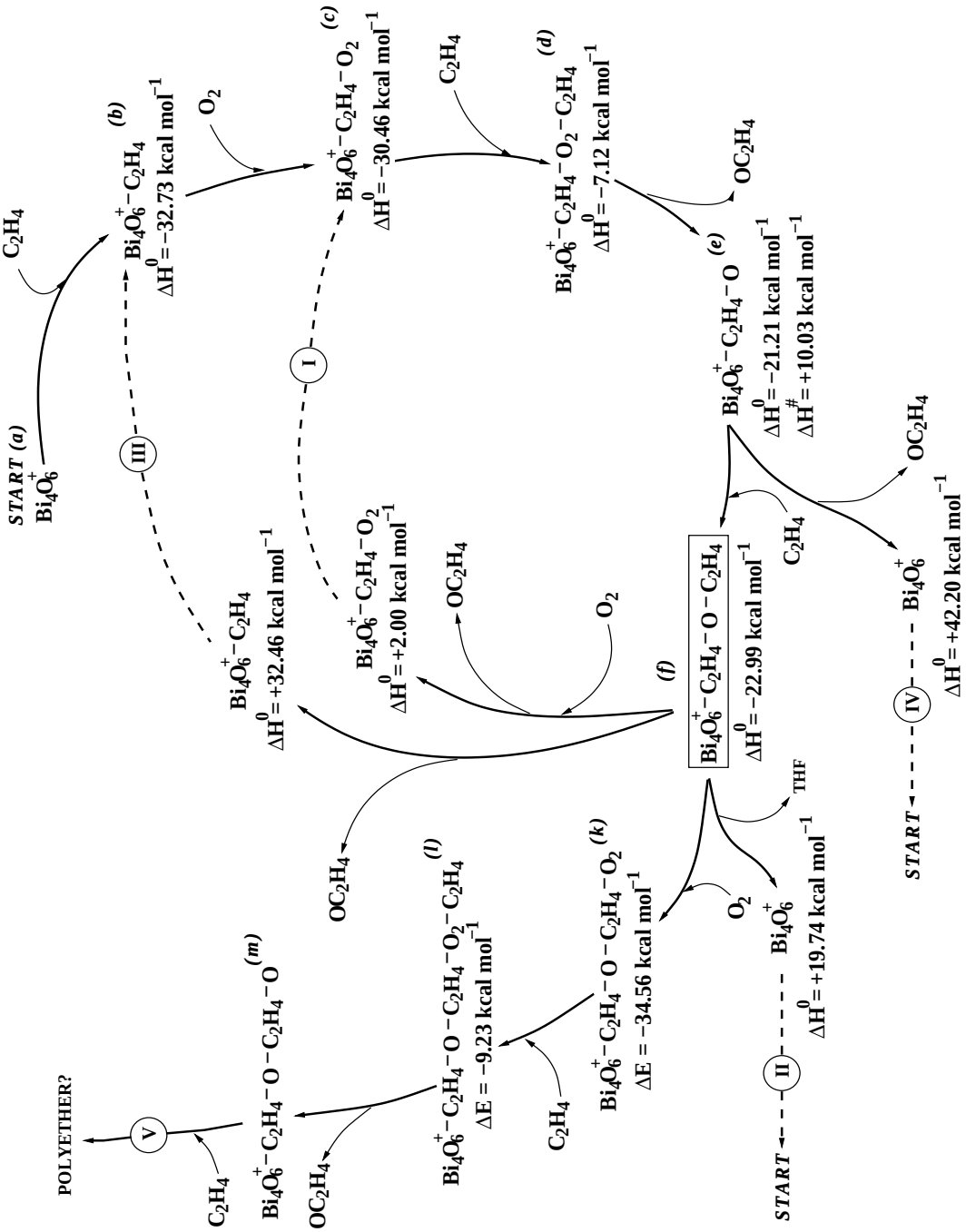

Figure 4.11: Thermodynamic cycle starting from $Bi_4O_6^+$ following Fig. 4.10 (right side) (steps a-f) extended by formation of chain though C_2H_4O units by adding molecular oxygen and ethene (steps k-m).

release an oxirane molecule to give back the $Bi_4O_6^+$ oxide, but this process is both thermodynamically and kinetically unfavorable since the reaction enthalpy amounts to $+42.9$ kcal mol^{-1}. By considering adduct (f) the paths II and III are also unlikely to occur due to endoergicity of $+19.7$ and $+32.4$ kcal mol^{-1}, respectively. Furthermore notice that in the case of the path III, the cycle closes to intermediate (b) and not to the $Bi_4O_6^+$. Path I is only slightly thermodynamically unfavorable, although from kinetics considerations this reaction is not likely to occur. In fact, the intermediate (f) is involved in a bi-molecular reaction with O_2. Namely an oxirane molecule is released and the cycle closes to intermediate (c), but the reaction mechanism would involve a first-order nucleophilic substitution reaction. Since the free molecular oxygen is not a very strong nucleophilic species and the involved carbon atom (cf. C_2 of Fig. 4.10) has a small fraction of negative charge (from NAO charge analysis population) it is to be expected that an high activation barrier would prevent the reaction to take place.

Fig. 4.11 reports also the path V, which can considered the most favorable one. By adding an O_2 molecule to the adduct (f) which retains radical properties, the adduct (k) can be formed due to a "chain mechanism", differing from adduct (c) by an additional OC_2H_4 "chain unit". The reaction enthalpy has been computed as -34.6 kcal mol^{-1} and as in the previously energetically favorable cases (such as (a) to (d)) the TS structure has not been located. The similarity of adducts (k) and (c) suggested us to investigate the possibility that a polyether chain supported on the $Bi_4O_6^+$ cluster can be formed. In fact, the peroxide species (l) differs from (d) also by an OC_2H_4 unit only. It is important to emphasize that the energetics of reaction path (f) to (l) compares well to the one calculated for (b) to (d) of Fig. 4.11 which means that the reaction along the path V could be favorable. Furthermore, Fig. 4.11 shows that once $Bi_4O_6^+$ species has been formed and has initiated the reaction giving rise to $Bi_4O_6^+$-C_2H_4-O-C_2H_4 (cf. adduct (f)), it plays a spectator role along the path V since the chain reaction proceeds by elongation through the OC_2H_4 units. Of course, species with high masses such as (k), (l) and (m) have not been detected experimentally since their masses are out of range belonging to $Bi_4O_y^+$ (y = 1-n) series and overlap with the oxide cluster with stoichiometry $Bi_5O_y^+$ (y = 1-n). Furthermore, the experimental setup consists of a very short reaction channel (allowing for the limited number of reactive collisions) in which only a small fraction of ethene is present in comparison with molecular oxygen, reducing the probability for detection of these species. Nevertheless, our theoretical findings concerning the path V suggest that the mechanism involving OC_2H_4 chain

units attached to $Bi_4O_6^+$ cluster might be an interesting process for future experimental investigations of the role of clusters as model systems for catalysis.

4.6 $Bi_xO_y^+$ $(x = 3, 4;\ y = 3 - 6)$ clusters and their interaction with propene

As reported in the section 4.5.1, the double bond of the ethene can be considered as the paradigm for small non-conjugated terminal π systems. This assumption holds in the case of propene in which the weak electron donor character of the methyl group does not induce particular charge splitting on the two carbon atoms involved in the π bond. As in the case of ethene, however, experimental evidence of the interaction of the bismuth oxide clusters with propene has been observed (cf. Fig. 4.1c and references [110] and [112]). We know (cf. Fig. 4.4) that the oxygen transfer reaction from the stoichiometric $Bi_3O_4^+$ cluster to the double bond is an unfavorable process and that the ethene π bond interacts with the cluster to form stable complexes (cf. Fig. 4.5). Furthermore, it has been shown that oxygen rich clusters such as $Bi_3O_5^+$ allows the π oxidation (cf. Fig. 4.6). In the case of propene, there are other possible reaction pathways. In fact, in addition to the reactivity of the π bond , the acidity of the methyl hydrogens of the hydrocarbon allows different reaction channels to occur.

In this section, we will present the role of the hydrogen transfer reactions in the formation of stable $Bi_3O_y^+(C_3H_6)$ $(y = 4,\ 5)$ complexes. Furthermore, the reactivity of the $Bi_4O_6^+$ cluster has been investigated by means of the chain reaction mechanism model proposed in section 4.5.3 by using propene as organic unsaturated substrate. It will be shown that also in this case the model gives satisfactory results in explaining the experimental findings.

4.6.1 The role of hydrogen transfer reactions in the oxidation of propene

Fig. 4.12 shows a reaction scheme involving the transfer of one of the methyl hydrogen atoms from the propene to the $Bi_3O_4^+$ cluster to form a stable compound. The process occurs by overcoming a reaction barrier of 17.47 kcal mol^{-1} and has a degree of exoergicity of 9.96 kcal mol^{-1}. The product of the reaction is a complex (cf. Fig. 4.12) in which the bismuth atom replaces the lost hydrogen of the methyl group of the

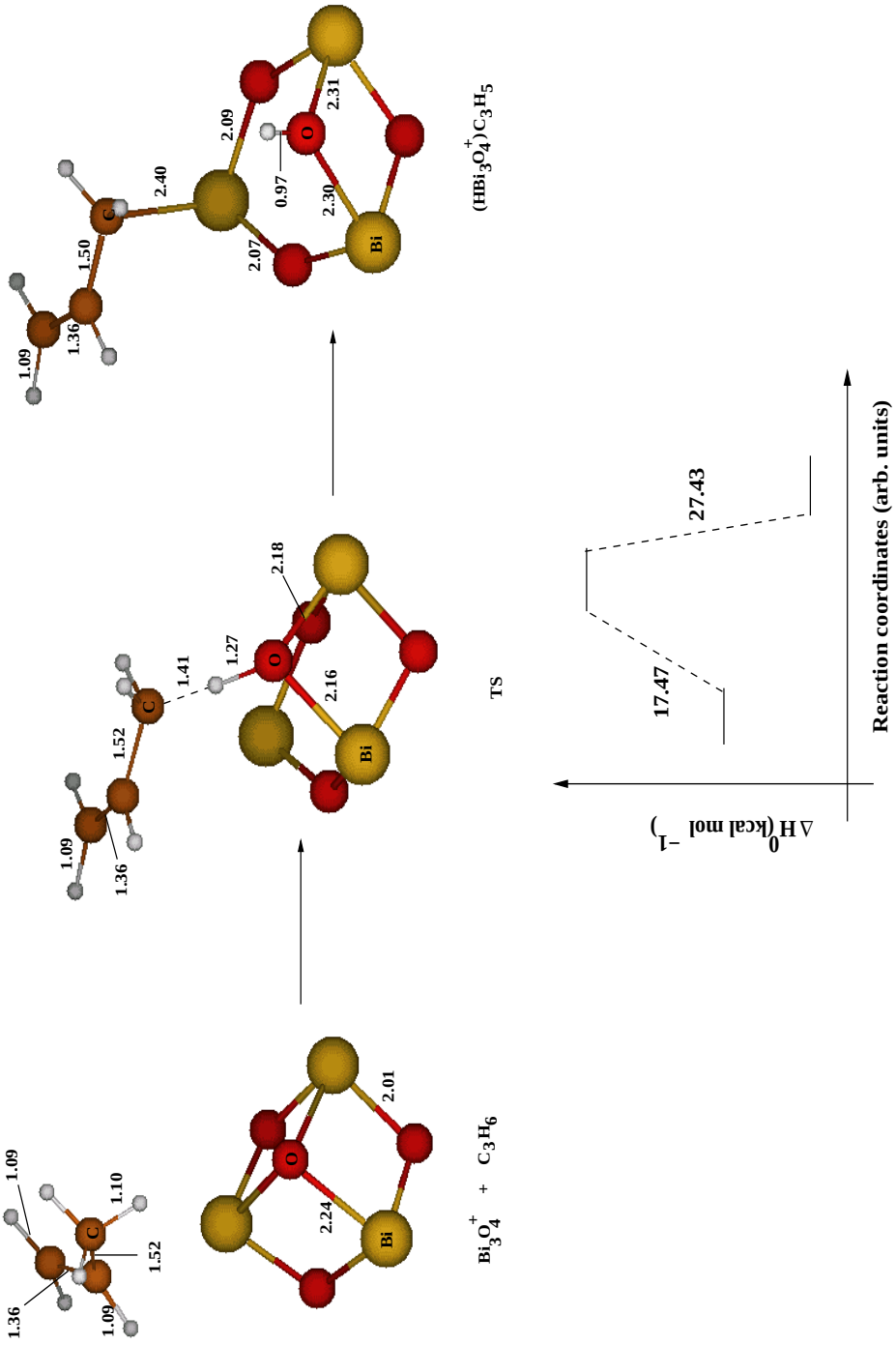

Figure 4.12: Structures of the reactants, TS and products as well as the energetics of the hydrogen transfer reaction $Bi_3O_4^+ + C_3H_6 \longrightarrow (HBi_3O_4^+)C_3H_5$.

propene, acting as an acidic center. In the TS structure the two C-C bond lengths (cf. 1.52 Å and 1.36 Å for the single and the π bond, respectively) of the propene are not affected by the transfer process and keep on values very close to those computed for the free molecule. Furthermore, there is no evidence of the formation of stable allyl intermediates. This is not unexpected, due to the post transition nature of the bismuth atom in the periodic table, which unables the metal to stabilize the delocalized bond of the allyl intermediate.

A different process involving the propene and the $Bi_3O_5^+$ cluster is reported in Fig. 4.13. In this case, the reaction proceeds through the formation of a partially oxidized intermediate. In the first step of the reaction, the hydrocarbon approaches the cluster with the central carbon (C_1) atom oriented along the guide-line of the principal vibrational mode of the dioxygen group of the cluster. In the TS I structure the O-O group of the $Bi_3O_5^+$ species is stretched from its computed equilibrium distance in the free cluster (cf. 1.46 Å) up to 1.75 Å, while the π bond of the hydrocarbon is elongated by 0.04 Å with respect to the computed value for the free molecule. At this stage of the reaction, care has been taken in order to ensure that the most likely reaction path from the TS I to the products will be followed. In fact, a reaction channel leading to the extraction of one oxygen from the $Bi_3O_5^+$ cluster to form OC_3H_6 also exists (cf. Fig. 4.14). In this respect, a particular computational technique which enables the user to investigate a reaction path by following the direction of the transition vector along its largest component (cf. Intrinsic Reaction Coordinates (IRC) [121]) and which ensures the convergence to the most likely product has been adopted. The result is the intermediate complex $(Bi_3O_5^+)C_3H_6$ I reported in Fig. 4.13 in which the dioxygen bond of the cluster is definitely broken and a three centers oxide species is formed. The reaction energy gain through this step is of about 50 kcal mol^{-1}, which is 30 kcal mol^{-1} more than in the case of the alternative pathway proposed by the mechanism of Fig. 4.14. The $(Bi_3O_5^+)C_3H_6$ I species can further evolve to form an even more stable complex by transferring one of the methyl hydrogens to one of the oxygen atoms of the cluster. The TS state structure of this second step (cf. TS II of Fig. 4.13) lies only 12.55 kcal mol^{-1} above the intermediate species (I) and shows how the process involves the shortening of the C_1-C_2 bond and the elongation of the C_2-C_3 bond. The product is a pseudo π alcoholic system in which the metal atom acts for an acid center bound to a C-O group. The last step is exoergic of about 20 kcal mol^{-1} and the $(HBi_3O_5^+)C_3H_5$ species evidences a strong since more than 60 kcal mol^{-1} is necessaryto break the

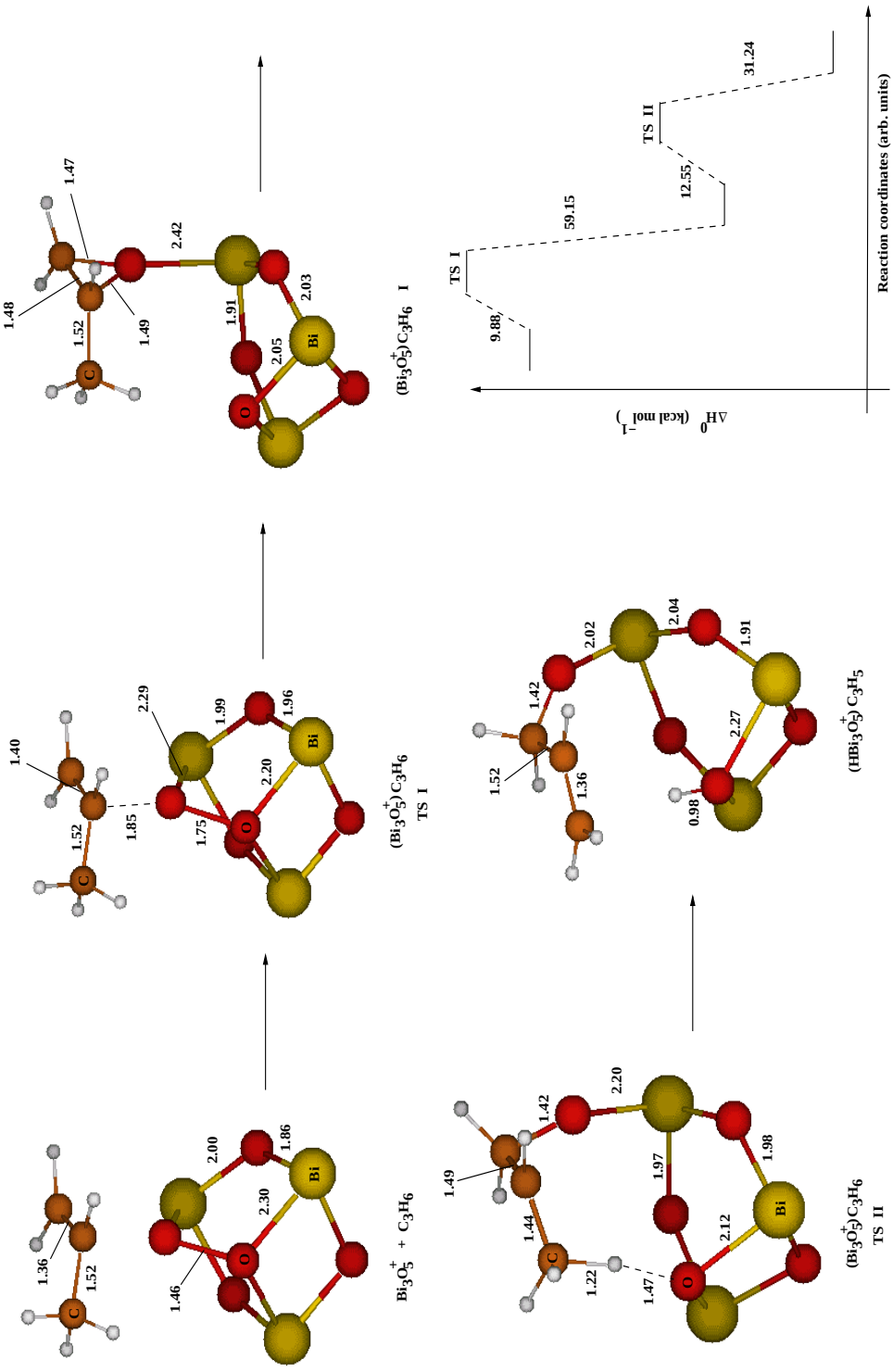

Figure 4.13: Structures of reactants, TS and products as well as the computed energetics of the two steps reaction involving propene and the $Bi_3O_5^+$ cluster.

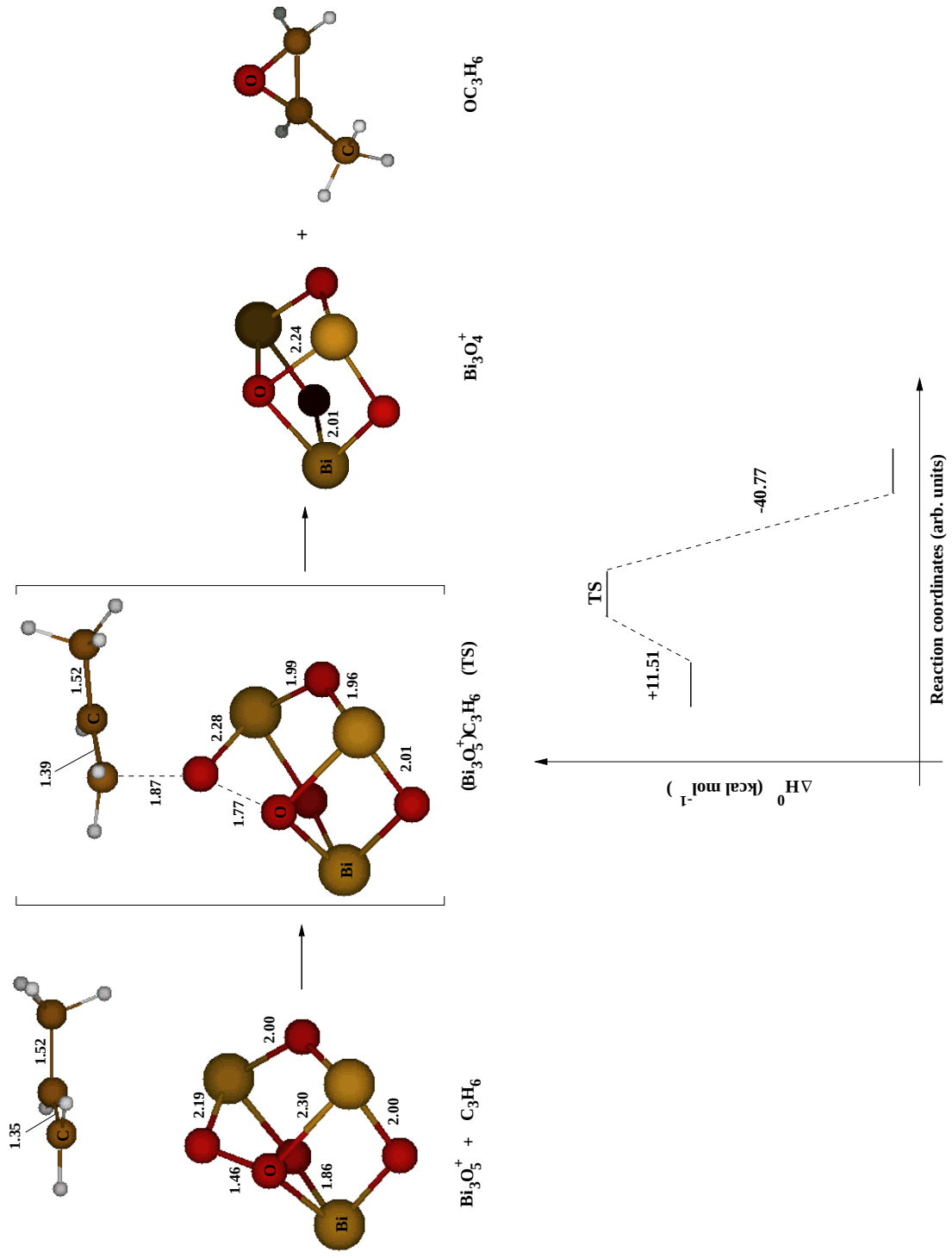

Figure 4.14: Structures of reactants, TS and products as well as the computed energetics of the π bond oxidation reaction of the propene by the $Bi_3O_5^+$ cluster.

Bi-O bond which keeps the hydrocarbon bound to the cluster.

In conclusion, clusters with stoichiometry $Bi_3O_y^+$ $(y = 4, 5)$ easily interact with propene. The reaction channels, however, differ from those involving ethene as reactant due to the possible transfer of the methyl hydrogens from the organic substrate to the oxygens of the cluster. In particular, it is evident that the $Bi_3O_5^+$ species can react with propene by two concurrent mechanisms leading to the formation of a stable $(HBi_3O_5^+)C_3H_5$ complex or to the direct oxidation of the alkene π bond. In the first case, a multistep process involving hydrogen transfer reactions is required while in the latter case the process proceeds straight to the oxidized product. Nevertheless, the computed reaction energies as well as the transition state energy barriers, evidence that the formation of the stable complex is favorable, in agreement with the experimental findings reported in Fig. 4.1c.

4.6.2 The $Bi_4O_6^+$ cluster as a promoter of chain reactions involving propene

Due to the presence of an unpaired electron localized at an oxygen atom, the $Bi_4O_6^+$ cluster has been identified as a particularly reactive radical species (cf. Sec. 4.4). Experimental findings evidenced that this cluster has a particularly high reactive cross section also by interacting with propene [112]. Of course, the C_3H_6 molecule has two different reactive centers which can influence this data. Thus, in order to approach theoretically the problem, the successful reactivity model proposed in the section 4.5.3 should be adopted by considering the energetics of different reaction paths involving the cluster interacting with the terminal or the secondary π carbon atoms in the propene. The results are schematically reported in Fig. 4.15. The path labeled by a) consider the terminal (C_1) carbon of propene as reactive center, whereas in the path b) the secondary (C_2) carbon has been considered as reactive. Both paths exhibit approximately the same reaction energy and it was not possible to locate any transition state structure. According to these calculations, both the intermediate complexes $(Bi_4O_6^+)C_3H_6$ I and II are equally likely to be formed and have approximately the same stability. Nevertheless, they substantially differ by the spin distribution which makes their further reactivity different. In fact, in the $(Bi_4O_6^+)C_3H_6$ I radical species, the unpaired electron is localized at the secondary carbon atom whereas in the intermediate II it is localized at the terminal carbon atom. According to the chain reaction mecha-

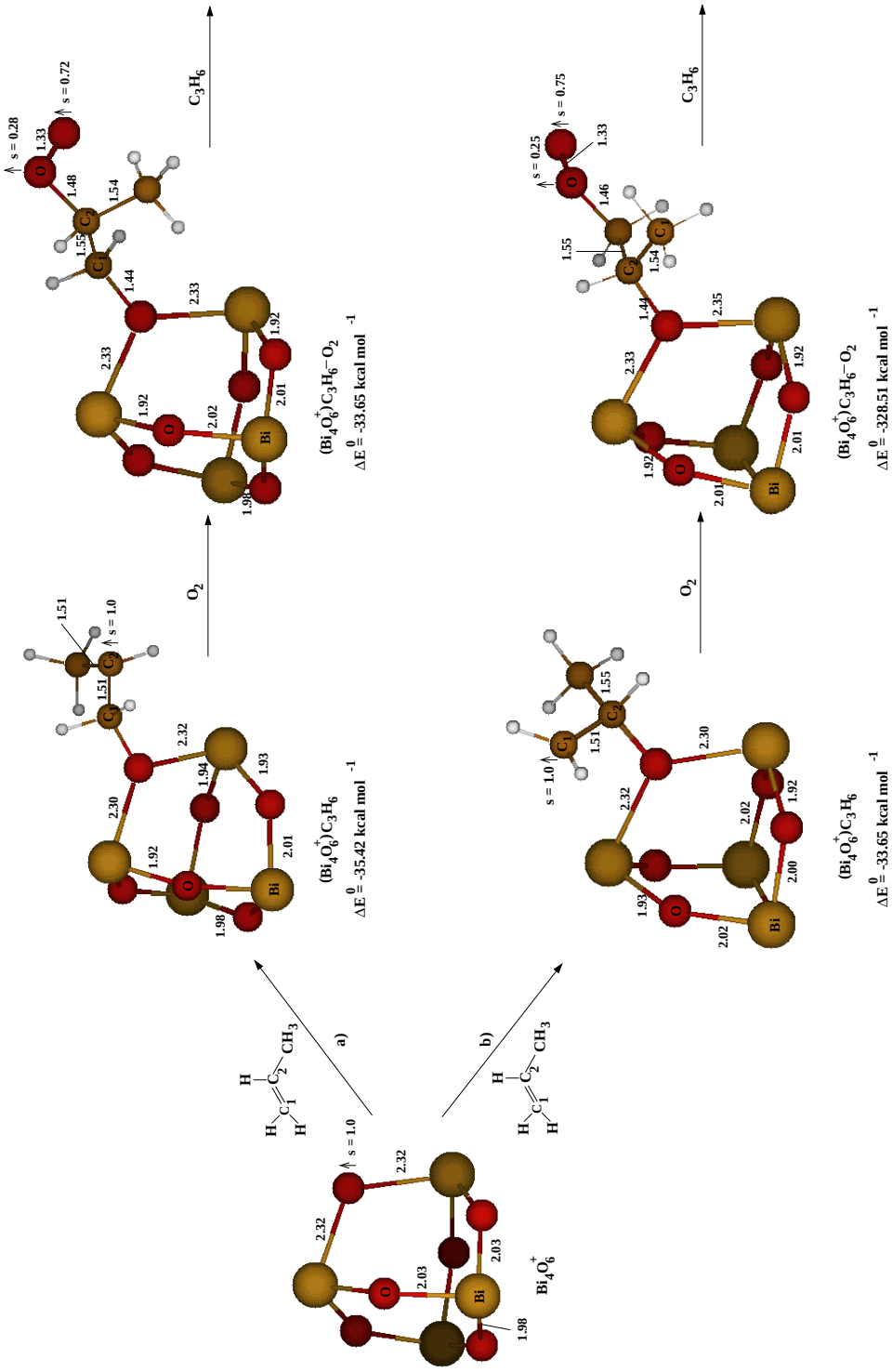

Figure 4.15: Reactants and intermediate structures for the reaction $Bi_4O_6^+ + C_3H_6 \longrightarrow Bi_4O_6^+C_3H_6$. Two paths are reported. In path a) the reactive center of the propene is the terminal carbon atom (C_1); in path b) the reactive center is the secondary carbon (C_2).

nism model of section 4.5.3, the $(Bi_4O_6^+)C_3H_6$ should further react with O_2 giving rise to superoxide complexes of stoichiometry $(Bi_4O_6^+)C_3H_6 - O_2$. The reactions occur with an energy gain of 27.97 and 28.51 kcal mol^{-1} for path a) and b), respectively. Furthermore, also in these cases no TS structures have been found confirming the extremely high reactivity of the radical species. The next step of the chain mechanism involves the reaction of the $(Bi_4O_6^+)C_3H_6O_2$ complexes with another propene molecule. Of course, every reactive step involving propene as substrate, can proceed by attaching a terminal or secondary carbon leading to different ramified products. However, calculations have shown that the energetics for the different reaction paths are comparable. As an example Fig. 4.16 reports the computed structures of two peroxide $(Bi_4O_6^+)C_3H_6 - O_2 - C_3H_6$ isomers (cf. I and II) which have been obtained by adding propene to the $(Bi_4O_6^+)C_3H_6 - O_2$ complexes of Fig. 4.15[4]. The next step of the chain mechanism model involves the dissociation of OC_3H_6 from the peroxides. We investigated the energetics of this process for both the $(Bi_4O_6^+)C_3H_6 - O_2 - C_3H_6$ I and II complexes. The resulting computed structures are reported in Fig. 4.16 labeled by $(Bi_4O_6^+)C_3H_6 - O$ I and II depending on the type of carbon atom is attached to the oxygen atom. The computed dissociation reaction energies are -19.52 and -16.58 kcal mol^{-1}, respectively and the corresponding reaction barriers are 8.47 and 7.58 kcal mol^{-1} evidencing a favorable process. Finally, the Fig. 4.16 also shows how the $(Bi_4O_6^+)C_3H_6 - O$ radical unit further reacts with propene allowing the chain reaction to proceed.

4.7 Summary and conclusions

Our systematic study of structural and electronic properties of the $Bi_3O_y^+$ $(y = 3 - 6)$ and $Bi_4O_y^+$ $(y = 6 - 8)$ clusters as well as their interaction with ethene and propene as reactive organic substrate based on density functional approach gives rise to three important findings:

I. Transfer of oxygen atoms from the stable clusters such as $Bi_3O_4^+$ is an energetically unfavorable process due to the breaking of strong Bi-O bonds. In the presence of molecular oxygen the clusters can be activated and the oxidation of unsaturated hydro-

[4]Of course, other two isomers were possible. In fact, labelling by X and Y the propene molecules reacting through the terminal or the secondary carbon atom, respectively and by I and II the two intermediate complexes $(Bi_4O_6^+)C_3H_6 - O_2$ of Fig. 4.15, one obtains the following combinations: IX, IY, IIX, IIY.

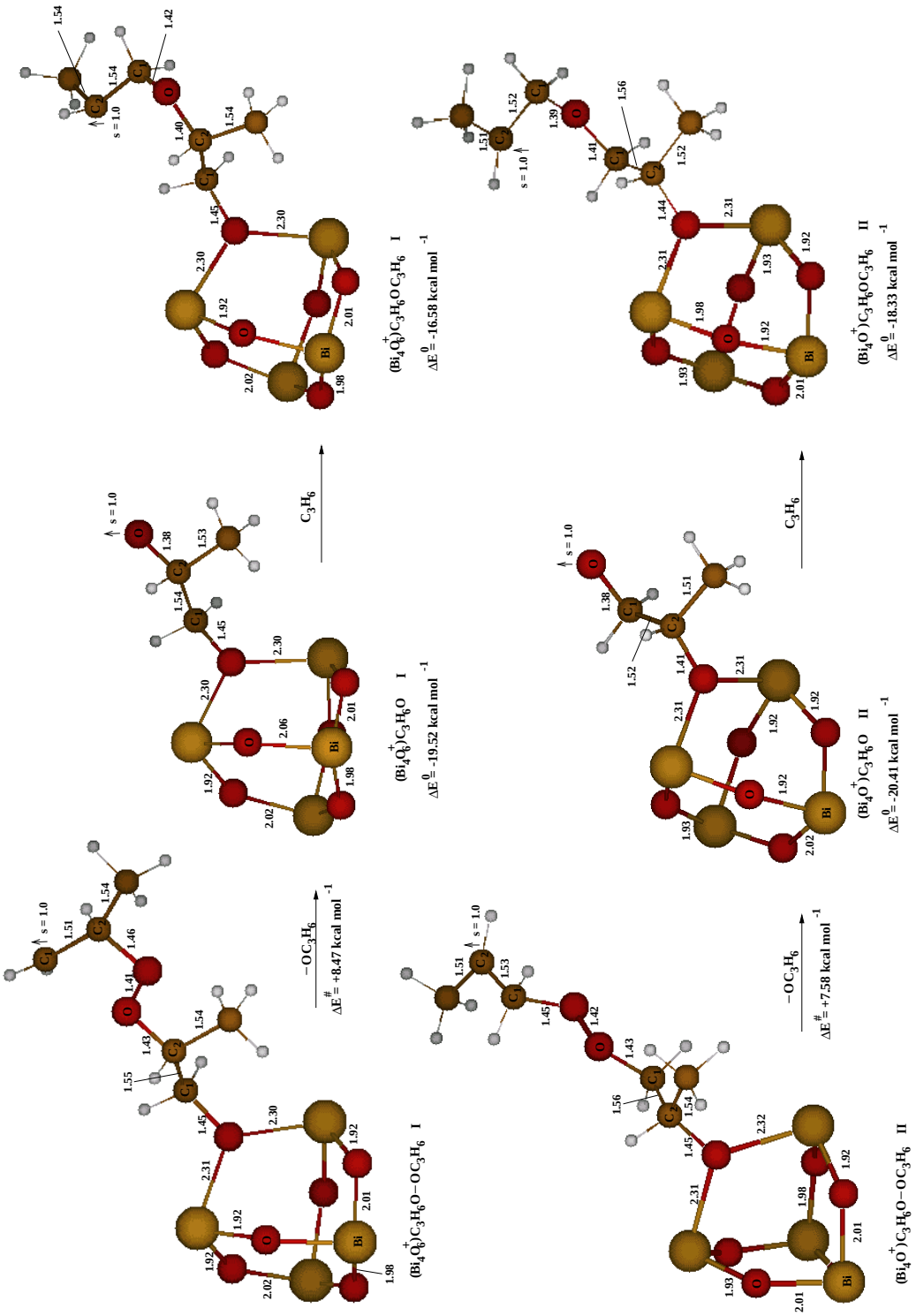

Figure 4.16: Structures and energetics of the further steps of the chain reaction mechanism model. The $(Bi_4O_6^+)C_3H_6 - O_2 - C_3H_6$ superoxide species dissociates to form $(Bi_4O_6^+)C_3H_6 - O$ radical complexes which further react with propene to form $(Bi_4O_6^+)C_3H_6 - O - C_3H_6$.

carbons might become feasible. However, ethene and propene reactivity differences have been pointed out. In details, the interaction of the clusters with propene can follow different reaction channels due to the presence of the methyl hydrogens which can be easily transferred from the hydrocarbon to the clusters.

II. The key role of the $Bi_4O_6^+$ cluster has been established. It interacts easily with both ethene and propene giving rise to a complex with a radical center located at a carbon atom which further reacts with molecular oxygen to form a superoxide unit. This is ready to further react with other hydrocarbon molecules to produce peroxide units which invoke a chain reaction.

III. The formation of chains with reactive radical units attached to the $Bi_4O_6^+$ cluster allows for possible oligomer formation from the energetic point of view. Also in this case, the behavior of propene differs from ethene, the former being characterized by two reactive π carbon atoms. The proposed reaction chain mechanism achieves the goal of explaining the experimental findings.

We can conclude that bismuth oxide clusters such as $Bi_4O_6^+$, retaining their identity, can play an important role in the presence of molecular oxygen for oxidation processes of alkenes.

Of course, whether the bismuth oxide clusters can act as catalysts still remains an open question. Indeed, from theoretical point of view a catalytic cycle can be set up, but additional experiments have to be carried out in order to confirm this prediction. Moreover, the temperature effects might be of large importance which have not been investigated in this work. This aspect should be addressed in the future work since molecular dynamics based on gradient corrected density functional methods can be applied in order to obtain the interpretation about temperature dependent reactivity of clusters.

Chapter 5

Zusammenfassung

Mit der vorliegenden Arbeit wurden neue Erkenntnisse bei der Aufklärung der Mechanismen, die für die Reaktivität von Übergangsmetall- und Metalloxid-Clustern verantwortlich sind, gewonnen. Dies ist aus zwei Gründen gelungen: Zum einen erlaubt die gradienten-korrigierte Dichtefunktional-Methode eine zuverlässige Beschreibung von strukturellen und energetischen Eigenschaften dieser Cluster, insbesondere durch die Entwicklung einer neuen Generation von Hybrid-Austausch- und Korrelations-Funktionalen im Rahmen der verallgemeinerten Gradienten-Näherung. Diese wurden erstmalig in entsprechenden quantenchemischen Programmen implementiert und getestet. Zum zweiten stellte die fruchtbare Zusammenarbeit mit den experimentellen Bereichen, insbesondere mit Herrn DC A. Fielicke im Arbeitskreis von Professor Rademann, eine Herausforderung für die Theorie dar, mittels der gewonnenen Erkenntnisse zur konzeptionellen Planung der Experimente beizutragen.

Die Reaktivität von Übergangsmetall-Clustern mit Liganden ist auf die ungesättigten Valenzbindungen zurückzuführen. An Hand des Ni-Tetramers haben wir gezeigt, dass die entsprechende Reaktivität mit einer starken Änderung der Natur der metallischen Bindung verbunden ist. Diese bestimmt damit auch die magnetischen Eigenschaften der Cluster. Bei Abwesenheit von CO-Liganden nimmt das Nickel-Tetramer einen Zustand grösstmöglicher Spin-Multiplizität ein, wobei die ungepaarten Elektronen in d-Orbitalen lokalisiert sind und die s-Elektronen für die metallischen Bindungen verantwortlich sind. Anlagerung von CO-Liganden führt zu einer drastischen Änderung der elektronischen Struktur des Ni-Tetramers, die mit abnehmendem Paramagnetismus verbunden ist. In voll karbonylierten Clustern ist die Stabilität nicht mehr durch die metallischen Bindungen verursacht, sondern erfolgt über Metall-Liganden-

Metall-Brücken.

Die Untersuchung der Reaktivität von Bismut-Oxid-Clustern stellt den Hauptteil der Arbeit dar. Auf der Basis der Dichtefunktional-Methode ergab unsere systematische Untersuchung der strukturellen und elektronischen Eigenschaften von $Bi_3O_y^+$ (y=3-6)- und $Bi_4O_y^+$ (y=6-8)-Clustern sowie ihre Wechselwirkung mit Ethen und Propen als reaktive organische Substrate drei wichtige Erkenntnisse:

I. Der Transfer von Sauerstoff-Atomen stabiler Cluster wie $Bi_3O_4^+$ ist energetisch ungünstig, da starke Bi-O Bindungen gebrochen werden müssen. In Anwesenheit von molekularem Sauerstoff können die Cluster jedoch aktiviert werden und die Oxidation von ungesättigten Kohlenwasserstoffen ermöglichen. Hierbei bestehen hinsichtlich der Reaktivität von Ethen und Propen Unterschiede. Insbesondere haben wir gefunden, dass die Wechselwirkung von Bismut-Oxiden-Clustern mit Propen verschiedenen Reaktionskanälen auf Grund der Anwesenheit von Methyl-Wasserstoff folgen kann, der leicht vom Cluster abstrahiert werden kann.

II. Die besondere Rolle von $Bi_4O_6^+$-Clustern bei massenspektrometrischen Modellreaktionen für Oxidationsprozesse von Alkenen wurde im Rahmen von Kettenreaktions-Mechanismen begründet. Dieser Cluster reagiert leicht sowohl mit Ethen als auch mit Propen zu einem Komplex mit einem Radikal-Zentrum, das an einem Kohlenstoff-Atom lokalisiert ist. Bei Anwesenheit von molekularem Sauerstoff entstehen hieraus Alkyl-Peroxyl-Radikale, die weiter mit Kohlenwasserstoff-Molekülen Peroxid-Einheiten bilden und die Kettenreaktion in Gang setzen.

III. Die Bildung von oligomeren Ketten, die an den $Bi_4O_6^+$-Cluster angelagert sind und reaktive Radikal-Einheiten enthalten, ist aus energetischer Sicht möglich. Auch in diesem Fall unterscheidet sich Propen von Ethen, da ersteres durch zwei reaktive π-Kohlenstoff-Atome charakterisiert ist. Dieser vorgeschlagene Kettenreaktions-Mechanismus diente auch zum Verständnis der experimentellen Ergebnisse.

Zusammenfassend haben wir gezeigt, dass Bismut-Oxid-Cluster wie $Bi_4O_6^+$, die unverändert bleiben, eine fundamentale Rolle für Oxidationsprozesse von Alkenen in Anwesenheit von molekularem Sauerstoff spielen. Ob Bismut-Oxid-Cluster als Katalysatoren dienen können, bleibt eine offene Frage. Aus theoretischer Sicht besteht die Möglichkeit für einen katalytischen Zyklus, was jedoch experimentell verifiziert werden muss. Darüber hinaus können auch Temperatureffekte wichtig sein, die in dieser Arbeit nicht untersucht wurden. Die Temperaturabhängigkeit der Reaktivität von Clustern ist ein wichtiger Aspekt zukünftiger Fragestellungen auf diesem Ge-

biet und kann im Rahmen einer Molekulardynamik auf der Basis von gradienten-korrigierten Dichtefunktional-Methoden behandelt werden.

List of Figures

List of Tables

Bibliography

[1] P. Fantucci V. Bonačić-Koutecký and J. Koutecký. In *Springer Series in Chemical Physics*, volume 52. Springer Verlag: Heidelberg, 1996.

[2] G. M. Pastor and K. H. Bennemann. Magnetic properties of transition-metal clusters. In W. Ekardt, editor, *Metal Clusters*. Wiley Series in Theoretical Chemistry, 1999.

[3] A. P. Alivisatos. *Science*, 271:933, 1996.

[4] D. Reichardt P. Fantucci V. Bonačić-Koutecký, J. Pittner and J. Koutecký. The quantum-chemical approach in metal clusters. In W. Ekardt, editor, *Springer Series in Chemical Physics*. Wiley Series in Theoretical Chemistry, 1999.

[5] D. Tománek Y. Wang and R. S. Ruoff. *Chem. Phys. Lett.*, 208:79, 1980.

[6] M. Pizzotti P. Fantucci, S. Lolli. *Inorg. Chem.*, 33:2779, 1994.

[7] A. Messiah. *Quantum Mechanics*, volume 1. North Holland Publishing Company, Amsterdam, 7 edition, 1972.

[8] E. B. Wilson Jr. L. Pauling. *Introduction to Quantum Mechanics With Applications to Chemistry*. Dover Pubns., 1985.

[9] E. Butkov. *Mathematical Physics*. Addison-Wesley Series in Advanced Physics, Addison-Wesley Publishing Company, 1968.

[10] P. W. Atkins. *Molecular Quantum Mechanics*. Oxford University Press, 2 edition, 1992.

[11] A. Szabo and N. S. Ostlund. *Modern Quantum Chemistry: Introduction to Advanced Electronic Structure Theory*. Dover Pubns., 1996.

[12] P. A. M. Dirac. *The Principles of Quantum Mechanics*. Oxford Clarendon Pressmic Press, 4 edition, 1958.

[13] H. B. Schlegel. Geometry optimization on potential energy surfaces. In *Modern Electronic Structure Theory Part I*. World Scientific Pubns., 1995.

[14] M. L. McKee and M. Page. In Kenny B. Lipkowitz and D. B. Boyd, editors, *Rev. in Computational Chemistry*, volume 4 of *271*. VCH Publishers, Inc., 1993.

[15] T. M. Apostol. *Mathematical Analysis*. Addison-Wesley Pub Co, 2 edition, 1974.

[16] D. A. Pierre. *Optimization Theory with Applications*. John Wiley and Sons, 1986.

[17] H. B. Schlegel C. Peng, P. Y. Ayala and M. J. Frisch. *J. of Comp. Chem.*, 17:1, 1996.

[18] C. Peng and H. B. Schlegel. *Isr. J. Chem.*, 33:449, 1993.

[19] T. A. Halgren and W. N. Lipscomb. *Chem. Phys. Lett.*, 49:225, 1977.

[20] P. Pulay. Analytical derivative technique and the calculation of vibrational spectra. In *Modern Electronic Structure Theory Part I*. World Scientific Pubns., 1995.

[21] P. C. Cross E. B. Wilson, J. C. Decius. *Molecular Vibrations*. Mc.Graw-Hill, New-Yor, 1955.

[22] F. Reif. *Fundamentals of Statistical and Thermal Physics*. McGraw-Hill International Edition, 1985.

[23] R. P. Feynman. *Statistical Mechanics. A set of Lectures*. The Advanced Book Program , Perseus Books; Reading, Massachussets, 1998.

[24] P. W. Atkins. *Physical Chemistry*. Oxford University Press, 4 edition, 1990.

[25] L. D. Landau and E. M. Lifsits. *Mechanica*. Ed. Mir, Moskow, 1975.

[26] B. C. Garrett D. G. Truhlar and S. J. Kilppenstein. *J. Phys. Chem.*, 100:12771, 1996.

[27] H. Eyring. *J. Chem. Phys.*, 3:107, 1935.

[28] R. P. H. Gasser and W. G. Richards. *An introduction to statistical thermodynamics*. WorldScientific Publishing Co. Pte. Ltd, 1995.

[29] D. G. Truhlar. Interpretation of activation energy. *Journal of Chemical Education*, 55:309, 1978.

[30] R. McWeeny. *Methods of Molecular Quantum Mechanics*. Academic Press; London, 2 edition, 1992.

[31] R. G. Parr and W. Yang. *Density Functional Theory of Atoms and Molecules*. Oxford University Press, 1989.

[32] F. Jensen. *An Introduction to Computational Chemistry*. John Wiley & Son Ltd., 1998.

[33] H. Kato H. Nakatsuji and T. Yonezawa. *J. Chem. Phys.*, 51:3175, 1969.

[34] T. Amos and Hall. *Proc. Roy. Soc. A.*, 263:483, 1961.

[35] D. Feller and E. R. Davison. In Kenny B. Lipkowitz and D. B. Boyd, editors, *Rev. in Computational Chemistry*, volume 8. VCH Publisher Inc, 1996.

[36] T. Helgaker and P. R. Taylor. Gaussian basis sets and molecular integrals. In *Modern Electronic Structure Theory Part I*. World Scientific Pubns., 1995.

[37] R. F. Steward W. J. Hehre and J. A. Pople. *J. Chem. Phys.*, 51:2657, 1969.

[38] J. S. Binkley and J. A. Pople. *J. Am. Chem. Soc.*, 102:939, 1980.

[39] J. A. Pople M. J. Frisch and J. S. Binkley. *J. Chem. Phys.*, 80:3265, 1984.

[40] D. Feller and E. R. Davison. In Kenny B. Lipkowitz and D. B. Boyd, editors, *Rev. in Computational Chemistry*, volume 4. VCH Publisher Inc, 1993.

[41] R. C. Raffenetti. *J. Chem. Phys.*, 58:4452, 1973.

[42] J. Almlöf and O. Gropen. In Kenny B. Lipkowitz and D. B. Boyd, editors, *Rev. in Computational Chemistry*, volume 8 of *271*. VCH Publishers, Inc., 1996.

[43] L. Szasz. *Pseudopotentials Theory of Atoms and Molecules*. Wiley, New York, 1985.

[44] P. Baybutt L. R. Kahn and D. G. Truhlar. *J. Chem. Phys.*, 65:3826, 1976.

[45] H. Bash W. J. Stevens and M. Krauss. *J. Chem. Phys.*, 81:6026, 1984.

[46] Y. S. Lee P. A. Christiansen and K. S. Pitzer. *J. Chem. Phys.*, 71:4445, 1979.

[47] W. C. Ermler Y. S. Lee and K. S. Pitzer. *J. Chem. Phys.*, 67:5861, 1977.

[48] M. L. Lutz T. R. Cundari, M. T. Benson and S. O. Sommerer. In Kenny B. Lipkowitz and D. B. Boyd, editors, *Rev. in Computational Chemistry*, volume 8. VCH Publishers, Inc., 1996.

[49] P. J. Hay and W. R. Wadt. *J. Chem. Phys.*, 82:270, 284, 299, 1985.

[50] P. Durand and J. C. Barthelat. *Theor. Chim. Acta*, 38:283, 1975.

[51] P. O. Löwdin. *Phys. Rev.*, 97:1474, 1955.

[52] E. R. Davidson S. R. Langhoff. *Int. J. Quant. Chem.*, 8:61, 1974.

[53] J. Pittner. *Ab Initio Study of Optical Properties of Neutral and Charged Pure and Mixed Alkali Metal Clusters*. VWF Verlag fuer Wissenschaft und Forschung Berlin GmbH, 1997.

[54] E. Davidson. *J. Comput. Phys.*, 17:87, 1975.

[55] R. J. Bartlett. Coupled-cluster theory: An overview of recent developments. In World Scientific Pubns., editor, *Modern Electronic Structure Theory Part I*, 271. 1996.

[56] G. E. Scuseria and T. J. Lee. *J. Chem. Phys.*, 93:5851, 1990.

[57] E. R. Davison. *Reduced Density matrices in Quantum Chemistry*. New York, Academic Press, 1976.

[58] P. Hohenberg and W. Kohn. *Phys. Rev.*, 136:864, 1964.

[59] W. Kohn and L. J. Sham. *Phys. Rev. A*, 140:1133, 1965.

[60] L. Wilk S. J. Vosko and M. Nusair. *Can. J. Phys.*, 58:1200, 1980.

[61] J. P. Perdew and Y. Wang. *Phys. Rev. B*, 45:13244, 1991.

[62] P. M. W. Gill J. A. Pople and B. G. Johnson. *Chem. Phys. Lett.*, 199:557, 1992.

[63] J. P. Perdew and Y. Wang. *Phys. Rev. B*, 33:8800, 1986.

[64] B. G. Johnson P. M. W. Gill and J. A. Pople. *Chem. Phys. Lett.*, 209:506, 1993.

[65] A. D. Becke. *Phys. Rev. A*, 38:3098, 1988.

[66] A. D. Becke. *J. Chem. Phys.*, 96:2155, 1991.

[67] R. Colle and A. Salvetti. *Theor. Chim. Acta*, 37:329, 1975.

[68] R. Colle and A. Salvetti. *J. Chem. Phys.*, 79:1404, 1983.

[69] W. Yang C. Lee and R. Parr. *Phys. Rev. B*, 37:785, 1988.

[70] J. P. Perdew. *Phys. Rev. B*, 33:8822, 1986.

[71] P. C. Redfern L. A. Curtiss, K. Raghavachari and J. A. Pople. *J. Chem. Phys.*, 106:1063, 1996.

[72] K. Raghavachari L. A. Curtiss, P. C. Redfern and J. A. Pople. *J. Chem. Phys.*, 109:42, 1998.

[73] T. Ziegler. *Can. J. Chem.*, 73:743, 1995.

[74] R. B. Ross B. B. Laird and T. Ziegler. *Chemical Applications of Density-Functional Theory*. Eds. ACS Symposium Series 629, Washington, 1995.

[75] J. Harris. *Phys. Rev. A*, 29:1648, 1984.

[76] A. D. Becke. *J. Chem. Phys.*, 98:132, 1993.

[77] A. D. Becke. *J. Chem. Phys.*, 107:8554, 1997.

[78] C. M. Pavlidou H. Stoll and H. Preuss. *Theor. Chim. Acta*, 49:143, 1978.

[79] A. D. Becke. *Int. J. Quantum Chem. Symp.*, 23:599, 1989.

[80] H. L. Schmider and A. D. Becke. *J. Chem. Phys.*, 108:9624, 1998.

[81] D. J. Tozer F. A. Hamprecht, A. J. Cohen and N. C. Handy. *J. Chem. Phys*, 109:6264, 1998.

[82] R. D. Amos. *CADPAC, The Cambridge Analytic Derivatives Package Issue 6*. Cambridge University, 1995.

[83] H-P. Baron R. Bauernschmitt S. Bocker M. Ehrig K. Eichkorn S. Elliott F. Furche F. Haase M. Haser H. Horn C. Huber U. Huniar M. Kattannek C. Kolmel M. Kollwitz K. May C. Ochsenfeld H. Ohm A. Schafer U. Schneider O. Treutler M. von Arnim F. Weigend P. Weis R. Ahlrichs, M. Bar and H. Weiss. *TURBOMOLE 5.2*. Universität Karlsruhe, Germany, 1985.

[84] H. B. Schlegel G. E. Scuseria M. A. Robb J. R. Cheeseman V. G. Zakrzewski J. A. Montgomery Jr. R. E. Stratmann J. C. Burant S. Dapprich J. M. Millam A. D. Daniels K. N. Kudin M. C. Strain O. Farkas J. Tomasi V. Barone M. Cossi R. Cammi B. Mennucci C. Pomelli C. Adamo S. Clifford J. Ochterski G. A. Petersson P. Y. Ayala Q. Cui K. Morokuma D. K. Malick A. D. Rabuck K. Raghavachari J. B. Foresman J. Cioslowski J. V. Ortiz B. B. Stefanov G. Liu A. Liashenko P. Piskorz I. Komaromi R. Gomperts R. L. Martin D. J. Fox T. Keith M. A. Al-Laham C. Y. Peng A. Nanayakkara C. Gonzalez M. Challacombe P. M. W. Gill B. Johnson W. Chen M. W. Wong J. L. Andres C. Gonzalez M. Head-Gordon E. S. Replogle M. J. Frisch, G. W. Trucks and J. A. Pople. *Gaussian G98 Rev. A. 5*. Gaussian, Inc., Pittsburgh PA, 1998.

[85] Wolfram Research. *Mathematica 2.2*. Inc. Champaign, IL, 1995.

[86] C. Adamo M. Bienati and V. Barone. *Chem. Phys. Lett.*, 311:69, 1999.

[87] A. J. Cohen and Y. Tantirungrotechai. *Chem. Phys. Lett.*, 299:465, 1999.

[88] P. C. Redfern L. A. Curtiss, K. Raghavachari and J. A. Pople. *J. Chem. Phys.*, 106:1063, 1997.

[89] P. M. W. Gill J. A. Pople and N. C. Handy. *Int. J. Quantum Chem.*, 56:303, 1995.

[90] G. E. Scuseira R. E. Stratmann and M. J. Frisch. *Chem. Phys. Lett.*, 257:213, 1996.

[91] G. W. Trucks L. A. Curtiss, K. Raghavachari and J. A. Pople. *J. Chem. Phys.*, 94:7221, 1991.

[92] D. J. Fox K. Raghavachari J. A. Pople, M. Head-Gordon and L. A. Curtiss. *J. Chem. Phys.*, 90:5622, 1989.

[93] G. W. Trucks K. Raghavachari L. A. Curtiss, C. Jones and J. A. Pople. *J. Chem. Phys.*, 93:2537, 1990.

[94] B. J. Duke and L. Radom. *J. Chem. Phys.*, 109:3352, 1998.

[95] J. Karwosky S. Fraga and K. M. S. Saxena. *Handbook of Atomic Data*. Elsevier, Amsterdam, 1975.

[96] F. A. Reuse and S. N. Kanna. *Chem. Phys. Lett.*, 77:234, 1995.

[97] C. E. Moore. *Atomic energy Levels*. NSRDS-NBS, Circular No. 467 US GPO Washington, 1952.

[98] G. Ganteför. private communication, 1996.

[99] R. Mulliken. *J. Chem. Phys.*, 23:1833, 1955.

[100] E. A. Keiter J. E. Huheey and R. L. Keiter. *Inorganic Chemistry: Principles of Structure and reactivity*. HarperCollins: New York, 1993.

[101] G. Wilkinson F. A. Cotton. *Advanced Inorganic Chemistry*. John Wiley & Son, New York, 1984.

[102] D. Cheilliah and G. W. Keulks. *J. Catal.*, 24:529, 1972.

[103] D. Burrington R. K. Grasselli. *J. Adv. Catal.*, 30:133, 1981.

[104] G. Centi and S. Perathoner. *Appl. Catal.*, 124:317, 1995.

[105] G. J. Hutchings S. H. Taylor, J. S. J Hargreaves and R. W. Joyner. *Appl. Catal. A*, 126:287, 1995.

[106] T. P. Snyder and C. G. Hill. *J. Catal. Rev.-Sci. Eng.*, 31 1 & 2:43, 1989.

[107] J. E. Bozik E. Swift and J. A. Ondrey. *J. Catal.*, 21:212, 1971.

[108] P. Ruiz B. Zhou, T. Machej and B. Delmon. *J. Catal.*, 132:183, 1991.

[109] B. Delmon. *Heterog. Chem. Rev. 1*, 219, 1994.

[110] A. Heidenreich M. Kinne and K. Rademann. *Angew. Chem. Int. Ed.*, 37:18, 1998.

[111] B. Kaiser M. Kinne, T. M. Bernhardt and K. Rademann. *Z. Phys. D*, 40:105, 1997.

[112] A. Fielicke and K. Rademann. *J. Phys. Chem. A*, 104:6979, 2000.

[113] H. Basch P. J. Jasien W. J. Stevens, M. Krauss. *Can. J. Chem. Phys.*, 98:5555, 1993.

[114] G. Herzberg K. P. Huber. *Molecular Spectra and Molecular Structure IV. Constants of Diatomic Molecules*. Van Nostrand Rehinold Co.: London, 1979.

[115] H. B. Schlegel A. G. Baboul. *J. Chem. Phys.*, 107:94, 1997.

[116] F. Weinhold A. E. Reed, L. A. Curtiss. *Chem. Rev.*, 88:899, 1998.

[117] J. Almlöf K. Faegri H. P. Luthi, J. H. Ammeter. *J. Chem. Phys.*, 77:2002, 1982.

[118] J. C. Robinsons S. H. Pullins J. Tucker R. B. King M. R. France, J. W. Buchanan and M. A. Duncan. *J. Phys. Chem. A*, 101:6214, 1997.

[119] S. Lolli P. Fantucci. *J. Mol. Catal.*, 82:131, 1993.

[120] C. Doornkamp. *The activation of oxygen by metal oxide catalyst*. Ponsen & Looijen bv: Wageningen, 4 edition, 1998.

[121] C. Gonzales and H. B. Schlegel. *J. Phys. Chem.*, 94, 1990.

Lebenslauf

von **Massimiliano Bienati**

04.06.1970	geboren in Premosello Chiovenda (Italien).
September 1976-Juni 1984	Besuch der Grundschule in Verbania (Italien).
September 1984 - Juli 1989	Besuch der Technischen Fachhochschule in Verbania (Italien).
Juli 1989	Abitur
November 1989 - Mai 1995 **Mai '95**	Studium der Chemie an der Universität Mailand. Diplomchemiker Hauptprüfung.
01.10.1995 - 31.10.1996	Wissenschaftlicher Mitarbeiter in der Gruppe von Prof. V. Bonačić-Koutecky an der Humboldt Universität zu Berlin, Forschungsthema: Strukturelle und Magnetische Eigenschaften von Nickel Clustern.
01.11.1996 - 31.12.1997	Wissenschaftlicher Mitarbeiter in der Gruppe von Prof. Piercarlo Fantucci an der Universität Mailand
01.01.1998 - 31.12.2000	Wissenschaftlicher Mitarbeiter an der Humboldt Universität zu Berlin. Beginn der Doktorarbeit in der Gruppe von Prof. V. Bonačić-Koutecky, Thema: Ab-initio Study of the Chemical Reactivity of Metal Clusters and Metal Oxide Clusters

List of pubblications

Massimiliano Bienati

1. M. Bienati, V. Bonačić-Koutecký and P. Fantucci, “The electronic structures and magnetic properties of the nickel tetramer and its partially carbonylated forms”, Eur. Phys. J. D, **9**, 467 (1999).

2. M. Bienati, V. Bonačić-Koutecky and P. Fantucci, “Theoretical Study of the Reactivity of Bismuth Oxide Cluster Cations with Ethene in the Presence of Molecular Oxygen”, J. Phys. Chem. A, **104**, 6983 (2000).

3. M. Bienati, C. Adamo and V. Barone, “The performance of a new hybrid Hartree-Fock/Kohn-Sham model (B98) in predicting vibrational frequencies, polarisabilities and NMR chemical shifts”, Chem. Phys. Lett. **311**, 69 (1999).

Erklärung

Hiermit erkläre ich, daß die Dissertation mit dem Titel "*Ab Initio Study of the Chemical Reactivity of Metal and Metal Oxide Clusters*" selbständig und nur unter Verwendung der angegebenen Literatur und Hilfsmittel von mir, Massimiliano Bienati, angefertigt wurde.

Berlin, den 22. 01. 2001

(Massimiliano Bienati)

This work has been supported by the Deutsche Forschungsgemeinschaft SFB 450 and partially by the Università degli Studi of Milan. It was carried out at the Walther-Nernst Institut für Physikalische und Theoretische Chemie, Humboldt Universität zu Berlin.

I would like to express my gratitude to Prof. Dr. Vlasta Bonačić-Koutecký for giving me the opportunity to accomplish my Ph.D thesis at the Humboldt University and for a constructive and stimulating guidance during my work. I extend my thanks to Prof. Piercarlo Fantucci for many stimulating discussions. I thank for the close collaboration with DC André Fielicke and Prof. Klaus Rademann of reactivity of bismuth oxide clusters. I thank Prof. Vincenzo Barone and Dr. Carlo Adamo for their support in the implementation of the new density functional theory code into the GAUSSIAN package. Further, I would like to thank Dr. Michael Hartmann and Dr. Jiri Pittner for their precious suggestions; Mr. Wihlelm Ruesing and Mr. Ettore Virzi for their help in solving any technical computer problem I had. Mrs. Katharina Pfaff for her patience in facing up all burocracy requirements related to my stay in Berlin; Mr. Heinrich Widmann for his generous hospitality and friendship.

I wish to extend my thanks to my parents who provided, encouragement, patience and strength for me to continue.